UNIVERSIDAD DE LA REPÚBLICA

FACULTAD DE INGENIERÍA

Doctoral thesis submitted in partial fulfillment of the requirements for the degree of

Doctor in Engineering, Applied Fluid Mechanics.

Response of the tropical convergence zones to extratropical thermal forcing

Author: MEng. Stefanie Talento

Advisor: PhD. Marcelo Barreiro

Submitted September, 2016

Abstract

Paleoclimatic data, 20th century observations and numerical simulations have all suggested the capability of the extratropics to trigger global teleconnection patterns and drive changes in the distant tropical regions mediated through atmospheric and ocean processes. The emerging general picture is that the Inter Tropical Convergence Zone (ITCZ) tends to shift toward the warmer hemisphere at the same time that the atmospheric energy transport is modified to favour the transport of energy to the colder hemisphere. Apart from paleo and 20th century climate implications, the extratropical to tropical teleconnection problem has also been related with the future climate as the projected pattern of temperature change for the 21st century presents an interhemispheric asymmetry with the strongest warming projected to occur over the Northern Hemisphere (NH) high latitudes.

This thesis aims to shed further light into the sensitivity of the tropical climate to an extratropical thermal forcing via a series of numerical simulations performed with an Atmospheric General Circulation Model (AGCM) coupled to either a low or a medium complexity ocean model, using realistic surface boundary conditions in all the cases. The behaviour of two convergence zones, the ITCZ and the South Atlantic Convergence Zone (SACZ), is the main focus of the work. The relative roles of the atmosphere, sea surface temperature (SST), land surface temperature (LST), hemispheric component of the forcing and tropical ocean dynamics are investigated and physical mechanisms mediating in the extratropical to tropical teleconnection are proposed and tested.

In simulations in which the AGCM is coupled to slab ocean and land models we find that if the tropical SSTs are not allowed to change in response to the extratropical forcing then the ITCZ response strongly weakens although it is not negligible in particular over the Atlantic Ocean and Africa. If, in addition to the tropical SST constraint, the LST over Africa is prevented to change the ITCZ response to the remote signal completely vanishes. Therefore, our results indicate that the ITCZ response to the extratropical forcing is not possible just trough purely atmospheric processes, but needs the involvement of either the tropical SST or the LST. The clear-sky longwave radiation feedback is highlighted as the main physical mechanism operating behind the land-based extratropical to tropical communication.

Regarding the SACZ, we present numerical evidence that indicates that it can be affected by an extratropical thermal forcing with a behaviour that does not replicate the ITCZ response of shifting toward the warmer hemisphere. In fact, we find that when the NH (Southern Hemisphere, SH) extratropics warm (cool), the SACZ experiences a significant weakening associated, mostly, to the NH component of the forcing. Our results indicate that 75% of the SACZ signal in response to the forcing is linked to the development of a secondary tropical convergence zone in the Atlantic Ocean around 20°N-30ºN, which depends on the tropical SST response. The remaining 25% of the signal can be explained through the development of a Walker-type of circulation between western tropical Africa and the SACZ, being this mechanism associated with the African LST reaction to the remote forcing.

To assess the role of the tropical ocean dynamics we analyse and compare simulations in which the AGCM is coupled either to a slab ocean model or to a combination of a Reduced Gravity Ocean model in the tropics and a slab model elsewhere. The inclusion of tropical ocean dynamics enables changes in the equatorial Pacific SST seasonal cycle, whose response to a NH (SH) high latitude warming (cooling) consists of a significant strengthening in the eastern portion of the basin. The annual mean response, however, is weaker than the signal the extratropical forcing would generate if only thermodynamic coupling was allowed, thus suggesting that tropical ocean dynamics tends to oppose the extratropical forcing in the mean. We further find that under an extratropical forcing the activity of the El Niño-Southern Oscillation weakens, which is consistent with a strengthening of the seasonal cycle through the previously proposed frequency entrainment mechanism.

Resumen

Datos paleoclimáticos, observaciones del siglo XX y simulaciones numéricas sugieren que los extratrópicos tienen la capacidad para desencadenar patrones de teleconexión globales y forzar cambios en las regiones tropicales, a través de de procesos atmosféricos y oceánicos. La imagen general que surge es que la Zona de Convergencia Inter Tropical (ZCIT) tiende a desplazarse hacia el hemisferio más cálido mientras que el transporte de energía atmosférico se modifica para favorecer la transferencia energética hacia el hemisferio más frío. Además de implicaciones paleoclimáticas y para el clima del siglo XX, el problema de la teleconexión desde los extratrópicos hacia los trópicos ha sido también relacionado con el clima futuro, dado que el patrón proyectado de cambio de temperatura para el sigo XXI presenta una marcada asimetría interhemisférica con un calentamiento acentuado en las latitudes altas del Hemisferio Norte (HN).

El objetivo de esta tesis es profundizar en el estudio de la sensibilidad del clima tropical a un forzante térmico extratropical mediante una serie de simulaciones numéricas realizadas con un modelo de circulación general de la atmósfera (MCGA) acoplado a modelos oceánicos de complejidad baja o media y utilizando, en todos los casos, condiciones de borde realistas. El comportamiento de dos zonas de convergencia, la ZCIT y la Zona de Convergencia del Atlántico Sur (ZCAS), es el foco principal del trabajo. Los roles relativos de la atmósfera, la temperatura de superficie del mar (TSM), la temperatura de superficie continental (TSC), la componente hemisférica del forzante y la dinámica de los océanos tropicales son investigados al mismo tiempo que mecanismos físicos que median en la teleconexión son propuestos y testeados.

En simulaciones en las que el MCGA se acopla a modelos tipo slab para océanos y continentes encontramos que si no se permite que la TSM tropical reaccione al forzante extratropical entonces la respuesta de la ZCIT se debilita notablemente pero sigue siendo significativa, en particular, sobre el océano Atlántico y África. Si, además de la restriction a la TSM tropical, no se permite que la TSC sobre África cambie entonces la respuesta de la ZCIT se desvanece completamente. Por lo tanto, nuestros resultados indican que la respuesta de la ZCIT a un forzante extratropical no es posible a través de procesos puramente atmosféricos, sino que necesita del involucramiento de o bien la TSM o bien la TSC tropical. Encontramos que la retroalimentación de radiación de onda

larga en cielo claro es el principal mecanismo físico operando detrás de la comunicación extratrópicos-trópicos a través del continente africano.

En cuanto a la ZCAS, presentamos evidencia numérica que indica que puede ser afectada por un forzante térmico extratropical con un comportamiento que no replica la respuesta de la ZCIT de desplazarse hacia el hemisferio más cálido. De hecho, encontramos que cuando los extratrópicos del HN (Hemisferio Sur, HS) se calientan (enfrían) la ZCAS experimenta un debilitamiento significativo asociado, mayoritariamente, a la componente del forzante localizada en el HN. Nuestros resultados muestran que el 75% de la señal de la ZCAS en respuesta al forzante está asociado al desarrollo de una zona de convergencia tropical secundaria en el océano Atlántico entre 20°N y 30°N, la cual es dependiente de la respuesta de la TSM tropical. El 25% restante de la señal puede ser explicado mediante el desarrollo de una circulación del tipo de Walker entre el oeste de África tropical y la ZCAS, estando este mecanismo asociado a la reacción de la TSC africana al forzante remoto.

Para evaluar el rol de la dinámica oceánica tropical analizamos y comparamos simulaciones en las que el MCGA se acopla o bien a un modelo slab oceánico o bien a una combinación de un modelo de gravedad reducida en los trópicos y un modelo slab en el resto de los puntos oceánicos. La inclusión de la dinámica oceánica tropical permite que se produzcan cambios en el ciclo estacional de la TSM del Pacífico ecuatorial, cuya respuesta a un calentamiento (enfriamiento) en latitudes altas del HN (HS) consiste en una intensificación significativa en la porción este de la cuenca. Sin embargo, la respuesta en términos de promedios anuales es más débil que la que el forzante generaría si únicamente una acople termodinámico estuviese permitido sugiriendo, por ende, que la dinámica oceánica tropical tiende a oponerse al forzante extratropical en promedio. Por otro lado, también encontramos que bajo la influencia de un forzante extratropical la actividad del fenómeno El Niño-Oscilación Sur se debilita, lo cual es consistente con la intensificación del ciclo estacional a través del ya propuesto mecanismo de arrastre de frecuencias.

Table of Contents

List of Figures

List of Tables

Chapter 1. Introduction

The climate of the Earth is determined by the global energy budget. For an equilibrium climate the net incoming shortwave solar radiation must be balanced by the outgoing longwave radiation, a process that involves multiple feedbacks internal to the climate system. On one hand, changes in the incoming solar radiation arise either from changes in the Sun's output or from changes in the planetary albedo. On the other hand, changes in the outgoing longwave radiation are produced by changes in the temperature or in the emissivity properties of either Earth's surface or atmosphere.

Nowadays, the Earth's radiative energy budget is not in balance but presents a slight surplus: the planet is absorbing more energy from the Sun than it is radiating back to space (Hansen et al., 2011). The energetic imbalance is estimated for the 2005-2010 period in 0.58+/- 0.15 W/m^2 and it is widely agreed that it is associated with the human-induced rapid changes to the atmospheric composition, via the greenhouse effect. Greenhouse gases (GHG) such as carbon dioxide, methane and nitrous oxide have long atmospheric lifetimes (decades to centuries) and, therefore, can accumulate in the atmosphere making it more opaque at infrared wavelengths, reducing the heat emission to the space. The energetic excess causes the planet to warm, being the global surface temperature linear trend for the 1880-2012 period estimated in 0.85+/- 0.2 °C (Hartmann et al., 2013).

Humanity and ecosystems are potentially vulnerable to changes in the climate system and the economic and ecological impacts could be large and serious. In recent decades changes in climate have been observed globally and some of them have been attributed to anthropogenic causes and not to natural climate variability. The impacts of the ongoing climate change are not restricted to changes in surface temperature, but also involve alterations of: global precipitation patterns, frequency or intensity of extreme events (droughts, floods, heat waves), tropical cyclones, ocean warming, ocean acidification, sea ice, ice sheets, glaciers and sea level. As the GHGs concentrations are expected to rise even further in the future climate, the study of climate changes induced by anthropogenic forcing and its separation from natural variability is of central relevance for the

scientific community.

1.1. Interhemispheric temperature asymmetry in the pattern of global temperature change and associated tropical changes

Figures 1.1 a and b show the evolution of the observed surface temperature anomalies zonal and hemispheric means, respectively, for the 1880-2015 period. As mentioned above, it is clear that during the 20th century the whole globe experienced a sustained warming, but the rate was not the same for the two hemispheres. From 1980 there is a significant amplification of the warming in the Northern Hemisphere (NH), poleward of 40ºN, as a result from the Arctic amplification and the warming of the NH landmasses (Collins et al., 2013; Flato and Boer, 2001; Friedman et al., 2013). Also a minimum warming is evident around 60ºS and has been attributed to deep ocean mixed layers and a consequent strong heat uptake in the Southern Ocean. Friedman et al. (2013) investigate the evolution of an interhemispheric temperature asymmetry index (ITA), defined as the difference between the hemispheric-mean surface air temperature anomalies (NH, minus Southern Hemisphere, SH; see Figure 1.1 c). A sudden ITA decrease is evident towards the late 1960's followed by a significant and sustained upward trend from the 1980's that continues until the present.

The drop of the ITA index by the end of the 1960's decade is associated with an interhemispheric sea surface temperature (SST) pattern, with cooling in the NH oceans (specially acute in the North Atlantic) and warming in the mid latitudes of the southern Atlantic and Indian Oceans. Thompson et al. (2010) argue that the rapid time scale of this interhemispheric SST shift signals an abrupt change in the oceanic meridional overturning circulation as the possible driver, suggesting a rapid freshening in the northern North Atlantic as the ultimate cause (known as the “Great Salinity Anomaly”; Dickson et al., 1988). Baines and Folland (2007) also suggest anthropogenic sulfate aerosols and internal variability as possible drivers. In fact, Friedman et al. (2013) find that, excepting a few cases, the Coupled Model Inter Comparison Project Phase 5 (CMIP5) historical simulations do not reproduce the observed ITA drop in the late 1960's, suggesting that internal variability might be playing a primary role. This interhemispheric SST pattern has been associated with tropical climate changes. Among the best known abrupt changes that occurred around the late

60's is the alteration of the precipitation regime in the African Sahel, which from 1967 to 1969 underwent a shift toward a persistent and severe drought that remained for two decades. Folland et al. (1986) find that a SST pattern characterized by an interhemispheric thermal gradient could be a possible driver to decadal wet and dry periods in the Sahel. In addition, Giannini et al. (2003) find that the observed record of SST is the main driver of the Sahel hydro-variability, as they are able to reproduce it by integrating an Atmospheric General Circulation Model (AGCM) forced with historical SST as the sole forcing. In particular, a configuration of a cooler NH and a warmer SH was associated with a period of Sahel drought starting in the late 1960s.

The upward trend seen in the ITA index (NH warming faster than SH) from 1980 is associated with a hemispherically asymmetric temperature pattern that features disproportionate warming in the Arctic and NH landmasses along with a moderate cooling in the eastern Pacific Ocean. The prominent Arctic amplification is associated with feedbacks from melting snow and sea-ice, water vapour, changes in the lapse-rate and increasing clouds while the Pacific Ocean cooling has been attributed to the Pacific Interdecadal Oscillation (see Friedman et al., 2013 and references therein). CMIP5 historical runs are able to reproduce this pattern, with very similar latitudinal gradients. Friedman et al. (2013) find that historical simulations with the combination of GHG and aerosols forcing are the ones that produce the best fit to the observed record, suggesting that until 1980 the GHG warming effect was largely compensated by the aerosols cooling effect, and only after regulations in aerosols were implemented the GHG effect was capable of producing the strongest impact.

The projections for the future climate tend to agree in the fact that global warming will not be uniform but will have an important hemispherically asymmetric component, with the NH warming faster that the SH as a result from the Arctic amplification and the warming of the NH landmasses. The ITA index introduced by Friedman et al. (2013) is projected to increase its upward trend well beyond the observed trend in the last decades of the 20th century.

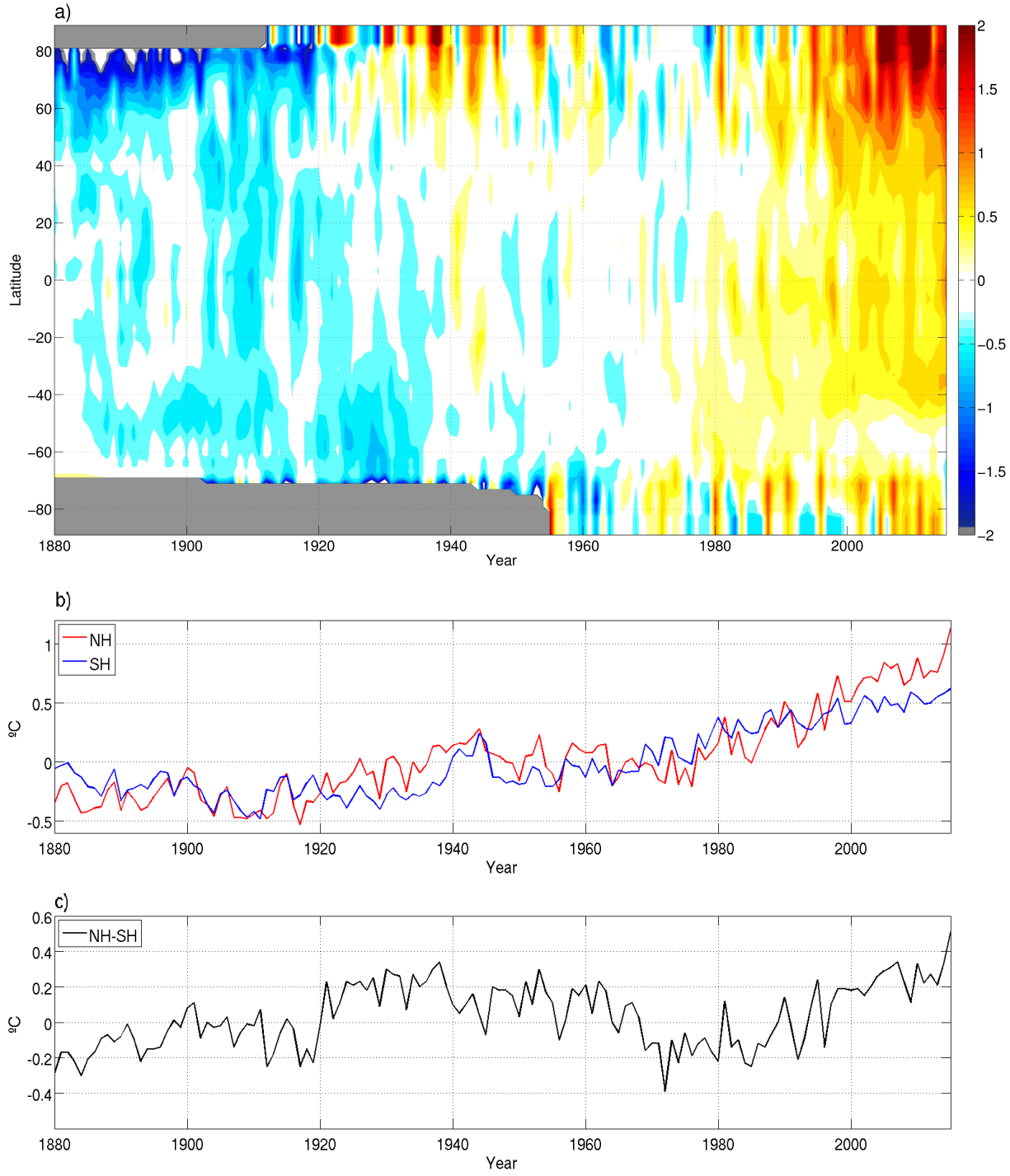

Figure 1.1: a. Time-latitude diagram of annual zonal mean temperature anomalies (°C). Gray areas indicate lack of data. b. NH and SH temperature anomalies (°C). c. ITA index (°C): NH minus SH temperature anomalies. Base period for anomaly calculation: 1951-1980. Data from GISTEMP (Hansen et al., 2010) at http://data.giss.nasa.gov/gistemp/)

CMIP5 models show that an increase in the ITA index in the 21st century is related to tropical

changes in the Hadley circulation and precipitation patterns. The future projections show that the ITA trend is associated with a significant weakening of the NH Hadley cell and a small strengthening of the SH Hadley cell. This asymmetry in the response of the overturning circulation might be explained by the added effects of the ITA (strengthening/weakening of the Hadley Cells in equal magnitudes) and of a uniform global warming (widespread weakening of the tropical circulation; Vecchi and Soden, 2007), leading to a partial compensation in the SH Hadley cell and producing only a moderate response. The ITA index projected trend is also associated with a positive trend in a tropical precipitation asymmetry index indicating a northward Inter Tropical Convergence Zone (ITCZ) shift, although the magnitude of this asymmetry is weaker than the expected from increasing the ITA (Friedman et al., 2013). Again, this behaviour might be related the overlapping effect of a uniform global warming, which is expected to promote a precipitation intensification (Held and Soden 2006). In particular, in the CMIP5 simulations the tropical precipitation asymmetric response is only significant from mid 21st century onwards.

1.2. Evidence for extratropical influence on the tropics: Paleoclimate and numerical simulations

The discussion of the previous section suggests that an interhemispheric temperature gradient (with largest anomalies in the extratropics) can induce changes in the tropical climate. This link can be materialized via any of the components of the climate system, and is usually known as teleconnection (Liu and Alexander, 2007). Tropical-extratropical teleconnections are typically conceived as the tropics driving the extratropics (Horel and Wallace, 1981; Hoskins and Karoly, 1981), being El Niño Southern Oscillation (ENSO) the most notorious example. However, the capability of the extratropics to drive the tropical regions has been also highlighted in studies analysing paleoclimatic proxies and numerical simulations. Both atmospheric and oceanic processes could be of relevance.

The greatest set of available evidence for the extratropical influence on the tropical climate comes from records of abrupt climate changes occurred during the last glacial period (between 100.000 and 15.000 years ago) and their global signatures (Chiang and Friedman, 2012).

Greenland ice-cores depict a series of abrupt warming events, known as Dansgaard-Oeschger (D/O) events (Dansgaard et al. 1993), in which rapid (3 years - few decades) and ample (~10ºC) warmings take place followed by more gradual cooling periods (Figure 1.2 a). Synchronous abrupt events are also recorded in the distant tropics, suggesting that the North Atlantic climate changes may have tropical correlates.

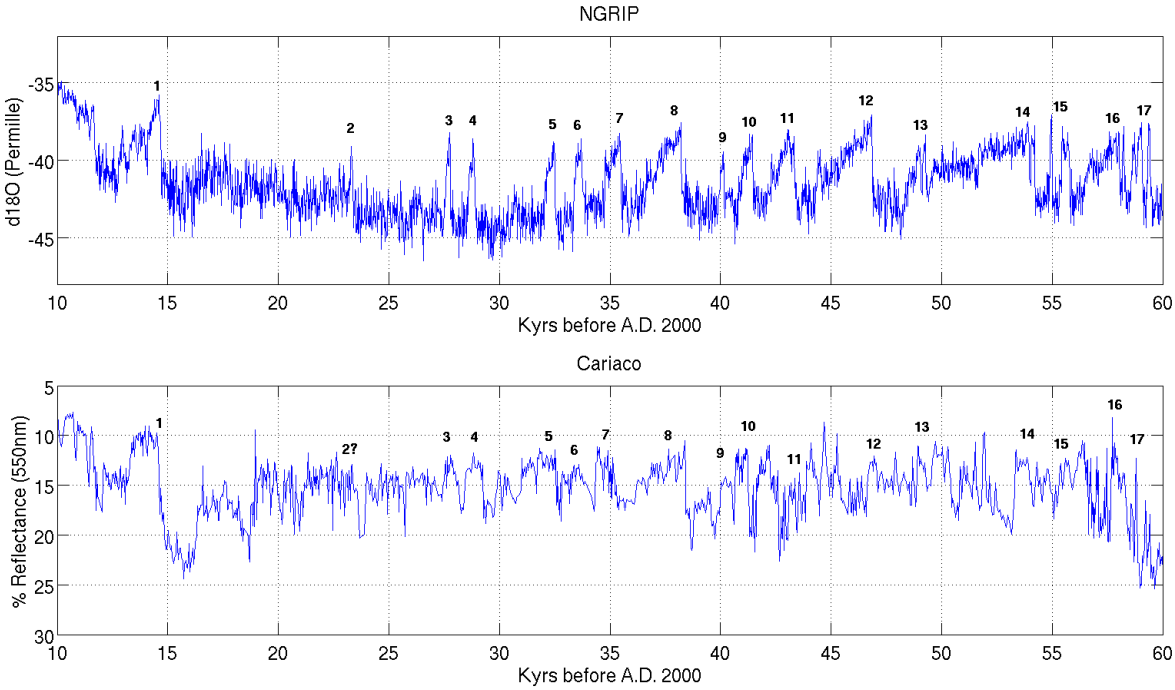

Figure 1.2: Paleoproxies from 10.000 to 60.000 years before A.D. 2000. a. Greenland temperatures as recorded by a stable oxygen isotope from the North GRIP ice core (Svensson et al., 2008) with 20 years resolution. D/O abrupt warm events are numbered. b. 550 nm (green wavelength) reflectance record from a sediment core in the Cariaco Basin (off Venezuela) (Peterson et al., 2000).

Paleorecords obtained in tropical South America and the surrounding Atlantic and Pacific oceans are among the best known. Peterson et al. (2000) analyse a sedimentary record for the last 90.000 years from the Cariaco Basin in the tropical Atlantic Ocean off the northern coast of Venezuela (Figure 1.2 b). The record reveals rapid changes in the hydrological cycle over land, considered to be associated to changes in the Atlantic ITCZ location, extremely well correlated with the Greenland temperature proxies during the Marine Isotope Stage 3 (59.000 - 29.000 years ago), within dating uncertainty: increased precipitation (northward ITCZ displacement) is associated with

warm Greenland events, and almost all the individual peaks in the data can be tied up with D/O events. Meanwhile, Wang et al. (2004) study a 210.000 years old record of wet periods in tropical northeastern Brazil from speleothem and travertine deposits. The find that the wet periods in their records, associated with a southward ITCZ shift, are synchronous with cold periods in Greenland, Heinrich events in the North Atlantic, periods of weak East Asian summer monsoon and periods of decreased river streamflow in the Cariaco Basin. In the Pacific Ocean, Koutavas and Lynch-Steiglitz (2004) study the marine ITCZ variability in the eastern portion of the basin for the last 30.000 years and find that it shifted southward when the NH was cooled by ice sheets at the Last Glacial Maximum (21.500 years ago).

In Asia, Wang et al. (2001) work with five stalagmites from the Hulu Cave in China (32ºN, 119ºE). The oxygen isotope records from Hulu bear a remarkable resemblance with oxygen isotope records from Greenland ice cores, for the period 11.000 - 75.000 years before the present, with individual events matched one for one with events in the Greenland D/O record. The authors find that there is a positive correlation between Greenland temperature and the ratio of summer to winter precipitation in eastern China and that, to the extent that changes in the ratio result from changes in summer precipitation, warmer Greenland temperatures are associated with a more intense summer East Asian Monsoon.

The general picture emerging from paleoclimatic evidence is that, within dating uncertainty, there is a synchronous behaviour between the high latitude North Atlantic Ocean temperatures and the tropical changes, being a rapid warming (cooling) of the North Atlantic associated with a northward (southward) displacement of the tropical precipitation. One of the possible questions to ask is: what triggers abrupt warming or cooling events in the high latitudes of the Atlantic Ocean? Changes to the strength of the Atlantic Meridional Overturning Circulation (AMOC) are often regarded as the main driver behind these events (Broecker et al., 1985).

The AMOC is characterized by a northward branch of warm and saline flow in the upper layers of the Atlantic Ocean together with a sinking region in the Greenland-Norwegian and Labrador seas and a southward branch of cold water flowing at depth (e.g., Bryden et al., 2005). This circulation transports heat from the South and tropical North Atlantic to the high latitudes of the North Atlantic Ocean, warming the climate there and in Europe. The AMOC presents multidecadal variability,

although there is no consensus on the physical mechanisms involved. Its low-frequency variability is usually associated with an anomalous northward heat transport in the upper Atlantic Ocean, which can affect the SST. Furthermore, modeling studies suggest that the SST signature of the AMOC resembles the observed Atlantic Multidecadal Oscillation (AMO; Zhang and Wang, 2013; see Figure 1.6): a strengthening of the AMOC favours a warm AMO phase.

The strongest evidence to associate the AMOC to global abrupt changes in climate comes from numerical simulations.

Vellinga and Wood (2002) produce a collapse of the AMOC in a coupled atmosphere-ocean model by applying a strong initial freshening to the top layers of the North Atlantic. Shortly after the salinity forcing is implemented global impacts are noticed: cooling of the entire NH (more pronounced in the North Atlantic) and a southward shift of the ITCZ over the Atlantic and eastern Pacific. Zhang and Delworth (2005) perform a similar experiment, with a different fully coupled model, confirm the results and further find a weakening signal over the Indian and Asian summer monsoons, consistent with the global synchronization suggested by paleorecords.

At that time a common hypothesis was that the communication of the extratropical signal was a pure oceanic teleconnection, mediated through altered ocean heat transports associated with the AMOC changes (for a review see Barreiro et al. 2008). However, studies analysing the relative roles of the atmosphere and the ocean in the global teleconnection pattern triggered by an extratropical forcing highlight that the main role is played by atmospheric-surface ocean processes. Chiang et al. (2008a) study the transient adjustment that follows an abrupt freshening of the North Atlantic and find that after an initial ocean baroclinic adjustment at the subtropical-subpolar gyre vicinity, the subsequent equatorward progression is materialized through evaporative cooling producing a southward ITCZ shift in 2 years from the initial perturbation. In the same direction, Liu and Yang (2003) asses the extratropical impact on the tropics quantifying the relative contributions from the atmospheric bridge and the oceanic tunnel by imposing an extratropical SST forcing in a coupled atmosphere-ocean model. They find that the impact on the tropical SST can be attributed mostly to atmospheric processes (70%). Although responsible for a minor part of the tropical SST response, the oceanic tunnel dominates the equatorial subsurface signal (80%). Barreiro and Philander (2008) find that an extratropical cloud reduction (which implies a decrease in the

planetary albedo), specially in the Southern Ocean, can impact the tropical climate producing a weakening of the cold tongues in the Pacific and Atlantic Oceans. They find that the atmospheric bridge plays the dominant role while the oceanic tunnel from the extratropics, on the other hand, tends to play a small role.

As a consequence, many recent studies have focused on the atmospheric bridge that connects an extratropical forcing with a tropical response. Chiang and Bitz (2005) and Broccoli et al. (2006) were among the first to propose such atmospheric mechanisms by performing experiments with AGCMs thermodynamically coupled to a motionless ocean (slab ocean model).

Chiang and Bitz (2005) impose an increase in the ice cover of the NH in an AGCM-slab ocean model and find that the marine ITCZ is shifted meridionally away from this hemisphere, altering the global Hadley circulation. This effect is found to be independent of the location of the imposed ice forcing. The authors propose that a subtropical wind-evaporation-SST (WES) positive feedback together with a marine ITCZ-SST feedback act as the main linkers of the high latitude forcing with the tropics. The subtropical WES mechanism is as follows: the NH ice increase cools and dries the atmosphere above it, cooling the entire high and mid latitudes by advection. Then, the associated surface pressure high (developed by hydrostatic adjustment in the atmospheric boundary layer; Biasutti et al., 2004) drives anomalous northeasterly winds which act to reinforce the prevailing trade winds, increasing evaporation and thus cooling the underlying SST, propagating the initial SST anomaly further south. Once the cold northern SST reaches the ITCZ latitudes the ITCZ-SST feedback is initiated: the meridional SST gradient induces surface pressure anomalies and an associated cross-equatorial flux, provoking a sourthward ITCZ shift and strengthened (weakened) northeasterlies (southeasterlies). Then, latent heat flux is increased to the north and decreased to the south, reinforcing the original SST gradient. The gradual southward ITCZ displacement produces changes in the Hadley circulation increasing the moisture transport to the warmer hemisphere, which becomes even warmer as a consequence of the greenhouse effect of water vapour. It is worth noting that, however, later studies by Kang et al. (2009) and Mahajan et al. (2011) demonstrated that the subtropical WES feedback is not fundamental in the extratropical to tropical teleconnection, as significant ITCZ displacements are still obtained even when disabling this mechanism.

On the other hand, Broccoli et al. (2006) impose equal and opposite extratropical thermal forcings

in a AGCM coupled to a slab ocean model and find results in agreement with Chiang and Bitz (2005): the ITCZ shifts towards the warmer hemisphere. They suggest that changes in the atmospheric transport by the altered Hadley circulation and transient and stationary eddies over the mid latitudes are the likely cause of the response, given the start point for an energy flux perspective on the extratropics to tropics teleconnection. Furthermore, Yoshimori and Broccoli (2008) argue that the ITCZ displacements are better correlated with the interhemispheric contrast in radiative forcing than with the interhemispheric temperature contrast.

The energy flux perspective was expanded as a diagnostic tool by Kang et al. (2008) and Kang et al. (2009) in a series of aquaplanet experiments with an AGCM coupled to a slab ocean model. Kang et al. (2008) find that when the northern extratropics are cooled and the southern extratropics are warmed the ITCZ shifts towards the warmer hemisphere and that this shift can be understood in terms of the degree of compensation between the imposed forcing and the resulting atmospheric energy transport in the tropics. They also highlight the role of cloud feedbacks. Kang et al. (2009) reexamine the aquaplanet simulations but using an AGCM without water vapour or cloud feedbacks. In this study they argue that the response of tropical atmospheric energy fluxes is determined primarily by the communication between the extratropics and the Hadley cell through eddy energy transport: an extratropical cooling results in an increased eddy energy transport into the cooled region, which acts to spread the cooling towards lower latitudes. When the cooling reaches the subtropics an anomalous Hadley circulation is developed, transporting energy to the cooler hemisphere. Since in a Hadley circulation moisture is transported in the opposite direction to energy, a positive moisture anomaly develops in the warmer hemisphere, shifting the ITCZ toward it. Schneider et al. (2014) build upon these studies analysing the ITCZ displacements from an energy flux perspective, and find an anticorrelation between the latitude of the ITCZ and the cross-equatorial atmospheric energy transport.

Recently, Cvijanovic and Chiang (2013) analyse the ITCZ response to a North Atlantic high latitude cooling applied to an AGCM coupled to a slab ocean, using realistic surface boundary conditions with special focus on the relative roles of tropical SST and energy flux changes. In idealized simulations with fixed tropical SST they find that the ITCZ shifts are not possible, therefore suggesting that the tropical SSTs are a more suitable driver of tropical precipitation shifts than the atmospheric energy fluxes.

In summary, paleoclimatic, 20th century observations and numerical evidence suggest that the extratropics have the ability to influence the tropical climate in a significant way. In particular, the generation of an interhemispheric thermal gradient has been suggested as one of the main triggers for tropical changes, with the ITCZ displacing toward the warmer hemisphere. Despite the fact that an energy framework has been developed linking ITCZ shifts to atmospheric energy constraints, a complete mechanistic view is still lacking.

1.3. Thesis objectives

The general objective of this thesis is to investigate the sensitivity of the tropical climate to an extratropical thermal forcing via a series of numerical simulations performed with an AGCM coupled to either a simple or a medium-complexity ocean model. The behaviour of two convergence zones, the ITCZ and the South Atlantic Convergence Zone (SACZ), is the main focus of the work. Changes in the intensity or position of these convergence zones play a major role in controlling the precipitation patterns in many countries. In particular, interannual and interdecadal variability of the ITCZ has resulted in prolonged periods of drought, with devastating societal and economic impacts, over northeastern Brazil (Hastenrath and Heller, 1977) and the African Sahel (Nicholson and Palao, 1993). Meanwhile, while SACZ' variability directly impacts the hydro-climate of the densely populated southeastern Brazil it also has indirect impacts over the climate of La Plata Basin, particularly over Uruguay (Vera et al., 2006).

Three specific objectives are highlighted. First, to quantify the relative roles played by the atmosphere, the tropical SSTs and the continental surface temperatures in the ITCZ response. Second, to investigate the SACZ response to an extratropical thermal forcing. Third, to estimate the role of the tropical ocean dynamics in transmitting the information from the extratropical to the tropical region.

To meet the first and second specific objectives we use the Abdus Salam International Centre for Theoretical Physics SPEEDY-ICTP AGCM (Molteni, 2003; Kucharski et al., 2006)

thermodynamically coupled to a motionless ocean model (slab ocean model). While the first objective intends to continue, and deepen, the line of work presented in Cvijanovic and Chiang (2013) the second objective points to investigate the impact of an extratropical forcing on a tropical feature different from the ITCZ (which has been the focus of most of the recent literature on the subject). For the third, and last, specific objective we perform a comparison between simulations in which the SPEEDY-ICTP AGCM is coupled to a global slab ocean model and simulations in which a Reduced Gravity Ocean (RGO) model is additionally coupled in the tropical oceans.

1.4. Inter Tropical Convergence Zone and South Atlantic Convergence Zone

This section provides a brief description of the main characteristics of the tropical precipitation features on which this thesis is focused: the ITCZ (primary focus over South America and the Atlantic Ocean sector and secondary focus over the Pacific Ocean) and the SACZ.

1.4.1. Inter Tropical Convergence Zone

The ITCZ can be defined in several ways, but here we will consider it as the narrow zonal belt of tropical deep convective clouds, below which lies the region that receives more annual precipitation on Earth (Figure 1.3). The belt shape of the tropical precipitation is generated as a consequence of the large-scale atmospheric circulation, in particular to the overturning Hadley circulation. The warm and moist trade winds converge near the surface, leading to ascension and subsequent cooling, condensation and precipitation. In the upper branch of the circulation the dry air masses diverge, flow away from the ITCZ and descend in the subtropics. To close the circulation this air returns to the ITCZ in the lower branch of the Hadley cell. This circulation in thermally direct, transporting energy from the low to the high latitudes, in the same direction as its upper branch.

Although the time-averaged solar radiation reaches its maximum precisely over the Equator, the ITCZ is not exactly symmetric relative to it. As a matter of fact, the tropical precipitation maximizes within the NH specially over the Atlantic and the eastern Pacific oceans where it migrates between 9°N in boreal summer and 2°N in austral summer (see Figure 1.4).

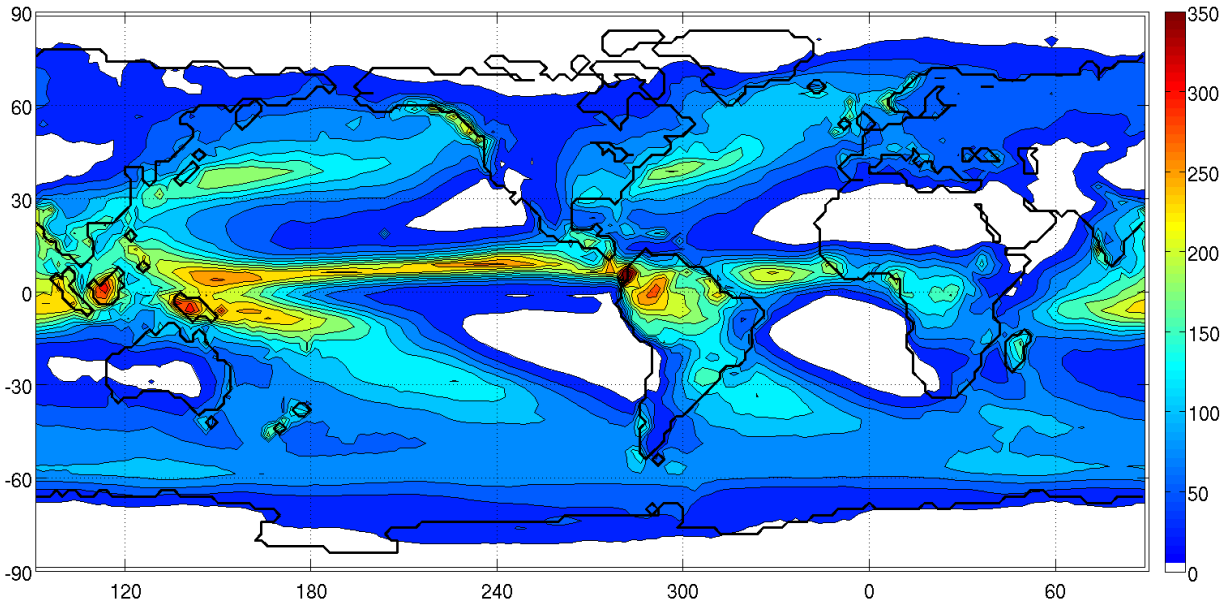

Figure 1.3: Annual mean precipitation. Data from GPCP (Adler et al., 2003) provided by the NOAA/OAR/ESRL for the period 1979-2014. Contour interval: 25 mm/month.

The distribution of global land masses and its induced asymmetric ocean temperature was one of the first mechanisms to be noted as a possible explanation for the northern skewness of the ITCZ (Philander et al., 1996). On the other hand, several studies have pointed out that the ITCZ hemispheric asymmetry is closely related to the hemispheric asymmetry in the atmospheric energy budget (Schneider et al., 2014): the ITCZ responds shifting towards the warmer hemisphere, being its mean position anticorrelated with the atmospheric energy transport. Frierson et al. (2013) calculate the top of the atmosphere (TOA) net radiation in each hemisphere and conclude that the SH receives slightly more net radiation that the NH, therefore, TOA radiation can not be the cause for the ITCZ skewness towards the north. In the present climate the NH is warmer than the SH and the main cause of that is northward heat transport exerted by the AMOC (Frierson et al., 2013). Thus, this reasoning suggests that the ITCZ mean position lies in the NH because it is warmer than the SH as a consequence of the northward heat transport in the Atlantic Ocean.

On interannual-decadal time scales, the ITCZ over the Atlantic Ocean presents variability correlated with the leading mode of SST variability: a dipole-like pattern with opposite signs at both sides of the Equator, termed the Atlantic gradient pattern. A warm north and cool south configuration is

associated with cross-equatorial surface winds (directed from the cool to the warm hemisphere), implying a northward displacement of the ITCZ (Chang et al., 1997). The mechanism behind this behaviour is based on the proposed by Lindzen and Nigam (1987): through hydrostatic adjustment (by differential heating of the boundary layer) a meridional SST gradient produces a sea level pressure gradient, generating a cross-equatorial flow (given the negligible effect of the Coriolis force). Chiang et al. (2002) confirm the former mechanism and note that the Atlantic ITCZ' sensitivity to this mode is extremely high compared, for example, with analogous SST gradients in the eastern Pacific. They explain this by stating that the SST anomalies in the eastern Pacific are symmetric about the Equator and, thus, do not trigger any pressure gradients; in the Atlantic, the asymmetry about the Equator allows for pressure gradients to generate, driving a significant cross-equatorial flow. Therefore, the theory indicates that important Atlantic ITCZ displacements can be initiated generating a tropical SST interhemispheric gradient.

1.4.2. South Atlantic Convergence Zone

The SACZ is a band of strong convective activity that extends in the NW-SE direction from the Amazon basin to the southeastern Atlantic Ocean whose peak season is the austral summer (December-February, DJF; Kodama, 1992; Marengo et al., 2010). Figure 1.5 displays the DJF precipitation mean for South America and the South Atlantic Ocean sector; the continental SACZ reaches 250 mm/month while the marine SACZ is slightly weaker with a maximum precipitation of 175 mm/month.

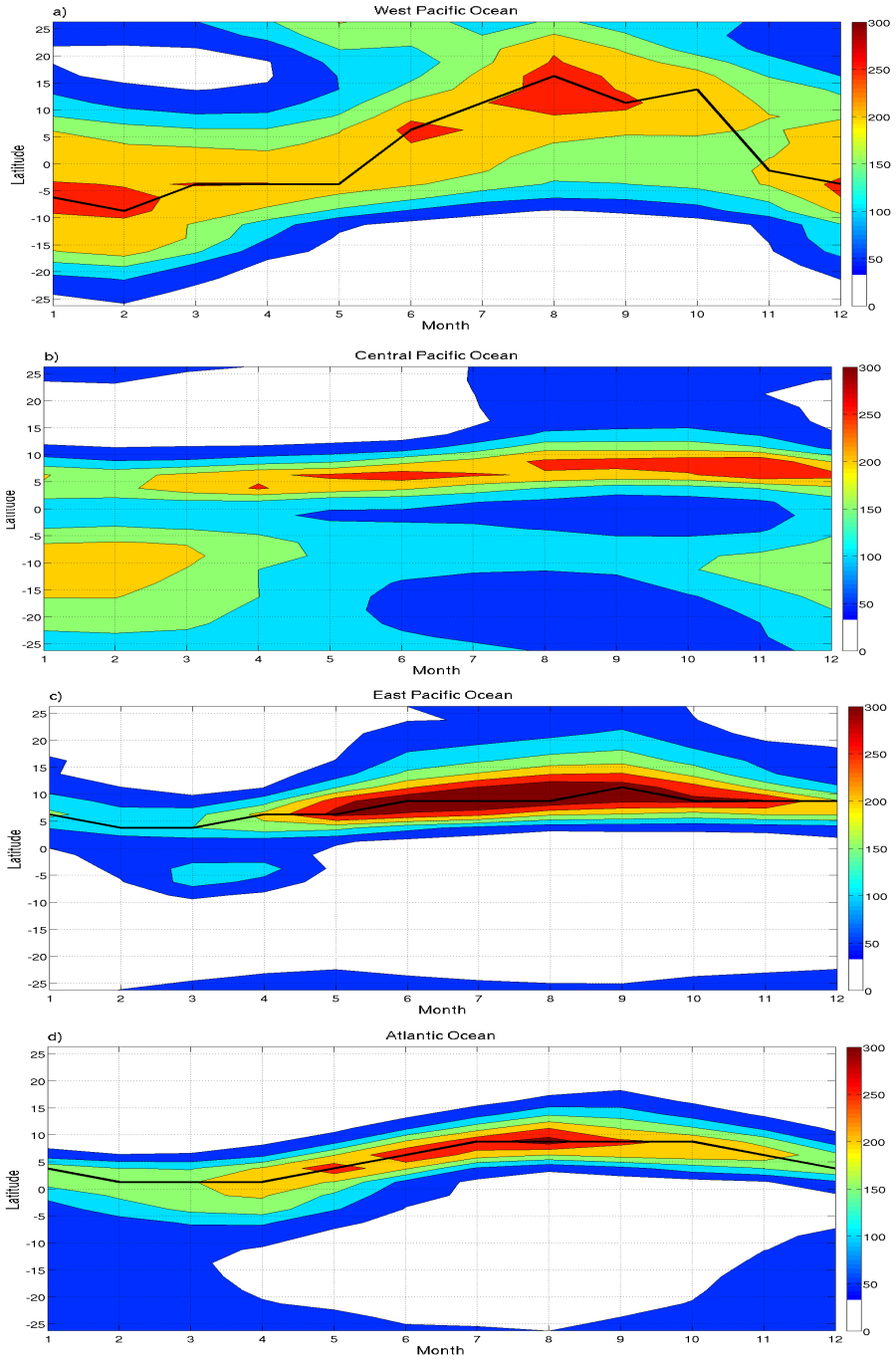

Figure 1.4: Time-latitude diagrams of seasonal cycle of ITCZ in different tropical regions. The black line indicates the estimation of the ITCZ position, except for the Central Pacific region. a. Western Pacific Ocean (110ºE-150ºE). b. Central Pacific Ocean (150ºE-220ºE). c. Eastern Pacific Ocean (220ºE-280ºE). d. Atlantic Ocean (310ºE-0ºE). Data from GPCP (Adler et al., 2003) provided by the NOAA/OAR/ESRL for the period 1979-2014. Contour interval: 50 mm/month.

Kodama (1993) finds that two conditions are necessary for the development of sub-tropical convergence zones (including the SACZ). First, a subtropical jet in the subtropical latitudes (30ºS-35ºS) and, second, a low-level poleward flow in the western boundary of the surrounding sub-tropical high. If the two former conditions are not quasi-stationarily satisfied, then, no or only weak precipitation develops in the subtropics. The low-level flow, indispensable for moisture convergence, is formed geostrophically between the subtropical high and a low pressure system developed by continental heating; this flow together with the subtropical jet produce a favourable configuration for frontogenesis and convective instability. In addition to these two ingredients, topography in central-east Brazil has proven to be fundamental for anchoring the SACZ in its present climatological location, as numerical simulations indicate that a southward SACZ shift will follow in the absence of these mountains (Grimm et al., 2007). In addition, Van der Wiel et al. (2016), although focusing on the South Pacific Convergence Zone, propose that the NW-SE diagonal orientation of the southern convergence zones is due to the zonally asymmetric component of the SST field. They argue that this SST component leads to stronger subtropical highs, enhancing the low level flow of moisture on its western flank.

A dipole-like pattern of variability in the SACZ and the South American Low Level Jet (SALLJ) has been identified in a broad range of time scales: from intra-seasonal (Nogués-Peagle and Mo, 1997) to inter-annual (Doyle and Barros, 2000), to centennial time scales (Talento and Barreiro 2012). Events with an intensification of the SACZ are associated with precipitation deficits over the subtropical plains of South America and a weak SALLJ.

Paleoclimatic evidence also points out that the SACZ presents variability on longer time-scales.

Stríkis et al. (2015) analyse speleothem records obtained from two caves in central-eastern Brazil and marine records from the western equatorial Atlantic. They recognize, at least, two events of widespread SACZ intensification (termed mega-SACZ; 18.1-16.66 kyears before present and 16.11-14.69 kyears before present) that occurred almost synchronously with Heinrich Stadial 1, a period characterized by massive depositions of ice-rafted debris in the North Atlantic Ocean and consequent cooling of the northern mid latitudes.

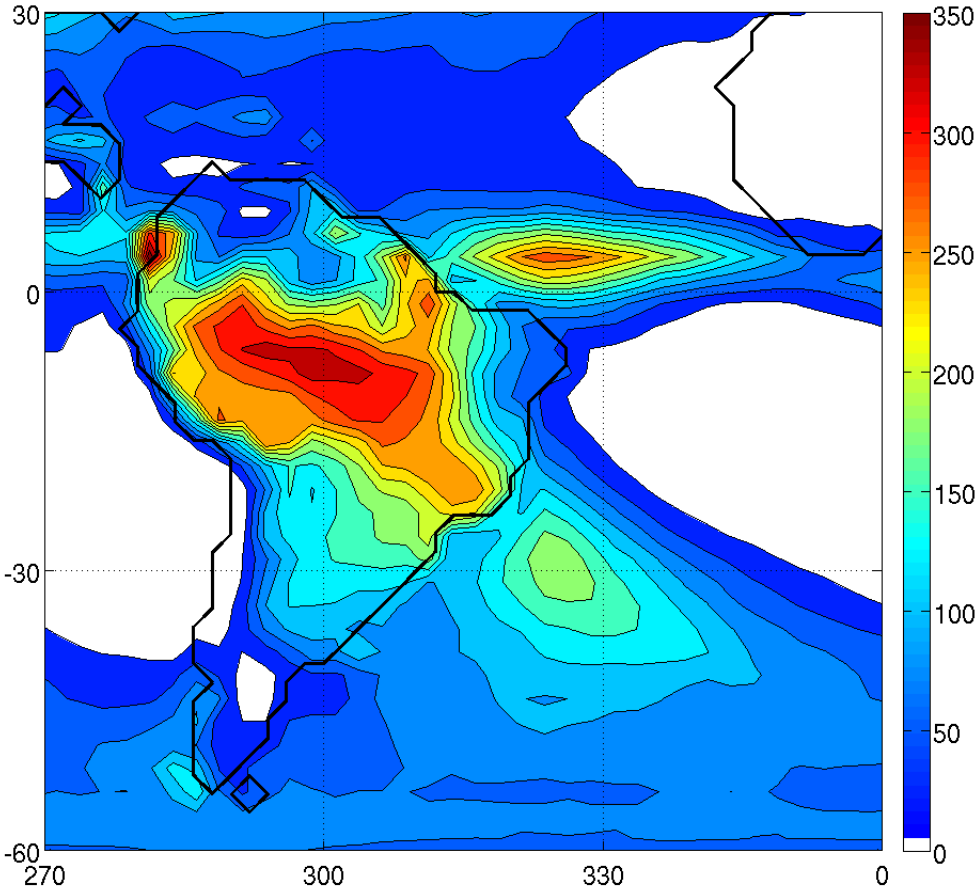

Figure 1.5: DJF mean precipitation in South America and the South Atlantic Ocean. Data from GPCP (Adler et al., 2003) provided by the NOAA/OAR/ESRL for the period 1979-2014. Contour interval: 25 mm/month.

Meanwhile, Chiessi et al. (2009) argue for the possible connection between the SACZ and the AMO. They use a 4500 years long marine sediment core from the western South Atlantic, indicative of the discharge variability in La Plata River Drainage Basin. The find a statistically significant oscillation with a period of 64 years and propose that this oscillation is associated with the AMO. They suggest that during periods of positive AMO (characterized by a widespread NH warming in the north Atlantic Ocean, see next section) a northward migration of the ITCZ and cooling of the western South Atlantic would lead to a decrease in the intensity of the SALLJ, producing a decrease in precipitation over La Plata Basin.

1.5. Atlantic Multidecadal Oscillation pattern

North Atlantic SST presents multidecadal (65-80 years) variability (Schlesinger and Ramankutty 1994; Delworth and Mann 2000). This mode has been termed the Atlantic Multidecadal Oscillation (AMO, Kerr, 2000) and is considered to be a natural mode of oscillation associated with fluctuations in the intensity of the thermohaline circulation in the North Atlantic (Delworth and Mann 2000).

A simple AMO index is defined as the SST anomaly in the North Atlantic Ocean (Equator-70ºN, 280ºE-0ºE) minus the global SST anomaly. The time series of this index as well as its regression pattern (obtained point by point by linearly regressing the AMO index against the local SST anomaly) are shown in Figure 1.6. Positive phases of the index occurred from the 30's to the 60's and from the year 2000 to the present. The spatial pattern depicts an hemispheric behaviour: generalized warming in the NH (with the largest magnitudes south of Greenland) and generalized cooling in the SH (with the largest magnitudes in the mid latitudes of the Atlantic Ocean). This north-south temperature contrast characteristic of the AMO SST pattern is the main inspiration for the extratropical thermal forcing used in the several numerical simulations performed in this thesis. The exact structure of the implemented forcing is described in each of the chapters (2-4).

1.6. Thesis outline

The remainder of this thesis is organized as follows. Chapters 2, 3 and 4 present the results organized as independent and self-contained entities. Chapter 2 details a paper entitled “Simulated sensitivity of the tropical climate to extratropical thermal forcing: Tropical SSTs and African land surface” as it appears in Talento and Barreiro (2015), published in Climate Dynamics. Chapter 3 is titled “Control of the South Atlantic Convergence Zone by extratropical thermal forcing” and comprises a manuscript currently under review (Talento and Barreiro, 2016). Chapter 4 “Sensitivity of the tropical climate to an interhemispheric thermal gradient: the role of ocean dynamics” is the basis for a manuscript in preparation for future publication. Finally, Chapter 5 presents the thesis summary and general conclusions.

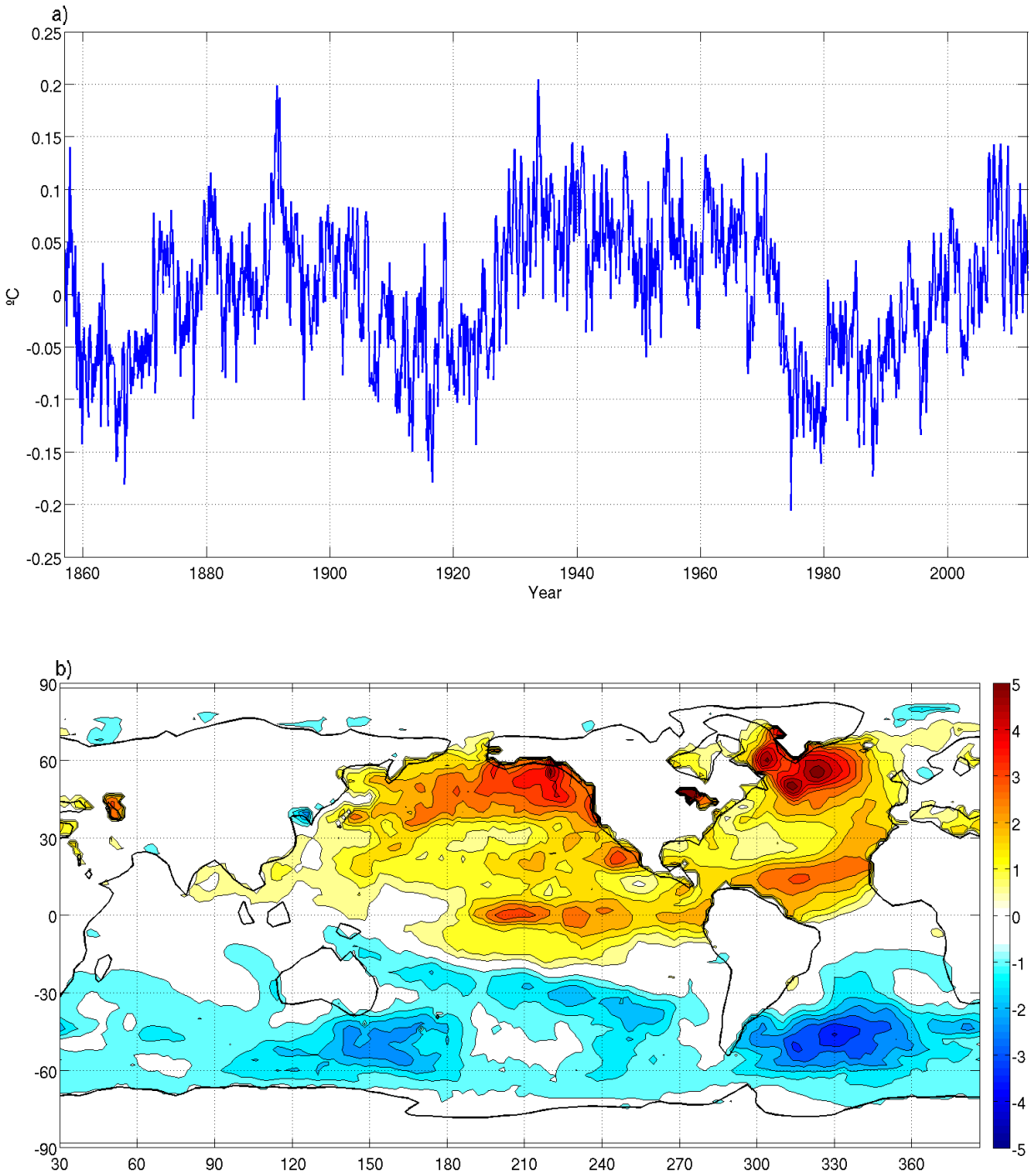

Figure 1.6: a. AMO index time series (°C). b. Regression of SST on AMO time series; contour interval: 0.5°C. Monthly data for the 1857-2013 period from NOAA_ERSST_V3 (Smith et al., 2008) at http://www.esrl.noaa.gov/psd/data

Chapter 2. Simulated sensitivity of the tropical climate to extratropical thermal forcing: Tropical SSTs and African land surface

Abstract

This study investigates the Intertropical Convergence Zone (ITCZ) response to extratropical thermal forcing applied to an atmospheric general circulation model (ICTP-AGCM) coupled to slab ocean and land models. We focus on the relative roles of the atmosphere, tropical sea surface temperatures (SSTs) and continental surface temperatures in the ITCZ response to the imposed forcing.

The forcing consists of cooling in one hemisphere and warming in the other poleward of 40°, with zero global average. Three sets of experiments are performed: in the first the slab ocean and land models are applied globally; in the second the tropical SSTs are kept fixed while the slab land model is applied globally; in the third, in addition, surface temperatures over Africa are kept fixed. Realistic boundary surface conditions are used.

We find that the ITCZ shifts towards the warmer hemisphere and that the stronger the forcing, the larger the shift. When the constraint of fixed tropical SST is imposed we find that the ITCZ response is strongly weakened, but it is still not negligible in particular over the Atlantic Ocean and Africa where the precipitation anomalies are of the order of 20% and 60%, respectively, of the magnitude obtained without the SST restriction. Finally, when the constraint of the African surface temperature is incorporated we find that the ITCZ response completely vanishes, indicating that the ITCZ response to the extratropical forcing is not possible just trough purely atmospheric processes, but needs the involvement of either the tropical SST or the continental surface temperatures. The clear-sky longwave radiation feedback is highlighted as the main physical mechanism operating

behind the land-based extratropical to tropical communication.

2.1. Introduction

Paleoclimatic studies and 20th century observations suggest that the extratropics have the capability to affect the tropical climate through the development of, both, atmospheric and oceanic teleconnections.

Paleoclimatic studies indicate that, for example, the marine Inter Tropical Convergence Zone (ITCZ) in the eastern Pacific Ocean shifts toward the south when the Northern Hemisphere (NH) is cooled by ice during maximal covering in glacial periods (Koutavas and Lynch-Stieglitz, 2004). In addition, evidence obtained in the Cariaco basin in the Caribbean Sea shows that changes in this region might be strongly correlated with high latitude climate, during the last glacial period and Holocene (Peterson et al., 2000; Hughen et al., 2000). Meanwhile, Wang et al. (2004) analyse records of the last 210 kyrs and find that wet periods in northeast Brazil, associated with a southward displacement of the ITCZ, may be synchronized with cold periods in Greenland and Heinrich events in the North Atlantic.

Regarding the 20th century climate, Folland et al. (1986) found that a sea surface temperature (SST) pattern characterized by an interhemispheric thermal gradient could be a possible driver to decadal droughts in the Sahel region and Giannini et al. (2003) were able to reproduce the Sahel precipitation variability prescribing the observed 20th century SST to an AGCM, In particular, a configuration of a cooler NH and a warmer Southern Hemisphere (SH) was associated with a period of Sahel drought starting in the late 1960s.

At the same time, numerical studies show that the tropical climate can be affected in several ways by anomalous conditions in the extratropics: abrupt descent of salinity in the North Atlantic, warming of surface oceanic waters in high latitudes, changes in clouds in high latitudes or extratropical thermal forcings.

The tropical effect of abrupt descents of salinity in the North Atlantic has been studied with focus on two aspects of the ocean dynamics: the thermohaline circulation (Manabe and Stouffer, 1995; Rahmstorf, 1995; Vellinga and Woods, 2002; Stouffer et al., 2006) and the wind-driven circulation (Gu and Philander, 1997; Boccaletti et al., 2004; Sun et al., 2004; Barreiro et al., 2008). Both circulations weaken in response to a decrease in the salinity levels and, as a consequence, there is a decrease in the heat transport toward the north as well as an ITCZ displacement to the SH.

The impact of increased SSTs in high latitudes has been analysed, for example, by Liu and Yang (2003) and Yang and Liu (2005). These authors find that the tropical SST response corresponds with half of the SST change imposed in the extratropical forcing region. In addition, they propose that the impact over the tropical SST is obtained through contributions from both the atmosphere and the ocean, being the contributions 70% and 30%, respectively. On the other hand, they suggest that the main influence comes from the SH, where the ocean/land proportion is higher.

Barreiro and Philander (2008) analyse the impact of the reduction of cloud cover in high latitudes. They conclude that such a change in the planetary albedo can lead to an extratropical and tropical warming and that the cold tongues in the Pacific and Atlantic oceans are weakened. They highlight that the temporal scale for the adjustment to the perturbation in the tropical Pacific can be considered in the range of rapid climate change, as it is of decades to centuries. Furthermore, Burls and Fedorov (2014) deepen on the idea that extratropical cloud cover can have an impact in the tropical regions and demonstrate that there is a near-linear relationship between the meridional gradient in cloud albedo between the tropics and mid-latitudes and the mean zonal SST gradient in the equatorial Pacific.

There are several works highlighting the impact an extratropical thermal forcing (materialized either by changes in the ice cover or by imposed heat fluxes) may have on the tropical climate. Simulations with either atmospheric or coupled models, in aquaplanet mode or with realistic surface boundary conditions, have all shown to shift the position of the ITCZ to the anomalously warm hemisphere.

Chiang and Bitz (2005) study the high latitude imposed ice influence on the marine ITCZ in an

atmospheric general circulation model (AGCM) coupled to a slab ocean model. They find that the ITCZ shifts in all the basins meridionally away from the hemisphere with the imposed ice cover. They propose that the imposed cooling is communicated to the tropics by a subtropical Wind-Evaporation-SST (WES) feedback: the anomalous ice induces a cooling and drying of the air and surface over high and mid latitudes, further progression of the cold anomalies occur in the Pacific and Atlantic northeasterly trade wind regions, where the WES feedback initiates progression of the cold SST to the tropical region.

Kang et al. (2008) and Kang et al. (2009) study the response of the ITCZ to an antisymmetric interhemispheric heat flux with zero global average, in an AGCM coupled to a slab ocean model in aquaplanet mode. They conclude that the ITCZ shifts toward the warmer hemisphere, that the magnitude of the shift increases with the amplitude of the forcing and that the tropical behaviour could be strongly dependent on the model convection scheme and cloud feedbacks. In particular, Kang et al. (2009) showed that the WES feedback is not fundamental as they performed simulations without this feedback and the ITCZ is still displaced to the warmer hemisphere. Schneider et al. (2014) build upon these studies analyzing the ITCZ displacements from an energy flux perspective, and find an anticorrelation between the latitude of the ITCZ and the cross-equatorial atmospheric energy transport.

Recently, Cvijanovic and Chiang (2013) analyse the ITCZ response to a North Atlantic high latitude cooling applied to an AGCM coupled to a slab ocean, using realistic surface boundary conditions focusing on the relative roles of tropical SST and energy flux changes (see also Chiang and Friedman, 2012). They argue that the ITCZ shifts are not possible without the tropical SST changes, therefore suggesting that the tropical SSTs are a more suitable driver of tropical precipitation shifts than the atmospheric energy fluxes.

In this study we examine the ITCZ response to an extratropical thermal forcing applied to an AGCM coupled to slab ocean and land models. In comparison with previous studies our simulations are performed with realistic surface boundary conditions, the extratropical forcing pattern consists of warming in one hemisphere and cooling in the other with zero global mean and the effect of the intensity of the forcing is investigated. In that sense this work can be seen as a continuation of that of Cvijanovic and Chiang (2013). Furthermore, the relative roles played by the atmosphere, the

tropical SSTs and the continental surface temperatures in the ITCZ response are investigated in a series of experiments designed to separate these influences. In the first series the slab ocean and land models are applied globally. In the second series, the tropical SST role is investigated through simulations in which the slab land model is applied globally while in the ocean the tropical SSTs are maintained fixed, applying the slab ocean model elsewhere. In this second series we will show that the ITCZ response does not completely vanish if the tropical SSTs are not allowed to change, in particular, over Africa and the Atlantic Ocean. This motivates the third series of experiments in which the role of the surface temperature over Africa is analysed by incorporating the constraint of fixed continental surface temperature over that continent. As will be shown, the role of the African land surface temperature (LST) is essential for maintaining the ITCZ response when the tropical SSTs are fixed and, therefore, the last part of this paper investigates the physical mechanisms connecting the extratropical signal to the continental surface temperatures over Africa, via a last experiment in which the clear-sky longwave radiation process is switched off.

The chapter is organized as follows: In Section 2.2 we introduce the model and the experiments. Results are presented in Sections 2.3, 2.4, 2.5 and 2.6. In Section 2.3 we present the experiments where the slab ocean and land models are applied globally. In Section 2.4 we analyse the role of the tropical SST. In section 2.5 the role of the African surface temperature is studied, while the physical mechanisms connecting the extratropical signal with the African surface temperatures are discussed in Section 2.6. Finally, in Section 2.7 we summarize the conclusions.

2.2. Model and experiments

The model used in this study is the Abdus Salam International Centre for Theoretical Physics (ICTP) AGCM (Molteni, 2003; Kucharski et al., 2006), which is a full atmospheric model with simplified physics. We use the version 41 of the model in its 8-layer configuration and T30 (3.75^{o}x3.75^{o}) horizontal resolution. Over ocean and land slab models are coupled. Present-day boundary surface conditions, orbital parameters and greenhouse forcing are used. In addition, a monthly-varying ocean heat flux correction is imposed in order to keep the simulated SST close to present-day conditions.

We design experiments in order to study the response of the ITCZ to extratropical thermal forcing, considering increasing intensity of the forcing.

The applied forcing pattern consists in cooling in one hemisphere and warming in the other poleward of 40°, applied only over ocean grid points, and with a resulting global average forcing equal to zero. This pattern is similar to the one used in Kang et al. (2008) and it is intended to represent the asymmetric temperature changes associated with glacial-interglacial and millennial-scale climate variability. The forcing pattern is superposed to a background state and is obtained as explained in the following paragraphs.

Let θ denote latitude, ψ longitude and lsm the land surface mask i.e. lsm=1 over land, lsm=0 over sea.

Consider h to be:

$$h(\theta,\psi) = -A\sin\left(\frac{\theta + 40}{50}\pi\right) * (1 - lsm(\theta,\psi)) \quad \text{for} \quad \theta \in [-90,-40]$$

$$h(\theta,\psi) = 0 \quad \text{for} \quad \theta \in [-40,40]$$

$$h(\theta,\psi) = -A\sin\left(\frac{\theta - 40}{50}\pi\right) * (1 - lsm(\theta,\psi)) \quad \text{for} \quad \theta \in [40,90]$$

where A (W/m^2) denotes the intensity of the forcing.

Then, let h_{SH} and h_{NH} be the integral of h over the SH and NH, respectively:

$$h_{SH} = \int_{\psi=0}^{\psi=2\pi} \int_{\theta=-\pi/2}^{\theta=0} h(\theta,\psi)\, d\theta\, d\psi$$

$$h_{NH} = \int_{\psi=0}^{\psi=2\pi} \int_{\theta=0}^{\theta=\pi/2} h(\theta,\psi)\, d\theta\, d\psi$$

Finally, the applied forcing pattern H is defined as:

$$H(\theta,\psi)=h(\theta,\psi) \quad \text{for} \quad \theta\in[-90,-40]$$

$$H(\theta,\psi)=0 \quad \text{for} \quad \theta\in[-40,40]$$

$$H(\theta,\psi)=\frac{-h_{SH}}{h_{NH}}*h(\theta,\psi) \quad \text{for} \quad \theta\in[40,90]$$

We consider values of A ranging from 0 to 35, every 5 W/m^2. A=0 denotes the control cases, as no forcing is applied. In Figure 2.1 we show the applied forcing pattern for the value of A=35 W/m^2. The sign convention selected is positive out of sea. Therefore, positive values of the forcing could be thought as representing a situation where the atmosphere is dry and colder than the ocean below it.

To analyse the relative roles of of the atmosphere, tropical SSTs and LSTs in the response to the imposed forcing we perform 3 series of experiments. For each experiment setup there is a control run (A=0) as well as perturbed runs (A different from zero). In the first series the slab ocean is applied globally. In the second series, the tropical (30ºS-30ºN) SSTs are kept fixed, while the slab ocean is applied elsewhere. In these first two experiments the slab land model is applied globally. Finally, in the third series the tropical (30ºS-30ºN) SSTs are kept fixed, the slab ocean model is applied elsewhere in the ocean and, also, the continental surface temperature over the African continent is kept fixed. In the experiments with fixed tropical SST, the prescribed tropical SSTs are the ones obtained in the control run with the global application of the slab ocean model. In the experiments with fixed surface temperature over Africa, the prescribed temperatures are the climatological temperatures of the land model. The experiments are named *global_slabs_A*, *fix_trop_SST_A* and *fix_trop_SST_fix_Africa_A*, respectively, with A denoting the strength of the forcing (varies from 0 to 35 W/m^2, every 5 W/m^2).

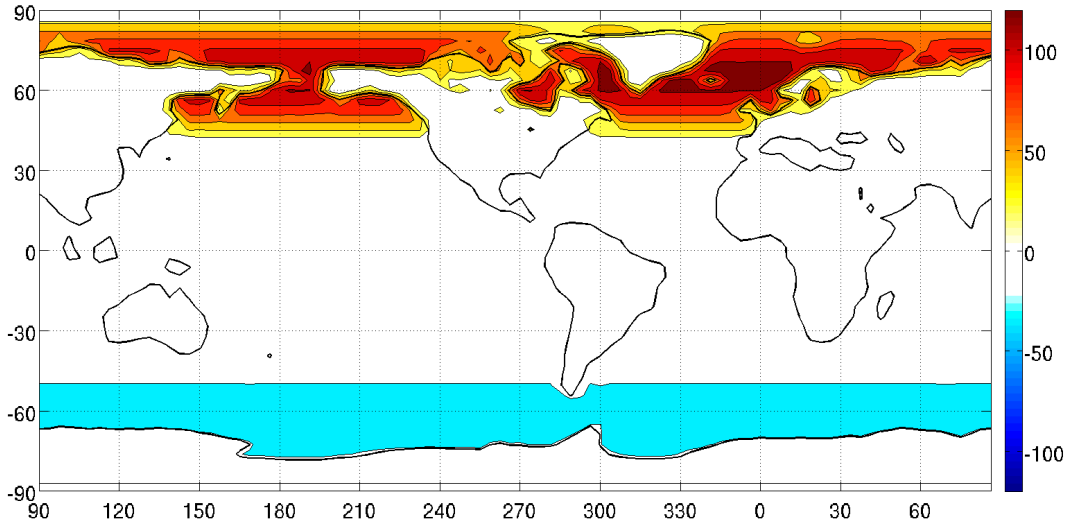

Figure 2.1: Forcing pattern H, for A=35 W/m^2 . The sign convention is positive out of sea. Contour interval: 20 W/m^2.

Moreover, we perform a fourth experiment to elucidate the mechanisms responsibles for the African LST reaction to the extratropical forcing. This experiment is a variation of *fix_trop_SST_A* experiment in which, in addition to the tropical SSTs constraint we incorporate the restriction of fixed clear-sky longwave radiation (see Section 2.6). The experiment name is *fix_trop_SST_fix_cslw_A.* As with all the other experiments, a corresponding control case (A=0) is calculated with this experiment configuration.

In all the simulations the model was run for 40 years and the last 10 are used for averaging. Running the simulations for 40 years proved to be more than enough to reach the equilibrium; a time scale of 10 years was estimated to be the time span necessary for adjustment (see Figure 2.14). In Table 2.1 we summarize the four series of experiments.

Table 2.1: Experiment summary. A denotes the strength of the forcing (varies from 0 to 35 W/m^2, every 5 W/m^2).

Experiment name	**Tropical SST fixed**	**Africa surface temperature fixed**	**Clear-sky longwave effect fixed**
global_slabs_A	No	No	No
fix_trop_SST_A	Yes	No	No
fix_trop_SST_fix_Africa_A	Yes	Yes	No
fix_trop_SST_fix_cslw_A	Yes	No	Yes

2.3. Tropical sensitivity to extratropical forcing

In this section we present the results of the experiment where the slab ocean and land models are applied globally: *global_slabs_A*. First we analyse the precipitation response to variations in the parameter A. Second, we focus on the case with maximal strength of the forcing (A=35 W/m^2) showing for different fields latitude–longitude, as well as zonal averages–height plots. These results are presented in the form of anomalies with respect to the associated control case (i.e. deviations of the forced run from the run with A=0 and the same experiment configuration). Lastly, we show the meridional atmospheric energy transport.

In Figure 2.2 we display the annual mean zonal averages of the precipitation anomalies for different values of the parameter A distinguishing total, oceanic and continental precipitation. Overall, the stronger the forcing the stronger the response in the zonal averages of the precipitation field. For total precipitation (Figure 2.2 a) the strongest responses are seen in the tropical region as well as in the northern high latitudes. In the tropics there are positive (negative) anomalies north (south) of 5ºN, indicating a northward shift of the ITCZ. In this region, both the intensity as well as the meridional position of the maximum anomalies change with A: as A increases so does the magnitude of the anomalies and the meridional shift of the ITCZ is largest. It is worth noting that in this region the intensity of the response is not linear, showing a very weak signal for A=5 W/m^2. In

high latitudes of the NH the anomalies are positive and with increasing magnitude as A increases. For this region the changes in the parameter A influence the intensity of the response but not the meridional pattern of the zonally averaged anomalies. Decomposing the total precipitation into oceanic and continental components we see that the general behaviour is very similar: increasing A leads to an increase in the magnitude of the anomalies and, in the tropical region, also to a slight change in the meridional position of the maximum anomalies.

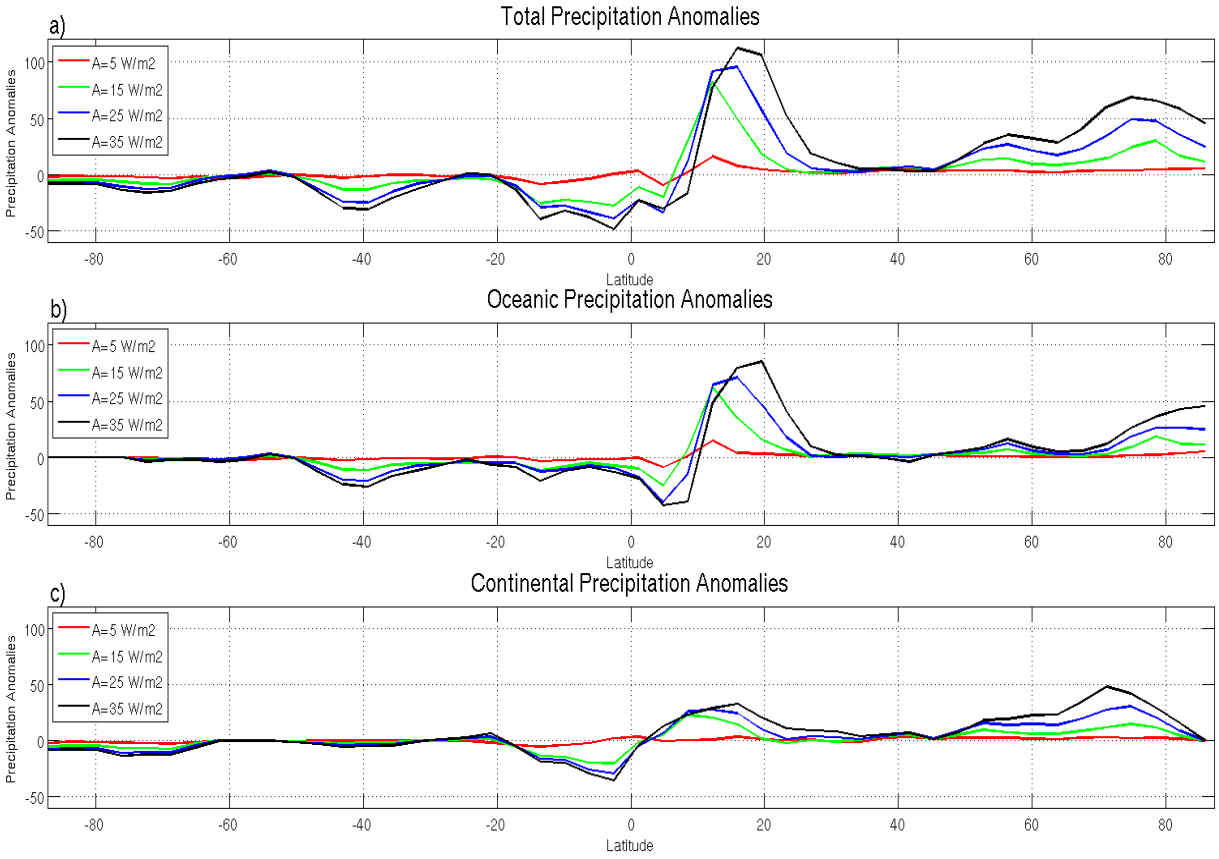

Figure 2.2: Annual mean zonal averages of: a. Total precipitation anomalies b. Oceanic precipitation anomalies c. Continental precipitation anomalies for several values of the parameter A and for the experiment with global slab ocean and land models: global_slabs_A. Units: mm/month.

In the following we will focus on the results for the maximal strength of the forcing A=35 W/m^2.

Near-surface air temperature (NSAT) anomalies are displayed in Figure 2.3 a. The response is a generalized warming in the NH and a generalized cooling in the SH, with the intensity of the

warming/cooling largest towards high latitudes. Maximum warming is about 17ºC in the northern Atlantic while the maximum cooling can be found in the Southern Ocean with a value of -14ºC in the Amundsen Sea. The NSAT anomalies in extratropics are quasi zonally symmetric. In the tropical region the main departures from the zonal symmetry can be found in the regions 20ºN-30ºN and 20ºS-30ºS in the Pacific Ocean where the zonal gradient is about 6ºC and 4ºC, respectively.

Over land the most extreme NSAT anomalies are seen over North America (up to 16ºC) and over Antarctica (around -8ºC). In latitudes lower than 30º the land response is most visible over the NH where the most extreme response is seen over the African continent (anomalies up to 10ºC centered at 25ºN, 30ºE), followed by the responses over North America (up to 5ºC anomalies) and Asia (up to 3ºC); in the SH low latitudes the signal is evident only over the Australian continent with negative anomalies of magnitude of the order of 1ºC.

Precipitation anomalies are shown in Figure 2.3 b. In the tropical Pacific and Atlantic oceans there is an increase (decrease) of precipitation north (south) of ~10ºN, indicating a northward shift of the oceanic ITCZ, consistent with Figure 2.2. The increase/decrease of precipitation is maximal toward the centre of the Pacific Ocean where it reaches ~350 mm/month. In the Indian Ocean there is no clear shift of the precipitation pattern. Continental precipitation is also affected, although in a weaker manner. A continental ITCZ displacement is also evident over both the African and the South American continents, with anomalies around 100mm/month over Africa and 200mm/month over South America. Extratropical precipitation changes are only important northward of 50ºN (positive anomalies) and to the west of South America around 45ºS (negative anomalies).

Near surface (950 hPa) wind anomalies are important only over ocean basins, in particular in the tropical Pacific and Atlantic Oceans, consistent with the ITCZ shift, and between 45ºS and 60ºS (Figure 2.4 a). In the tropical Pacific the anomalies are located between 5ºN and 20ºN, exceeding the 10 m/s in the centre of the basin and with north-east direction. In the Atlantic the anomalies are located in the band 5ºN-15ºN being of importance (around 9 m/s) toward the west of the basin. Finally, in the Southern Ocean there is a band of westerly anomalies between 45ºS and 60ºS with intensities that range from 7 m/s to a maximum over 10 m/s in the region 190ºE-240ºE.

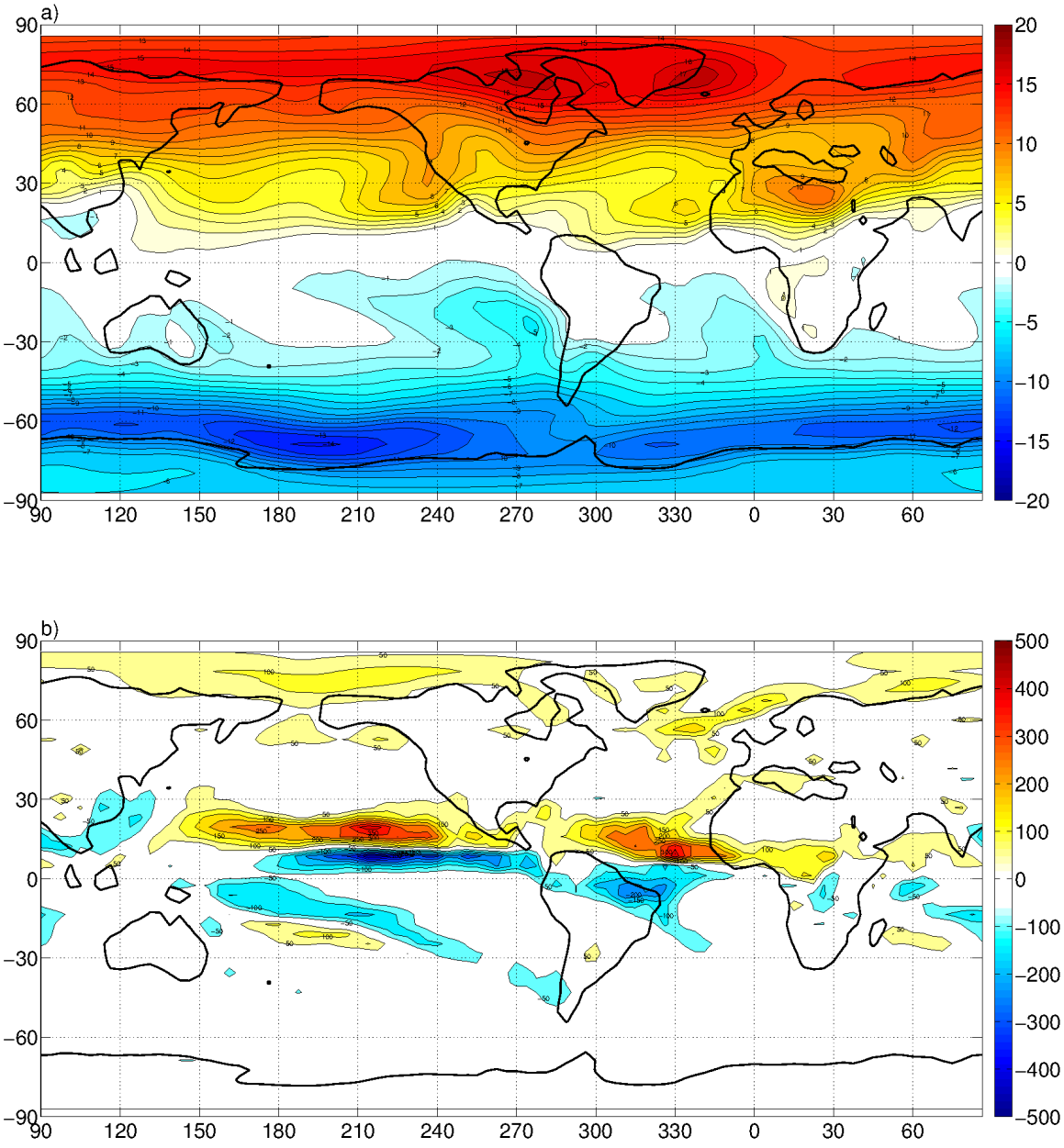

Figure 2.3: Annual mean anomalies with respect to the control of: a. NSAT (contour interval: 1ºC) b. Precipitation (contour interval: 50 mm/month) for the experiment with global slab ocean and land models and A=35 W/m^2: *global_slabs_35*.

In upper levels the anomalous wind field shows easterly anomalies from 30ºS until 60ºN and westerly anomalies from 40ºS until 60ºS (Figure 2.4 b). The strongest anomalies are found in the region Equator-30ºN and represent a weakening of the subtropical jet, consistent with a decrease in

meridional temperature gradient. Thus, wind anomalies in the tropics are baroclinic and result from the change in the distribution of latent heat release due to the ITCZ shift. In the SH extratropics, on the other hand, the wind anomalies have a barotropic structure.

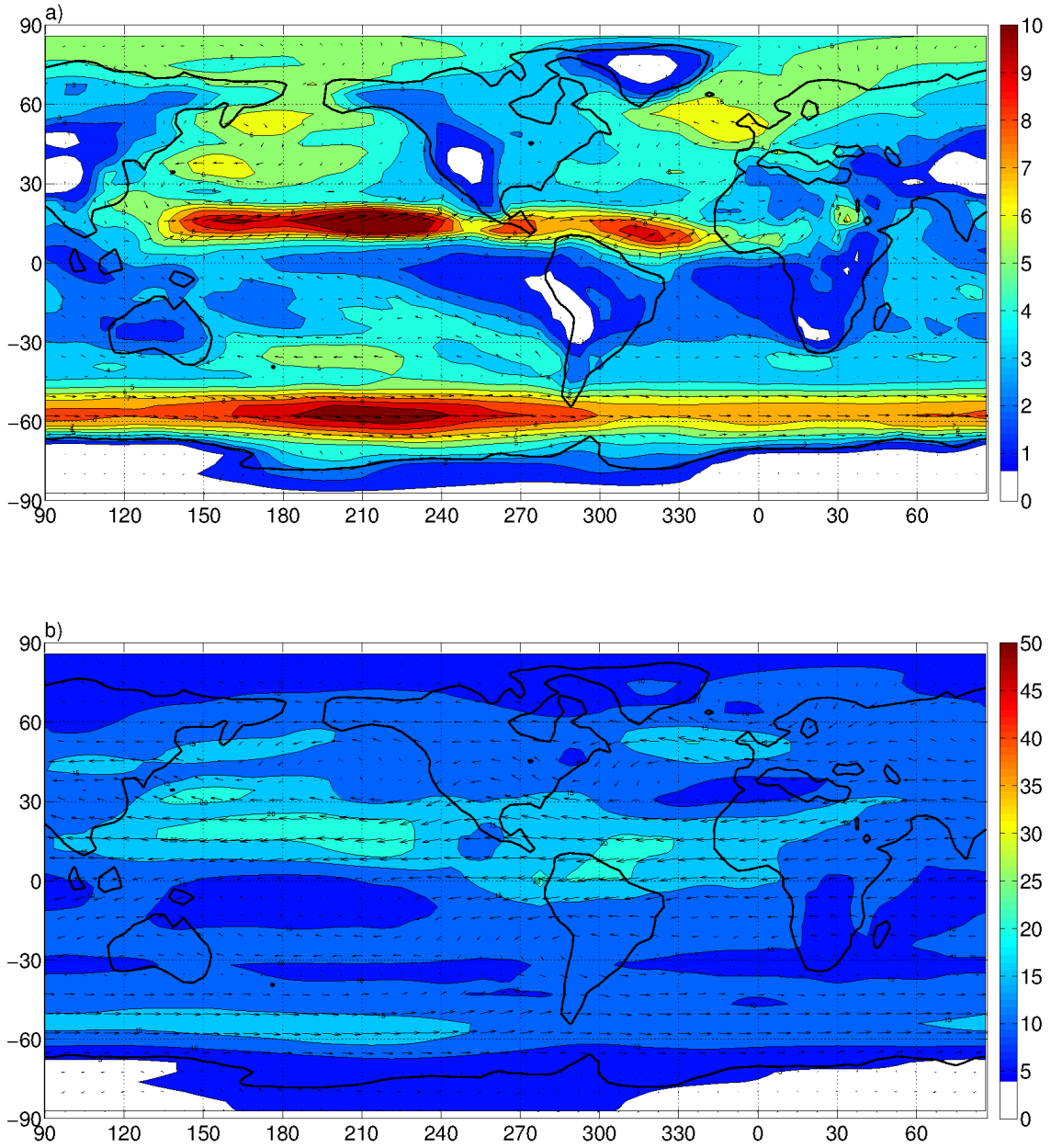

Figure 2.4: Annual mean anomalies with respect to the control of: a. wind at 950 hPa (arrows indicate wind direction, colors indicate wind magnitude, contour interval: 1m/s) b. wind at 200hPa (arrows indicate wind direction, colors indicate wind magnitude, contour interval: 5m/s) for the experiment with global slab ocean and land models and A=35 W/m^2: *global_slabs_35*.

Next we show zonal averages, which will be denoted by square brackets. Temporal means will be denoted by an over bar and deviations from the temporal mean by primes.

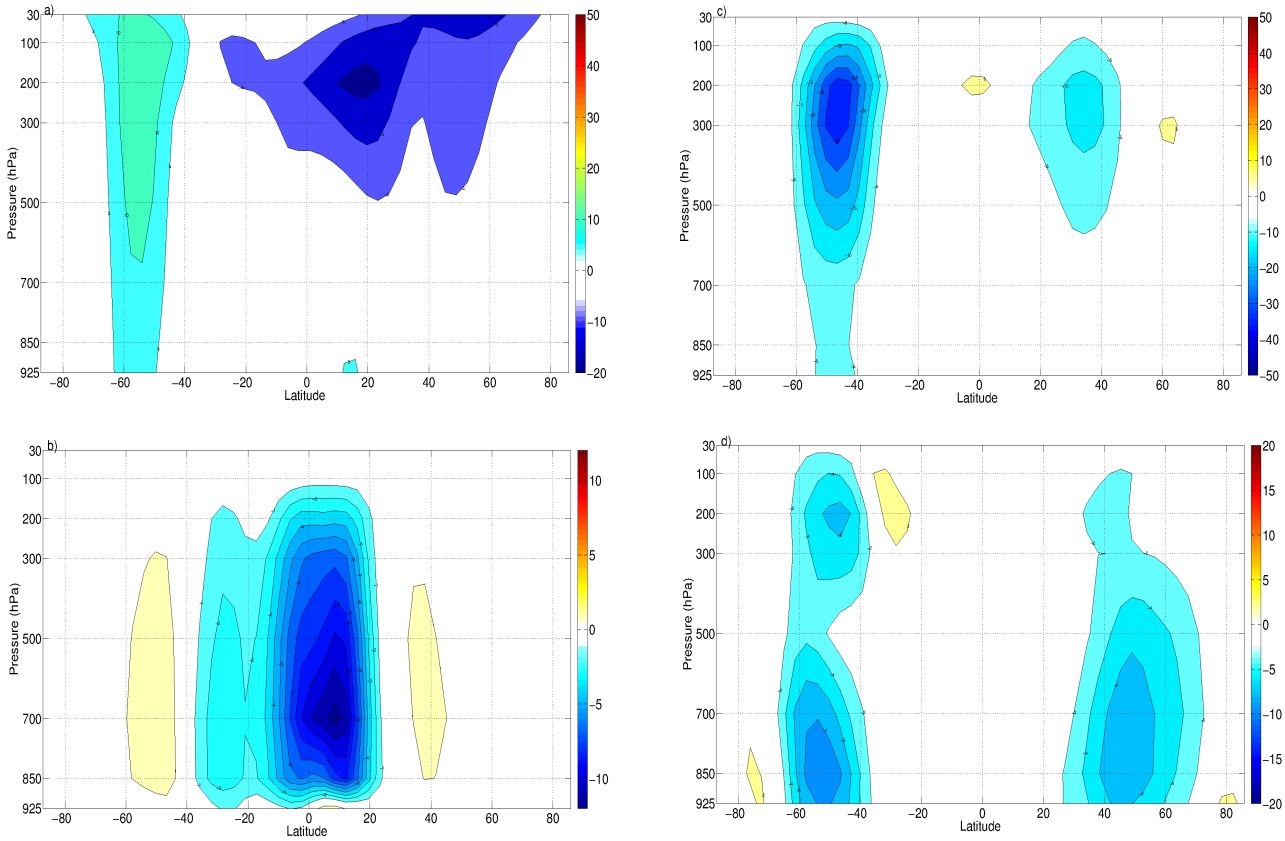

Figure 2.5: Annual mean anomalies with respect to the control of: a. Zonally averaged zonal wind with height [ū] (contour interval: 5 m/s) b. Mean Meridional Overturning Circulation Stream Function $[\overline{\Psi_M}]$ / 10^{10} (contour interval: 1 kg/s) c. Mean Meridional Momentum Transport by eddies $[\overline{u'v'}]$ (contour interval: 5 m^2/s^2) d. Mean Meridional Heat Transport by eddies $[\overline{v'T'}]$ (contour interval: 2 mK/s) for the experiment with global slab ocean and land models and A=35 W/m^2, *global_slabs_A.*

Figure 2.5 a displays anomalies with respect to the control run of the zonally averaged zonal wind ([ū]). There are two distinct anomaly patterns. The first one is a region of positive anomalies located in the latitude band 60ºS-40ºS with a clear barotropic structure and a maximum of 12 m/s located near the 200 hPa level between 60ºS-50ºS. The second one is a region of negative anomalies that comprises the latitudes 10ºS-80ºN upward from the 500 hPa level, with a maximum of 15 m/s at

20ºN and 200 hPa.

To get insight into the mean meridional circulation it is useful to consider the mass streamfunction Ψ_M defined as (e.g. Hartmann 1994): $\Psi_M = \frac{2\pi a \cos(\theta)}{g} \int_0^p [v] dp$ where a is Earth's radius, θ the latitude, g gravity, p pressure and v meridional wind. In Figure 2.5 b we present the changes with respect to control of the mean meridional overturning circulation stream function $[\overline{\Psi_M}]$. Negative anomalies in the tropical region indicate a northward displacement of the uplift region along with an intensification of the southern Hadley cell and a weakening of the northern Hadley cell. Although much weaker there is also a response in the Ferrel cells: the southern cell is intensified and the northern cell weakened.

Anomalies of meridional momentum transport performed by eddies $([\overline{u'v'}])$ are only of importance above 700 hPa and mostly negative, with one maximum in each hemisphere (Figure 2.5 c). In the SH the anomalies are maximum between 60ºS and 40ºS with magnitudes that exceed the 30 m^2/s^2, while in the NH the maximum anomalies are weaker and located closer to the Equator (between 40ºN and 30ºN) with a maximum of 10 m^2/s^2. These negative anomalies imply an intensification (weakening) of the transport from the tropics to high latitudes in the SH (NH). In addition, it is worth noting that such fluxes drive a poleward intensification of the zonal flow in the SH: as (e.g. Holton 2004) $\frac{du}{dt} \alpha - \frac{d\overline{[u'v']}}{dy}$ in the case shown by Figure 2.5 c, the meridional gradient of $[\overline{u'v'}]$ is positive (negative) on the equatorward (poleward) side of the minimum centered at (50ºS, 250 hPa), forcing a poleward shift of the mid-latitude jet in the SH. The latitude of strengthening of the mid-latitude jet coincides with the latitude of maximum SST gradient anomaly (50ºS-60ºS) consistent with the driving role of the lower atmosphere temperature gradient in the behaviour of the jet (e.g. Lorenz and Hartmann, 2001).

In Figure 2.5 d we show the anomalies of the meridional heat transport by eddies $([\overline{v'T'}])$. The anomalies are fundamentally negative, maximal in the latitude bands 60ºS-40ºS and 40ºN-60ºN close to surface and also at the jet level. The SH anomaly is stronger than the northern counterpart. As was the case with momentum transport, these negative anomalies imply an intensification

(weakening) of the eddy heat transport form the tropics to high latitudes in the SH (NH).

Finally, Figure 2.6 a displays the meridional atmospheric energy transport for the control case and the experiment with A=35 W/m^2. As previous studies have shown (e.g. Schneider et al, 2014) the energy flux equator is displaced northward in the forced case, as the atmospheric transport diminishes (increases) towards the NH (SH).

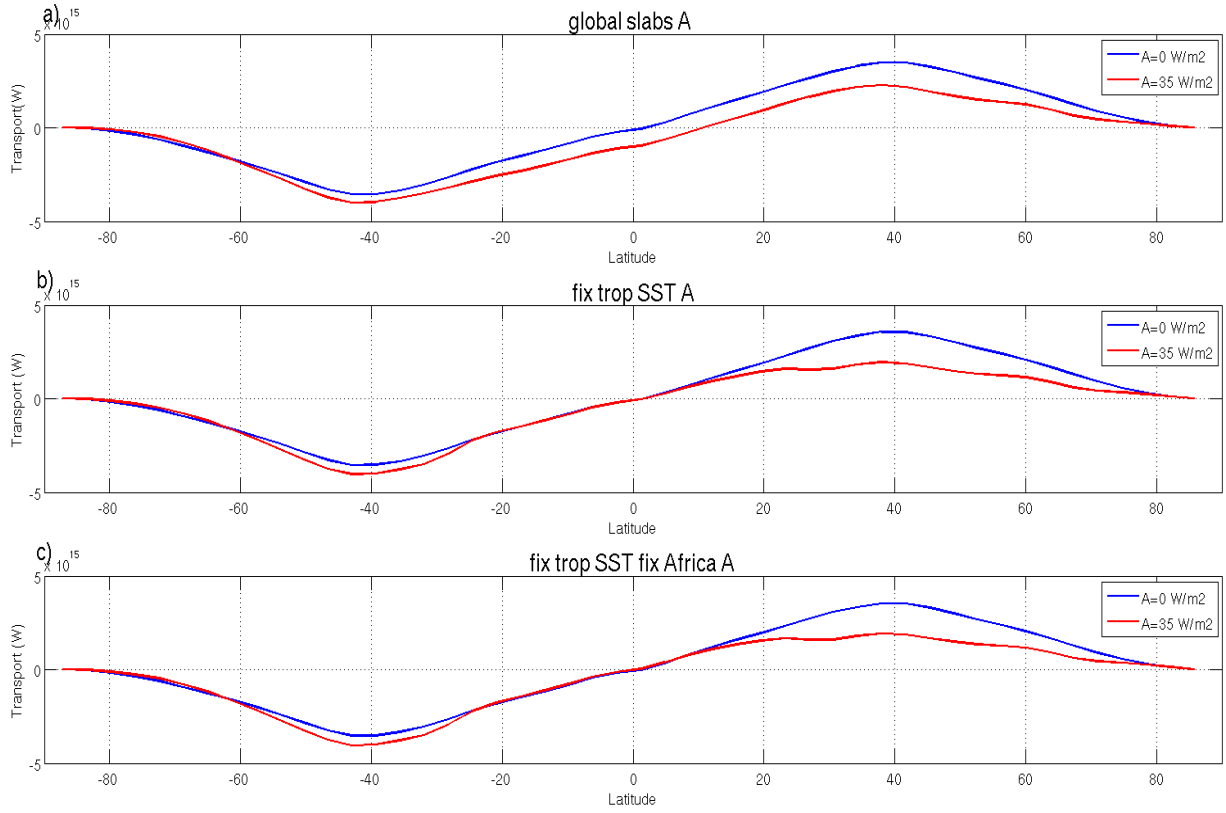

Figure 2.6: Northward atmospheric energy transport for the experiments: a. *global_slabs_A*, *b. fix_trop_SST_A and c. fix_trop_SST_fix_Africa_A for* A=0 (control cases) and A=35 W/m^2.

2.4. Role of the tropical SST

In this section we present the results of the experiment where the tropical SST are kept fixed and the slab ocean model is applied elsewhere, the land model is applied globally: *fix_trop_SST_A*. The anomalies are calculated with respect to the associated control case. Again, we start by analysing the dependence of zonal precipitation anomalies on the intensity of the forcing. We then focus the

analysis on the case with the maximum forcing, A=35 W/m^2.

Figure 2.7 shows the annual mean zonal averages of the precipitation anomalies (distinguishing total, oceanic and continental precipitation) for the experiment *fix_trop_SST_A* for different values of A. For the total precipitation field the most important anomalies occur in high latitudes of the NH. In this region, the stronger the forcing the stronger the positive precipitation anomalies and no meridional changes in the anomalous response are evident with the increase of A. The mechanism behind this behaviour is possibly related to the increase in specific humidity due to the warming of the region (not shown). Meanwhile, in the tropics the response is much weaker than that obtained for the experiments with global slab ocean and land models, although the signal is not null. We should note that close to the Equator there is a weak positive (negative) anomaly north (south) of 5ºN, that could indicate a timid response of the ITCZ, slightly shifting to the north. The decomposition of total precipitation into oceanic and continental indicates that both components present the stronger response in the NH high latitudes (both with positive anomalies increasing in magnitude with A); in the tropical sector the oceanic precipitation displays weak negative anomalies from the Equator to 10ºN while in the continental part some positive and also weak anomalies are seen from 10ºN to 20ºN.

As increasing the intensity of the forcing pattern mainly led to an increase in the response we will now only analyse more in detail the response for the maximal strength of the forcing A=35 W/m^2.

NSAT anomalies are depicted in Figure 2.8 a. Evidently, anomalies over sea in the tropics are zero given that the prescribed SST for that region coincides with the SST of the corresponding control case. Over the oceans the anomalies are positive (negative) in the northern (southern) extratropics, with increasing absolute magnitude toward the poles. For both hemispheres the anomalies over sea are very close to being zonally symmetric although there are some asymmetries in the Southern Ocean and to the west of the North American continent.

As was the case with the experiment *global_slabs_A* there is a generalized continental warming (cooling) in the NH (SH). In extratropics the response is very similar to the one obtained in the previous experiment (compare Figures 2.3 a and 2.8 a). However, some differences are seen in

particular with the extent of the continental warming in the region equatorward of 30ºN: in Asia now the warming only reaches 1ºC, in North America 3ºC and in Africa 8ºC, hence, indicating a 2ºC lower response than in the experiment with the global slab ocean model.

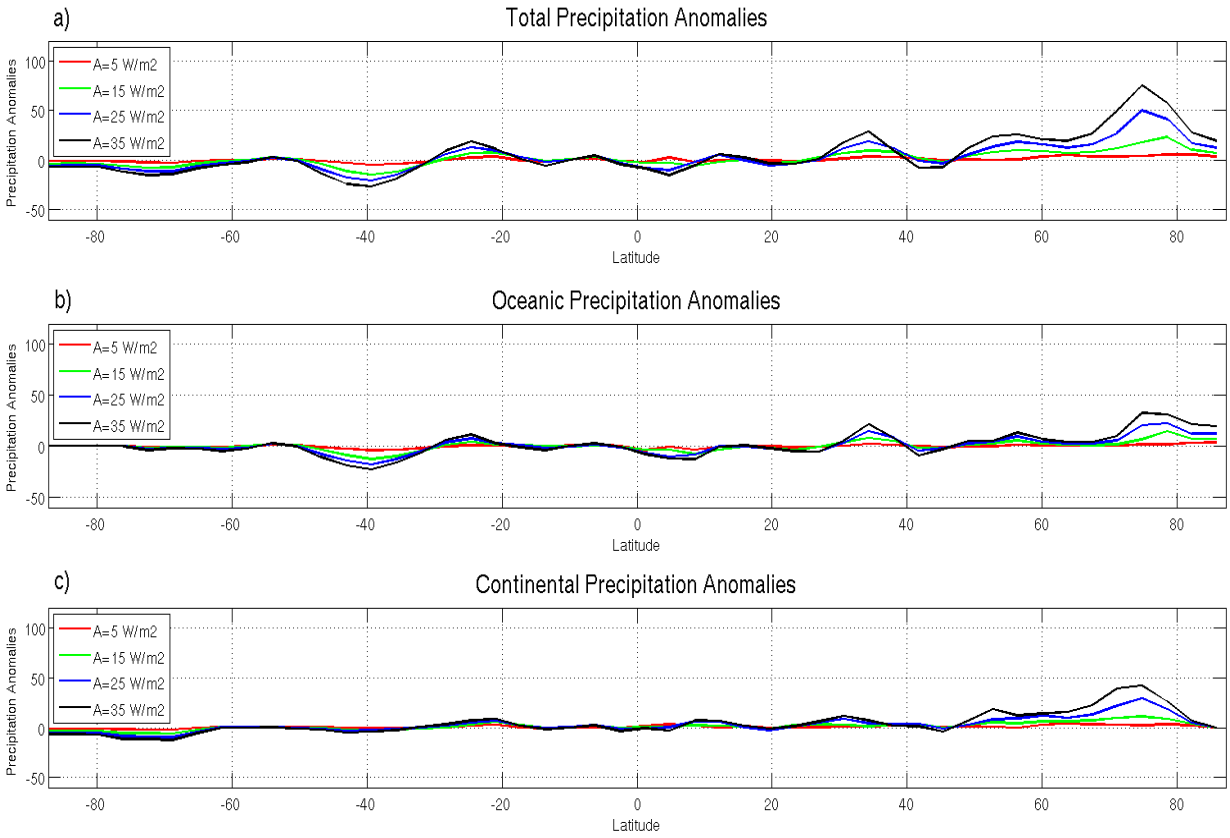

Figure 2.7: Same as Figure 2.2 for the experiment with fixed tropical SST, global slab land: *fix_trop_SST_A.*

Precipitation anomalies in extratropics are very similar to the ones obtained when the tropical SST restriction was not imposed (Figure 2.8 c). On the other hand, the tropical response is very different: the only place where there are signs of a northern shift in the ITCZ is over equatorial western Africa and over the Atlantic Ocean, with anomalies of the order of 50 mm/month. To better quantify the changes in precipitation we select three tropical precipitation indices: precipitation anomalies over the Sahel (8°N-15°N, 350°E-30°E), precipitation anomalies over the tropical Atlantic Ocean (5°N-12°N, 322°E-341°E; considering northern half minus southern half) and precipitation anomalies over South America (10°S-Eq, 300°E-322°E). Figure 2.9 indicates the regions considered. In Table

2.2 we calculate the values of those indices for the experiment *fix_trop_SST_35* relative to the same indices for the experiment *global_slabs_35*. We see that over Africa the response in the experiments with fixed tropical SST represents more than half (58%) of the response obtained when the slab ocean model is applied globally, indicating that for this region the tropical SSTs are important but not crucial in determining changes of precipitation forced by an extratropical source. On the other hand, over the Atlantic Ocean and South America the response in the experiments with restricted tropical SST has a magnitude of 19% and 13%, respectively, of the response obtained without such restriction, therefore indicating that for these regions the role of the tropical SSTs is much more important.

As expected, tropical surface and upper level wind anomalies in this experiment are practically null (Figures 2.10 a and 2.10 b), with the exception of some southwesterly surface anomalies over east Africa in the latitude band Equator-15ºN. The extratropical anomalies are very similar in structure to those obtained when the slab ocean model is applied globally, although in upper levels in the NH a slight weakening of the mid-latitude jet can be appreciated.

Figure 2.11 a shows the zonally averaged zonal wind ($[\bar{u}]$) anomalies with respect to the corresponding control run. Once again, the main difference with the experiment applying the slab ocean model globally is that the tropical anomalies almost vanish. In extratropics, the SH barotropic and positive anomaly pattern is still present showing an increase in the mid latitude jet; in the NH extratropics the negative anomaly is slightly stronger and evidences the weakening of the jet.

Regarding the mean meridional circulation changes, seen through $[\overline{\Psi_M}]$ anomalies, it is evident that the Hadley circulation is almost not affected with the tropical SST constraint imposed in this experiment (Figure 2.11 b).

The eddy meridional momentum and heat fluxes are displayed in Figures 2.11 c and 2.11 d, respectively. In both transports there is a subtle weakening of the transport from the tropics to the Poles, with respect to the experiment with global slab ocean model application.

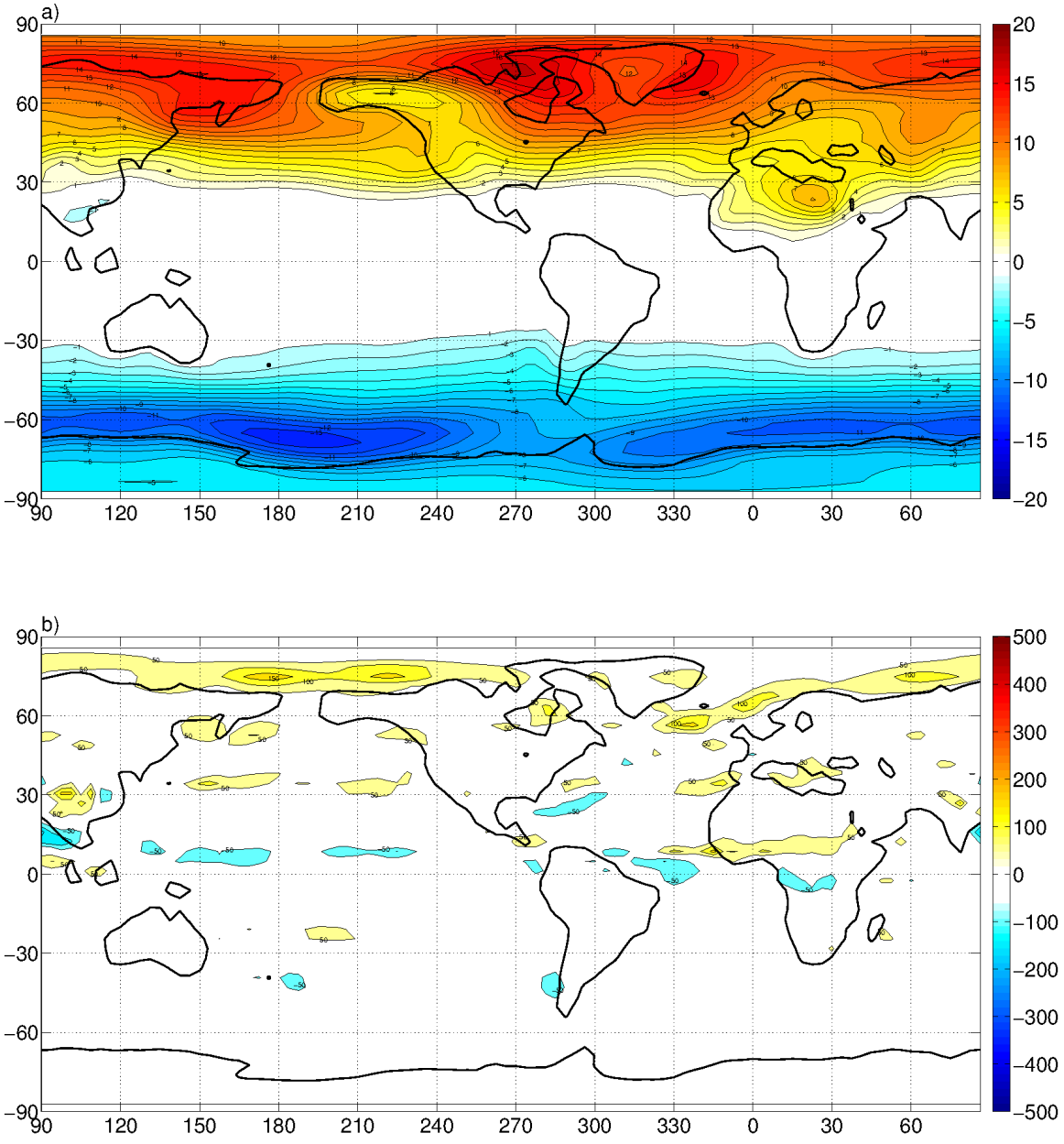

Figure 2.8: Same as Figure 2.3 for the experiment with fixed tropical SST, global slab land: *fix_trop_SST_35* except that the control run is the one corresponding to this experiment setup.

The meridional atmospheric energy transport for this experiment is shown in Figure 2.6 b. On the contrary of what occurred in the experiments global_slabs_A, the energy flux equator does not show any appreciable displacement from the control case when the forcing is applied, consistent with the fact that the ITCZ shifts are negligible when averaged zonally.

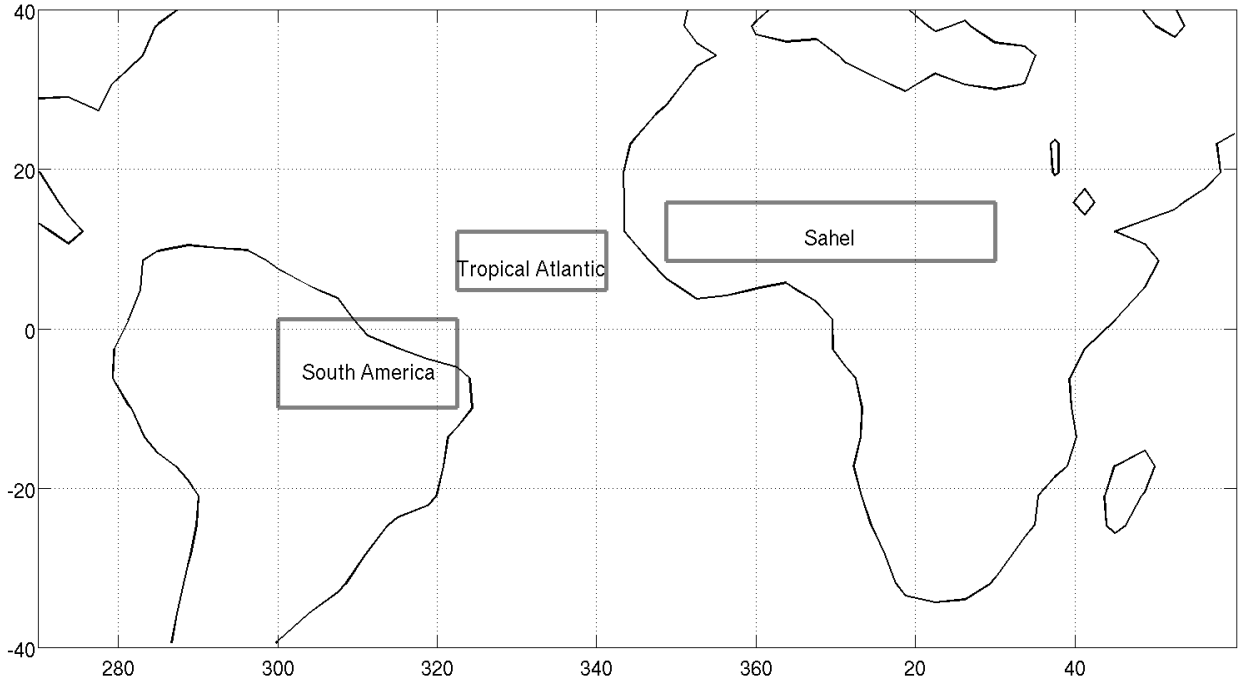

Figure 2.9: Regions where the precipitation indices are calculated: Sahel (8°N-15°N, 350°E-30°E), Tropical Atlantic (5°N-12°N, 322°E-341°E) and South America (10°S-Eq, 300°E-322°E).

Bearing in mind the precipitation anomalies shown in Figure 2.8 b, which shows that the main tropical response to the extratropical forcing when the tropical SSTs are kept fixed and A=35 W/m^2 is a northern shift in the ITCZ over western Africa and the Atlantic Ocean, in Figure 2.12 we restrict the view to that tropical sector (300ºE-30ºE) and show the total, oceanic and continental zonal mean precipitation variations with the parameter A in that region. For this restricted tropical sector we clearly see that the ITCZ response seen for the case of maximal strength of the forcing is still present for lower values of A. The ITCZ response consists in a northward displacement, increasing in magnitude with the strength of the forcing and is mostly due to the continental precipitation signal.

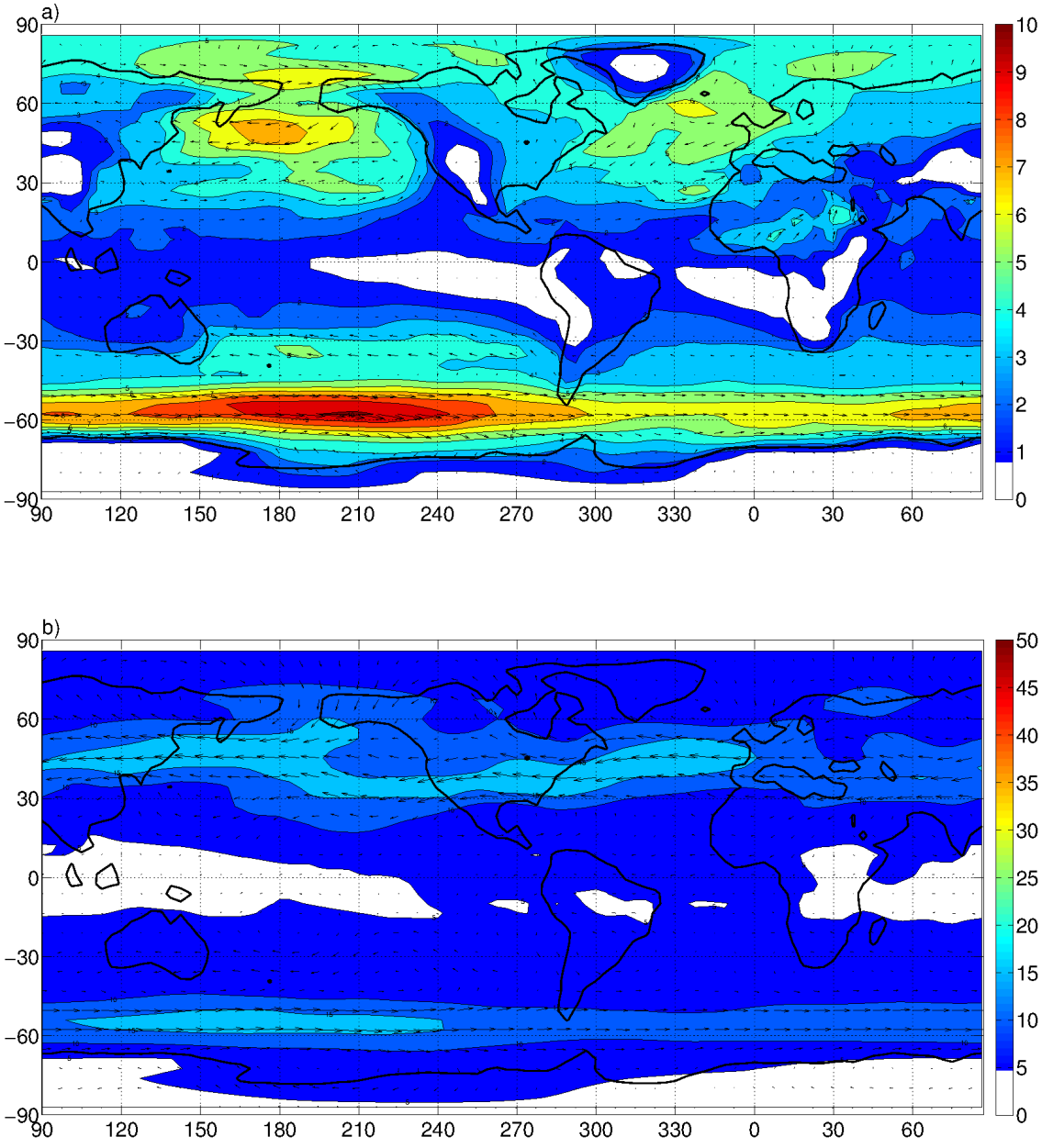

Figure 2.10: Same as Figure 2.4 for the experiment with fixed tropical SST, global slab land: *fix_trop_SST_35* except that the control run is the one corresponding to this experiment setup.

In summary, from the results of this sub section, we can conclude that when the extratropical forcing is applied and the tropical SST is not allowed to react in consequence, the tropical precipitation response is weak but still not negligible, specially over Africa and the Atlantic Ocean

where the ITCZ shows a northward displacement which increases its magnitude with the strength of the forcing. This tropical response is more important over the continent than over the ocean and seems related to the fact that the surface temperature over the African continent is greatly affected by the forcing while the SSTs are maintained fixed. With this motivation, in the next section we show the results for a series of experiments where, in addition, the surface temperature over Africa is kept fixed.

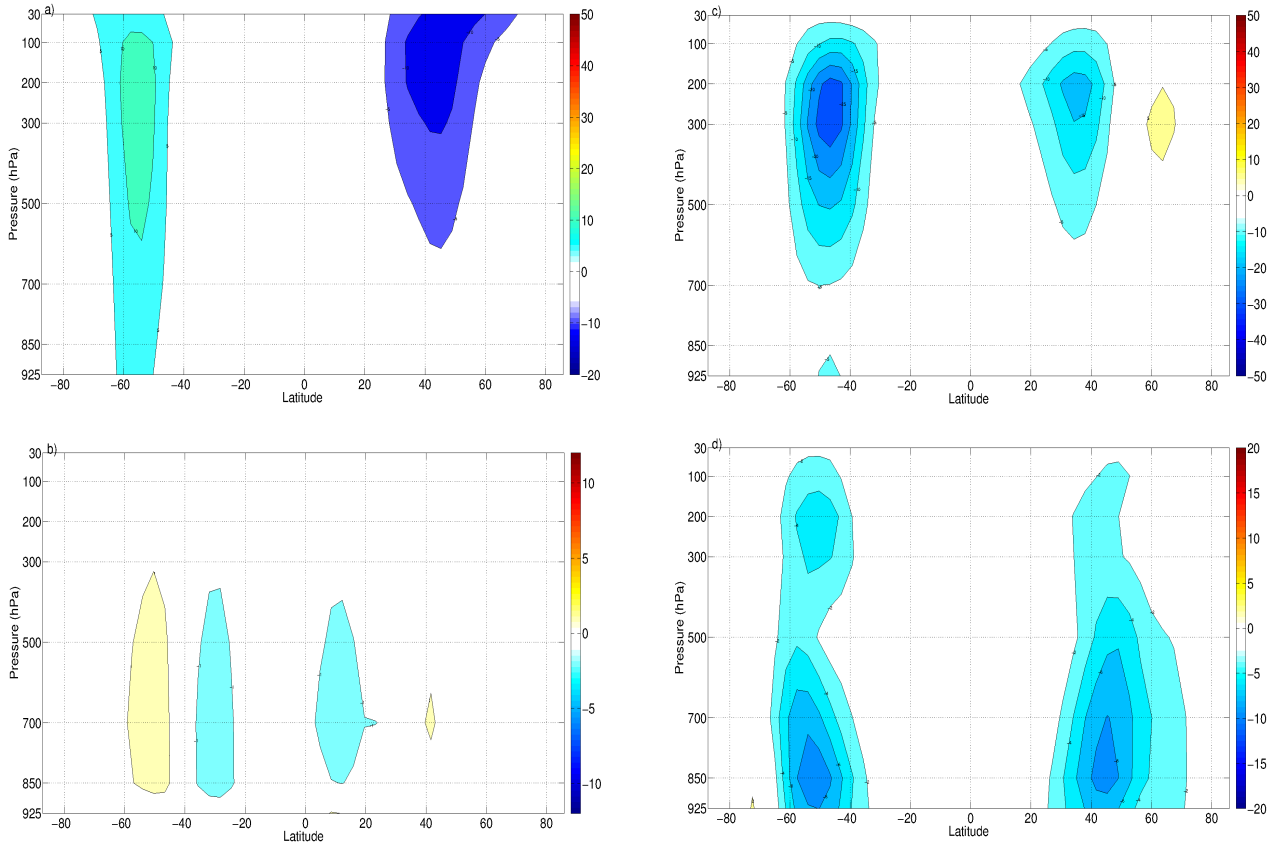

Figure 2.11: Same as Figure 2.5 for the experiment with fixed tropical SST, global slab land: *fix_trop_SST_35* except that the control run is the one corresponding to this experiment setup.

2.5. Role of African continental temperature

In this section we present the results of the experiment where the tropical SST are kept fixed, (the slab ocean model is applied elsewhere) and the LST over Africa is kept fixed, applying the slab land

model elsewhere: *fix_trop_SST_fix_Africa_A*. As was the case before, anomalies are calculated with respect to the corresponding control case and we will only show the results for the maximum strength of the forcing A=35 W/m^2. For this experiment we will focus on the fields: NSAT, precipitation and atmospheric meridional energy transport as the other fields investigated previously show little change with respect to the experiment where the tropical SSTs were fixed.

The NSAT anomalies over sea do not differ between the experiments *fix_trop_SST_fix_Africa_35* and *fix_trop_SST_35* (Figure 2.13 a vs. Figure 2.8 a). Differences in tropical temperatures are however seen over land as temperatures over Africa are prescribed (Figure 2.13 b versus Figure 2.8 b).

In Figure 2.13 b, we show the precipitation anomalies. For this experiment tropical precipitation changes are almost not present, in particular the anomalies over Africa and the tropical Atlantic are essentially zero. On the contrary, in the extratropics, the anomalies are very similar to those obtained without constraining the African land temperatures. For a more quantitative vision in Table 2.2 we calculate the values of the precipitation indices (Sahel, Atlantic and South America) for the experiment *fix_trop_SST_fix_Africa_35* relative to the same indices for the experiment *global_slabs_35*. For this experiment we see that the precipitation responses are very weak compared with the experiment in which the two slab models are applied globally and never exceed 15% in magnitude, indicating that when both the tropical SSTs and the LST are not allowed to react to the extratropical forcing, the precipitation response almost vanishes. Moreover, comparison among the indices clearly indicates that rainfall over the Sahel is the one that is most influenced by the surface warming over Africa. The Atlantic ITCZ shift is also controlled by the African temperatures, while precipitation over South America shows almost no response.

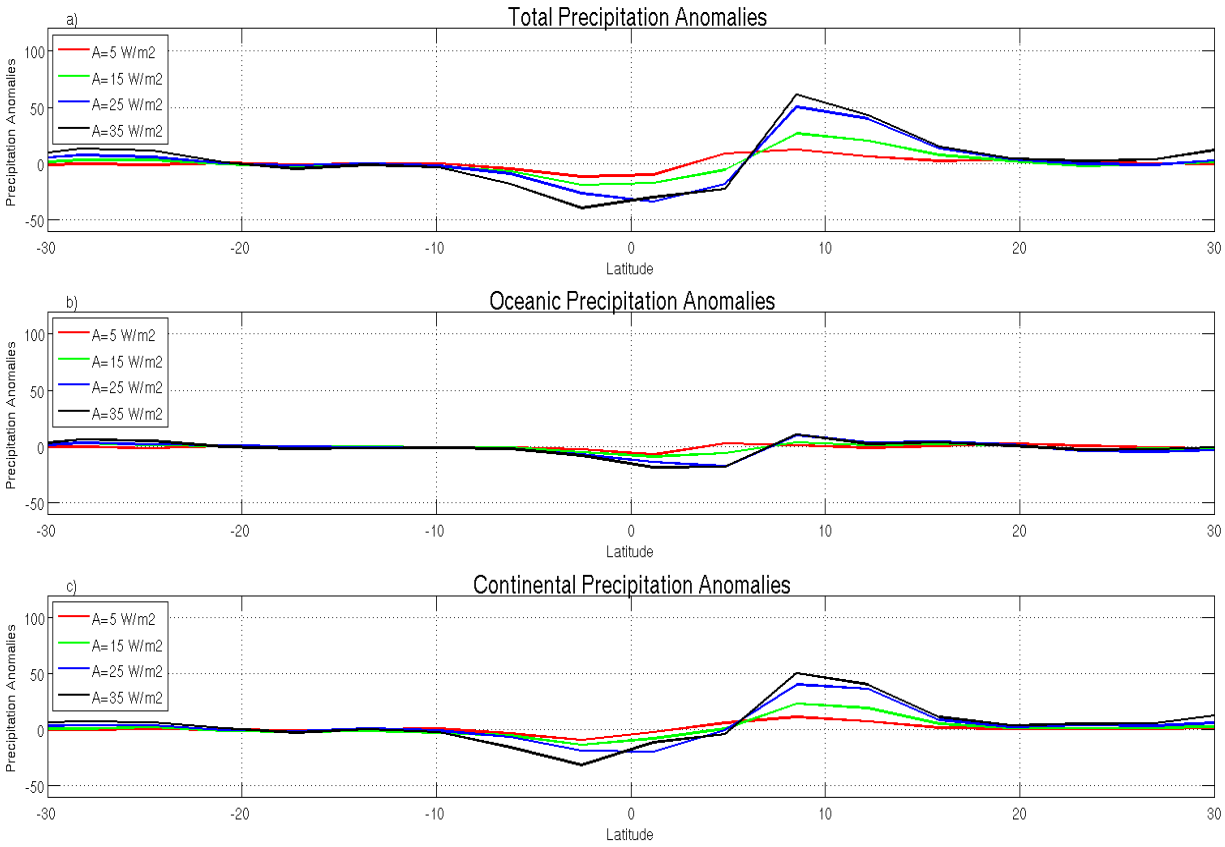

Figure 2.12: Annual mean zonal averages in the region 300ºE-30ºE of: a. Total precipitation anomalies b. Oceanic precipitation anomalies c. Continental precipitation anomalies, shown in the tropical sector (30ºS-30ºN) for several values of the parameter A and for the experiment with fixed tropical SST, global slab land: *fix_trop_SST_A.*

Table 2.2: Value of the Sahel, Tropical Atlantic (northern half minus southern half) and South America precipitation indices for the experiments fix_trop_SST_35 and fix_trop_SST_fix_Africa_35 relative to the values for the experiment global_slabs_35.

	Sahel	**Tropical Atlantic**	**South America**
fix_trop_SST_35	58%	19%	13%
fix_trop_SST_fix_Africa_35	15%	4%	11%

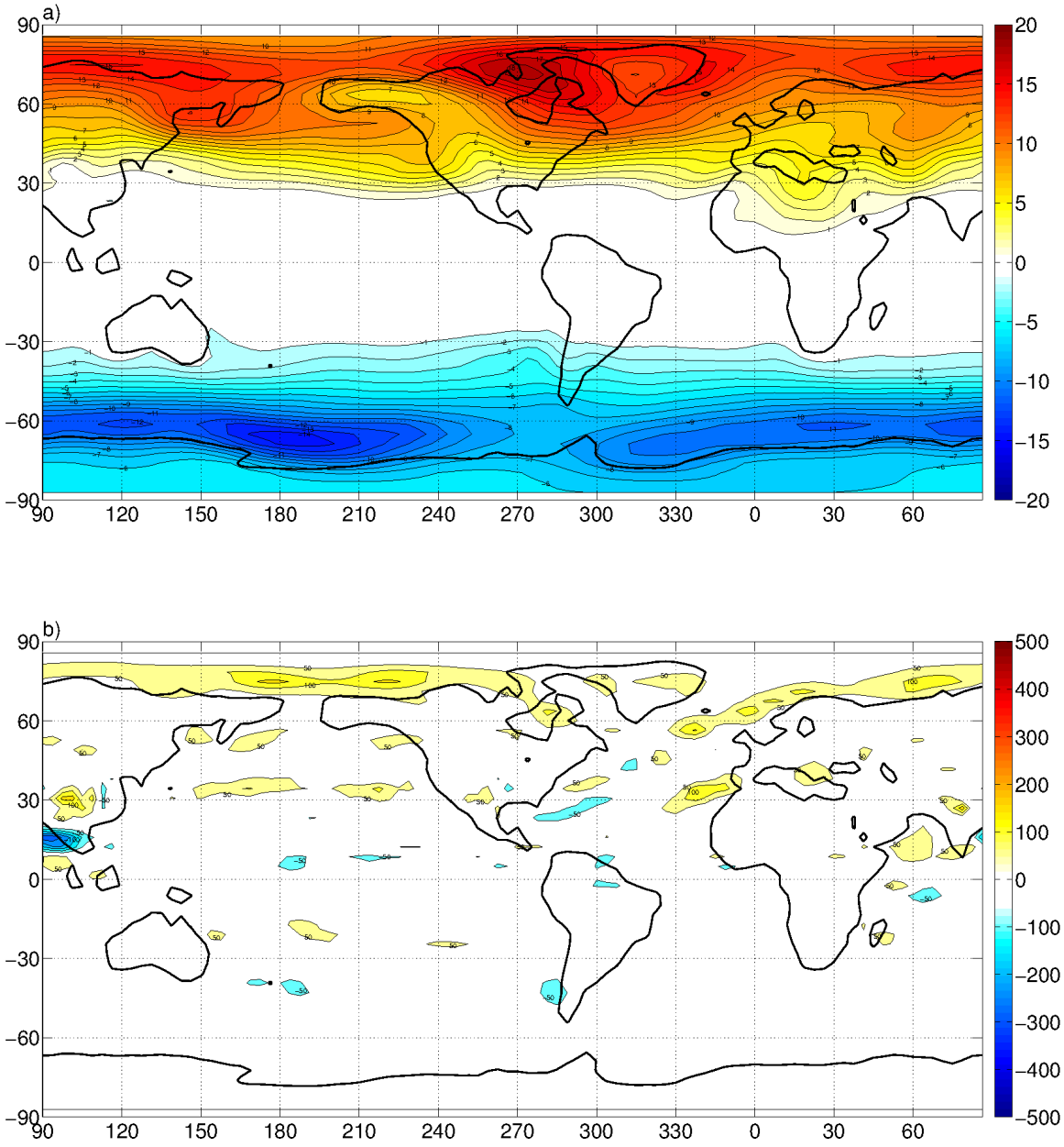

Figure 2.13: Same as Figure 2.3 for the experiment with fixed tropical SST, fixed surface temperature over Africa: *fix_trop_SST_fix_Africa_35* except that the control run is the one corresponding to this experiment setup.

2.6. Physical mechanisms: Teleconnection between extratropics and African LST

As we have shown in the previous section, the role of the LST over Africa is essential for obtaining an ITCZ response to the imposed extratropical forcing when the tropical SSTs are not allowed to react. Hence, in this section we try to answer the question: which are the physical mechanisms that make the African LST change once the extratropical forcing is imposed?

We start by analysing the surface energy balance in the experiment *fix_trop_SST_35* in the region of the maximum African LST response (15°N-30°N, 15°E-30°E).

Surface fluxes play a key role in the land temperature response. Thus, to validate model results we first determine how well the control run (*fix_trop_SST_0*) simulates the surface energy fluxes in this African region. Table 2.3 presents a comparison with two reanalysis products: NCEP-NCAR (Kalnay et al., 2006) and ERA40 (Uppala et al., 2005), using data from years 1979-2001. The values for net shortwave radiation are quite different in the reanalysis and the model value lies between them. On the other hand, the net longwave radiation has similar magnitudes in both reanalysis products as well as in the simulation. The sensible heat term is the one with largest difference between reanalysis products (a factor of 2), and the simulation result for this term lies between the values given by the two reanalysis. Lastly, the latent heat flux term is practically negligible in the reanalysis and in the simulation, although the simulation somewhat overestimates the value given by the reanalysis. Thus, overall, the model simulates the surface energy balance adequately.

Figure 2.14 displays, for the region of maximum temperature response, the annual-means of average LST anomalies and the terms of the surface energy balance: net shortwave radiation, net longwave radiation, sensible heat flux and latent heat flux. As can be seen in the LST time series, the stationary state is reached after ~10 years of simulation with an average warming of 5-6°C. The same time scale for equilibrium is seen in all the terms of the surface energy balance. However, the net surface heat flux is nonzero even after the stationary state has been reached. This is because the energy equation in the land model posses a small damping term with a time scale of 40 days to

prevent the LST to drift away from the climatological mean (Molteni, 2003). This damping term is small compared to the other terms involved in the energy balance, with exception of the latent heat flux, which does not play a role here. For example, for the region of interest (15°N-30°N, 15°E-30°E) in the experiment fix_trop_SST_0 (fix_trop_SST_35) the corrective term is of the order of 7W/m^2 (11W/m^2). Hence, except for the damping term, Figure 2.14 shows that the energy balance is reached mainly between the radiative terms, with the sensible heat flux playing a secondary role. The sum of the radiative terms plus the sensible heat flux is directed downward, in the same direction as the longwave radiation. Thus, the warming of the continent in this region appears to be related to the longwave radiation effect.

Table 2.3: Annual mean values of surface net shortwave radiation, net longwave radiation, sensible heat flux and latent heat flux in the region (15ºN-30ºN, 15ºE-30ºE) for NCEP-NCAR Reanalysis (years 1979-2001), ERA40 Reanalysis (years 1979-2001) and the experiment fix_trop_SST_0.

	NCEP-NCAR Reanalysis	**ERA40 Reanalysis**	***fix_trop_SST_0***
Net Shortwave Radiation (W/m^2)	210	149	200
Net Longwave Radiation (W/m^2)	115	111	127
Sensible Heat Flux (W/m^2)	86	38	52
Latent Heat Flux (W/m^2)	8	3	14

The longwave radiation effect can be decomposed into clear-sky and cloud components. Given that cloud changes are not particularly important in the region, we speculate that the clear-sky component must be the one playing the dominant role. To demonstrate this we designed a new experiment (fix_trop_SST_fix_cslw_A) in which, in addition to the prescribed tropical SSTs, the

clear-sky component of the longwave radiation is maintained fixed globally. Again, we perform runs in which the extratropical forcing is applied (A different from zero), as well as an associated control run (A=0, i.e. no forcing), all of them sharing the same experimental configuration.

In the parametrization scheme for longwave radiation (see Molteni, 2003 for more details) the infrared spectrum is partitioned into four bands: between 8.5 and 11 μm, the band of strong absorption by CO_2, the aggregation of regions with weak or moderate absorption by water vapour and the aggregation of regions with strong absorption by water vapour. For each band and model layer a transmissivity is computed as a function of layer depth, specific humidity and cloud properties. The effect of clouds is modeled as a decrease in the transmissimity in the first band. To inhibit clear-sky longwave changes, we modify the transmissivity in the two water vapour bands, replacing in the transmissivity computation at each time step the calculated specific humidity by a climatological specific humidity (in this case climatology is obtained computing the monthly averages of the last 10 years of simulation of the control run).

As Figure 2.14, Figure 2.15 displays the results for the experiment with fixed clear-sky longwave radiation: *fix_trop_SST_fix_cslw_35*. The time-scale to achieve the stationary state is unchanged (~10 years). The LST response is still of warming but more moderate (values between 3°C and 4°C) while the predominant terms in the surface energy balance are the shortwave radiation and the sensible heat flux.

Finally, in Figure 2.16 we show the NSAT and precipitation anomalies (with respect to the associated control case) for the experiment with prescribed tropical SSTs and clear-sky longwave radiation. Over sea, the NSAT response is very similar to the one obtained without the restriction over the longwave radiation. On the other hand, the NSAT anomalies over Africa are clearly weaker, with a maximum of 5°C over central Sahara desert, while the ITCZ response is almost completely suppressed (Figure 2.8 versus Figure 2.16).

So, how does the African LST change once the extra-tropical forcing is imposed? We hypothesize the following mechanism. Once the forcing is imposed, a general warming occurs in the region of application in the NH (poleward of 40°N), leading to an increase in the specific humidity there (not

shown). Changes in the circulation advect humidity towards the African continent (note the westerly anomalies from the Atlantic into the Sahara in Figure 2.10), therefore increasing the humidity there and enhancing the clear-sky longwave greenhouse effect that leads to a warming of the surface beneath. As the warming is associated with a decrease in the regional sea level pressure (not shown) it drives the ITCZ northward over the continent. Some other processes may also play a role in explaining the remaining warming.

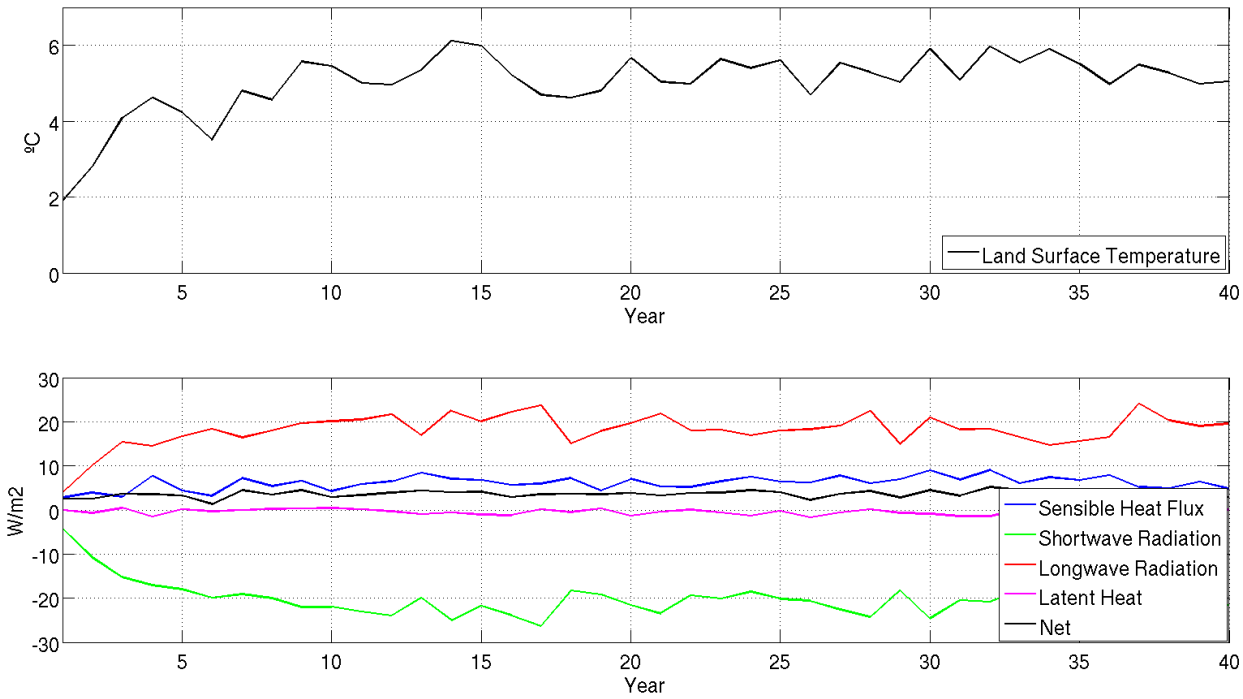

Figure 2.14: Annual mean anomalies with respect to the control of: a. LST b. Shortwave radiation, longwave radiation and sensible heat flux, in the region (15°N-30°N, 15°E-30°E) for the experiment *fix_trop_SST_35*.

2.7. Summary and conclusions

We investigated the response of the ITCZ to extratropical forcing in an AGCM coupled to slab ocean and land models, with realistic surface boundary conditions. We imposed an oceanic heat flux forcing, with zero global mean, consistent of warming in the NH and cooling in the SH and analysed the changes obtained when averaging over a 10-year period. The relative roles of the

atmosphere, tropical SSTs and continental surface temperature over Africa were investigated in three series of experiments. Finally, the mechanisms behind the land-based extratropical to tropical communication were studied.

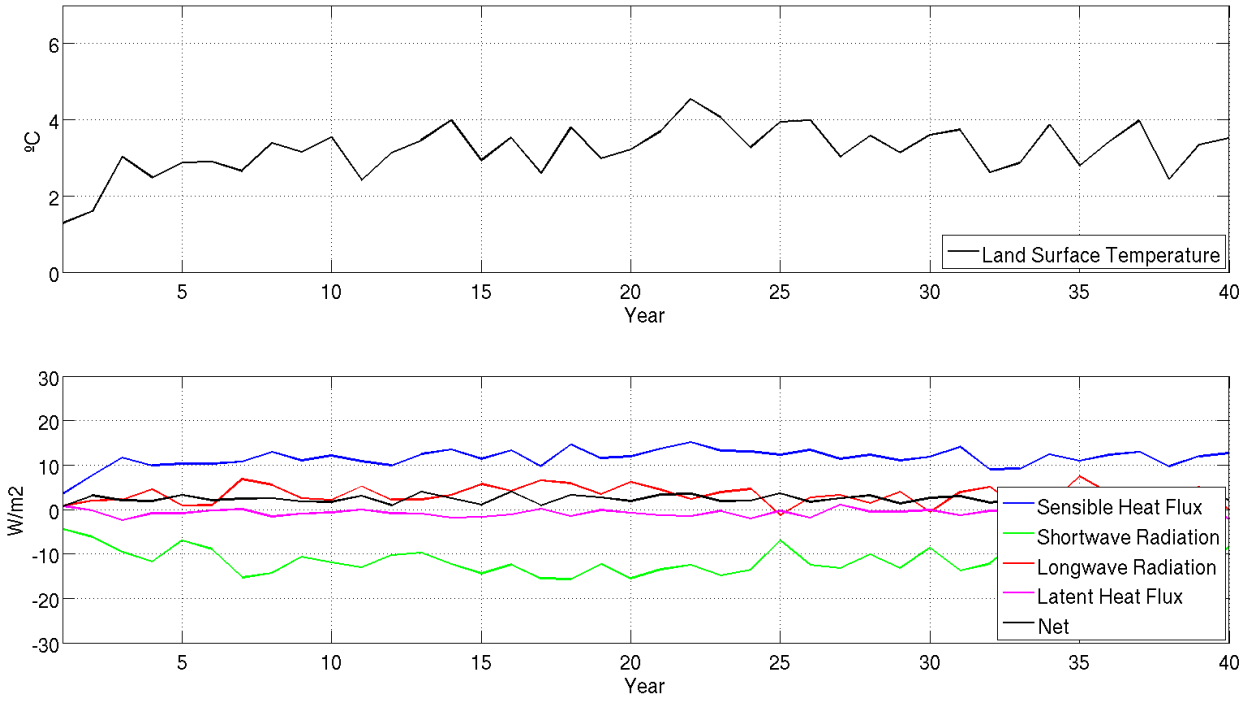

Figure 2.15: Same as Figure 2.14 for the experiment with fixed tropical SST, global slab land and fixed clear-sky longwave radiation *fix_trop_SST_fix_cslw_35* except that the control run is the one corresponding to this experiment setup.

In the simulation where the slab ocean and land models are applied globally our results are consistent with previous results in the sense that the ITCZ shifts toward the warmer hemisphere and that the magnitude of the shift increases with the magnitude of the forcing. In this case we also attribute the ITCZ displacement mainly to the tropical cross-equatorial SST gradient, a finding consistent with previous studies. However, some aspects of our simulations differ from previous works: in particular, we found that the magnitude of the tropical precipitation zonal mean maximum increases with the magnitude of the forcing at the same time that no changes to the width of the ITCZ are noticed, while Kang et al., (2008) found that this maximum gets weaker and the ITCZ widens. As has been shown before the ITCZ control by the SST results extremely sensitive to the

deep-convection scheme implemented (e.g. Liu et al., 2010; Song and Zhang, 2009; Lin, 2007) and, as a consequence, we hypothesize that the differences found might be due the use of different AGCMs, and therefore different parameterizations. Switching between realistic surface boundary conditions and an aquaplanet configuration might also play a role. With respect to heat and momentum atmospheric transports we found that both react to the extratropical forcing by increasing (decreasing) the amount transfered from the tropics to the SH (NH) in order to compensate the anomalous cooling (warming) of the hemisphere. Transports performed by the mean circulation respond to the forcing with an intensification (weakening) of the southern (northern) Hadley and, to a lesser extent, Ferrel cells in the SH (NH). Meanwhile the changes in the fraction of the transport performed by transient eddies are found to be stronger in the SH, where they drive a poleward intensification of the zonal flow in the SH. An integration of the former leads to a net meridional atmospheric transport increased (decreased) to the SH (NH) and a consequent displacement of the energy equator towards the warmer hemisphere.

In the simulations in which the slab land model is applied globally but in the ocean the tropical SSTs are not allowed to change we found that the ITCZ response notably weakens. However, there is still some non negligible ITCZ response in particular over the Atlantic Ocean and Africa. In these regions the magnitude of the precipitation anomalies is of the order of 20% and 60%, respectively, of that obtained when the tropical SST constraint was not applied. Cvijanovic and Chiang (2013) performed a similar experiment and also found that by disabling the tropical SST reaction the ITCZ response almost disappears, although in their results significant tropical precipitation changes were essentially not present in any location. This discrepancy in the ITCZ response could be caused by the use of different AGCMs. Based on our results the tropical SSTs are extremely important but not necessary in order to obtain a shift of the ITCZ to the warmer hemisphere, in particular over the Atlantic Ocean and Africa. With respect to atmospheric transports, as a direct consequence of the stillness of the tropical SSTs, the mean meridional circulation shows almost no response in the tropical region while the effect over the Ferrel cells and the transports performed by eddies is similar to the obtained without the SST constraint. Regarding the physical mechanism we hypothesize that, in the absence of an interhemispheric SST gradient in the tropical region, the continental surface temperature over Africa is the one responsible for the ITCZ displacements.

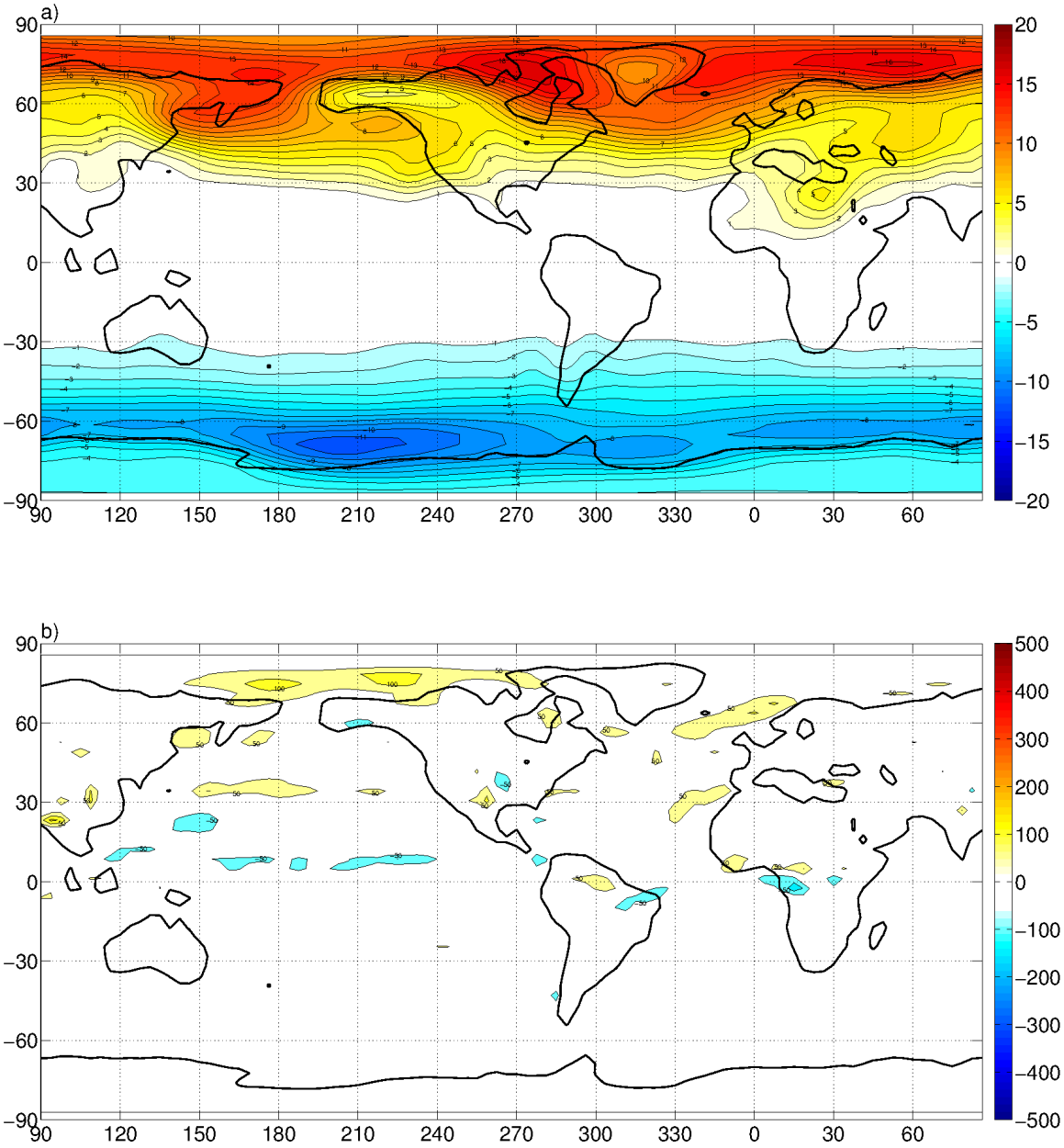

Figure 2.16: Same as Figure 2.3 for the experiment with fixed tropical SST, global slab land and fixed clear-sky longwave radiation *fix_trop_SST_fix_cslw_35* except that the control run is the one corresponding to this experiment setup.

With this motivation in mind we performed the third set of simulations in which fixed surface temperatures over Africa are imposed as an additional constraint. In this case we found that the ITCZ response completely vanishes, indicating that the ITCZ response to the extratropical forcing is

not possible just trough purely atmospheric processes, but needs the involvement of either the tropical SST or the continental surface temperatures. An additional experiment showed that an enhancement of the clear-sky longwave greenhouse effect plays a fundamental role in the warming over northern Africa. The warming is associated with a local decrease in sea level pressure that drives the ITCZ shift.

It is worth noting that the relevance of the surface air temperature over the Sahara desert as a driver of the Sahel rainfall variability has been previously highlighted, both in observations and model simulations by Haarsma et al. (2005).

Further work is planned in order to understand the role of the tropical ocean dynamics in the communication of the extratropical signal to the tropical region.

Chapter 3. Control of the South Atlantic Convergence Zone by extratropical thermal forcing

Abstract

The response of the South Atlantic Convergence Zone (SACZ) to an extratropical thermal forcing is investigated in a series of simulations performed with an atmospheric general circulation model coupled to a slab ocean model. Three sets of experiments are performed, varying the extratropical forcing. In the first the forcing consists of warming of the Northern Hemisphere (NH) and cooling of the Southern Hemisphere, with zero global average. In the second and third experiments, the former forcing is divided into its northern and southern components to asses their relative roles in affecting the SACZ. In all the cases realistic surface boundary conditions are implemented.

We find that during its peak in austral summer the SACZ weakens in response to the extratropical forcing and that such weakening is mostly due to the NH component of the forcing. We find that 75% of the SACZ signal in response to the forcing is linked to the generation of a secondary tropical convergence zone in the Atlantic Ocean around 20°N-30ºN, which generates an anomalous Hadley circulation with subsidence over the SACZ. This mechanism appears to be dependent on the tropical ocean response, as it weakens significantly when the simulation is repeated not allowing the tropical sea surface temperatures to change in response to the forcing. The remaining 25% of the signal can be explained through the development of a Walker-type of circulation between western tropical Africa and the SACZ, being this mechanism dependent on the African land surface temperature reaction to the remote forcing.

3.1. Introduction

The capability of an extratropical thermal forcing to affect the tropical climate has been suggested in studies analysing paleoclimatic data (Wang et al., 2004), 20th century observations (Folland et al., 1986) and numerical simulations (Chiang and Bitz, 2005; Kang et al., 2008, 2009; Cvijanovic and Chiang, 2013; Talento and Barreiro, 2015). The Intertropical Convergence Zone (ITCZ) has been the most studied feature and the general picture emerging from these studies is that the ITCZ tends to shift toward the warmer hemisphere. However, there is evidence supporting the idea that other features of the tropical climate might be affected by such an extratropical influence. In particular, the South Atlantic Convergence Zone (SACZ) stands out as one of such possibly affected features.

The SACZ is a summertime elongated convective belt orientated diagonally (in the NW-SE direction) extending from the Amazon basin to southeastern Brazil and the South Atlantic Ocean (Kodama, 1992; Carvalho et al., 1994). The SACZ presents variability in many timescales from intraseasonal to decadal (Vera et al., 2006). On interannual timescales a dipole-like structure, with centers of opposite sign over SACZ and southeastern South America (SESA), emerges as the main pattern of variability (Doyle and Barros, 2002). Van der Wiel et al. (2016) elaborate on the mechanisms that promote the diagonal orientation of the southern convergence zones (they focus on the South Pacific convergence zone, SPCZ, noting that comparable mechanisms apply to the SACZ). Through a series of numerical simulations they test the influence of several atmospheric boundary conditions and conclude that the zonally asymmetric component of the sea surface temperature (SST) is the key condition leading to the diagonal configuration. The authors argue that this component of the SST field leads to strong subtropical highs that provide warm moist air to the convergence zones and then, if the dynamical forcing is adequate, deep convection will be triggered producing precipitation.

The notion that the SACZ might react to extratropical stimulus is supported by both paleoclimatic data and numerical simulations.

Stríkis et al. (2015) present a multi-proxy paleoprecipitation reconstruction of areas affected by SACZ and ITCZ during Heinrich stadial 1 (HS1). Heinrich stadials occur as massive depositional

episodes of ice-rafted debris in the north Atlantic Ocean, implying an abrupt cooling of the northern midlatitudes of this basin. The authors find that the HS1 footprint is characterized by a southward shift of the ITCZ as well as an intensification of the SACZ, being the response to the Northern Hemisphere (NH) forcing synchronous.

Meanwhile, Chiessi et al. (2009) analyse the possible impact of the Atlantic Multidecadal Oscillation (AMO) on the South American Monsoon System using 4500 years-long proxy records of the La Plata River discharge variability. They suggest that during periods of positive AMO (characterized by a widespread NH warming in the north Atlantic Ocean) a northward migration of the ITCZ and cooling of the western South Atlantic would lead to a decrease in the intensity of the South American Low Level Jet, producing a decrease in precipitation over La Plata Basin.

Junquas et al. (2012) analyze the summer precipitation variability over SESA and SACZ under a global warming scenario in the CMIP3 simulations. They find that the future summer (December to February: DJF) precipitation variability over SESA and SACZ has a strong projection on the changes of the above mentioned dipole-pattern activity. Their results indicate that in a global warming scenario, in which the NH is expected to warm faster than the Southern Hemisphere (SH), there is an increase in the frequency of the positive phase of the dipole leading to wetter conditions over SESA and dryer ones over SACZ.

The existence of an interhemispheric thermal gradient in which the NH is warmer than the SH has been already noted in 20th century observations in Friedman et al. (2013). The interhemispheric temperature asymmetry (ITA) annual mean (NH minus SH) shows an abrupt descent in the late 60's while a linear upward trend is noticed from the 80's.

Although for the 20th century no significant signal has been found linking SACZ precipitation and the ITA, following Junquas et al. (2012) some signal is expected to arise during the 21st century when the ITA is projected to rise continuously.

In this study we further explore the mechanisms through which the SACZ may respond to an

extratropical thermal forcing. To do so we conduct a series of simulations performed with an atmospheric general circulation model (AGCM) coupled to a slab ocean model, prescribing realistic surface boundary conditions. In our first series of simulations the imposed extratropical forcing consists of warming of the NH and cooling of the SH, with zero global average. In order to determine which component of the extratropical forcing most affects the SACZ we conduct two complimentary experiments in which the former forcing is divided into its northern and southern components, respectively. The relative role of the tropical SSTs in the communication of the remote signal will be assessed in a experiment in which the slab ocean model will be turned off over the tropics. As will be shown, when the tropical SSTs are not allowed to change there is still some signal over the SACZ and Africa, fact that motivates the last experiment in which the role of the African land surface temperature (LST) is investigated, not allowing it to change in response to the remote forcing.

The chapter is organized as follows: In Section 3.2 we introduce the model and the experiments. Results are presented in Sections 3.3 and 3.4. In Section 3.3 we present the experiments where the slab ocean model is applied globally. In Section 3.4 we analyse the relative roles of the tropical SST and LST over Africa. Finally, in Section 3.5 we summarize the conclusions.

3.2. Model and Experiments

The model used in this study is the Abdus Salam International Centre for Theoretical Physics (ICTP) AGCM (Molteni 2003; Kucharski et al. 2006) which is a full atmospheric model with simplified physics. We use the model version 41 in its 8-layer configuration and T30 (3.75ºx3.75º) horizontal resolution. A slab ocean model is coupled. Present-day boundary surface conditions, orbital parameters and greenhouse forcing are used. A monthly-varying ocean heat flux correction is imposed in order to keep the simulated SST close to present-day conditions.

Three extratropical forcing patterns are implemented. The first forcing pattern consists in cooling in one hemisphere and warming in the other poleward of 40°, applied only over ocean grid points, and with a resulting global average forcing equal to zero. This pattern is similar to the one used in Kang

et al. (2008) and Talento and Barreiro (2015) and it is intended to represent the asymmetric temperature changes associated with glacial-interglacial and millennial-scale climate variability. It may also represent the asymmetric SST pattern characteristic of the global warming trend. The forcing pattern is superposed on a background state and is obtained as explained in the following paragraphs. The second and third forcing patterns are obtained as the NH and SH components of this forcing, respectively.

Let θ denote latitude, ψ longitude and lsm the land surface mask i.e. lsm=1 over land, lsm=0 over sea.

Consider h to be:

$$h(\theta,\psi) = -A\sin\left(\frac{\theta+40}{50}\pi\right)*(1-lsm(\theta,\psi)) \quad \text{for} \quad \theta\in[-90,-40]$$

$$h(\theta,\psi) = 0 \quad \text{for} \quad \theta\in[-40,40]$$

$$h(\theta,\psi) = -A\sin\left(\frac{\theta-40}{50}\pi\right)*(1-lsm(\theta,\psi)) \quad \text{for} \quad \theta\in[40,90]$$

where A (W/m^2) denotes the intensity of the forcing.

Then, let h_{SH} and h_{NH} be the integral of h over the SH and NH, respectively:

$$h_{SH} = \int_{\psi=0}^{\psi=2\pi}\int_{\theta=-\pi/2}^{\theta=0} h(\theta,\psi)\,d\theta\,d\psi$$

$$h_{NH} = \int_{\psi=0}^{\psi=2\pi}\int_{\theta=0}^{\theta=\pi/2} h(\theta,\psi)\,d\theta\,d\psi$$

Finally, the forcing pattern H, with components on both hemisphere, is defined as:

$$H(\theta,\psi)=h(\theta,\psi) \quad \text{for} \quad \theta\in[-90,-40]$$

$$H(\theta,\psi)=0 \quad \text{for} \quad \theta\in[-40,40]$$

$$H(\theta,\psi)=\frac{-h_{SH}}{h_{NH}}*h(\theta,\psi) \quad \text{for} \quad \theta\in[40,90]$$

taking just the NH or the SH component of H the second and third forcing patterns are obtained.

We only consider the forcing patterns corresponding to the value A=35W/m^2 (see Figure 3.1 for the pattern with components in both hemispheres). The sign convention selected is positive out of sea. Therefore, positive values of the forcing could be thought as representing a situation where the atmosphere is dry and colder than the ocean below it so that there is a strong ocean-to-atmosphere net heat flux. Alongside with the three perturbed runs associated with each of the forcing patterns a Control run in which no forcing is applied is implemented using the same model configuration. The experiments are named *nh+sh_forcing*, *nh_forcing*, *sh_forcing* and *Control*, respectively.

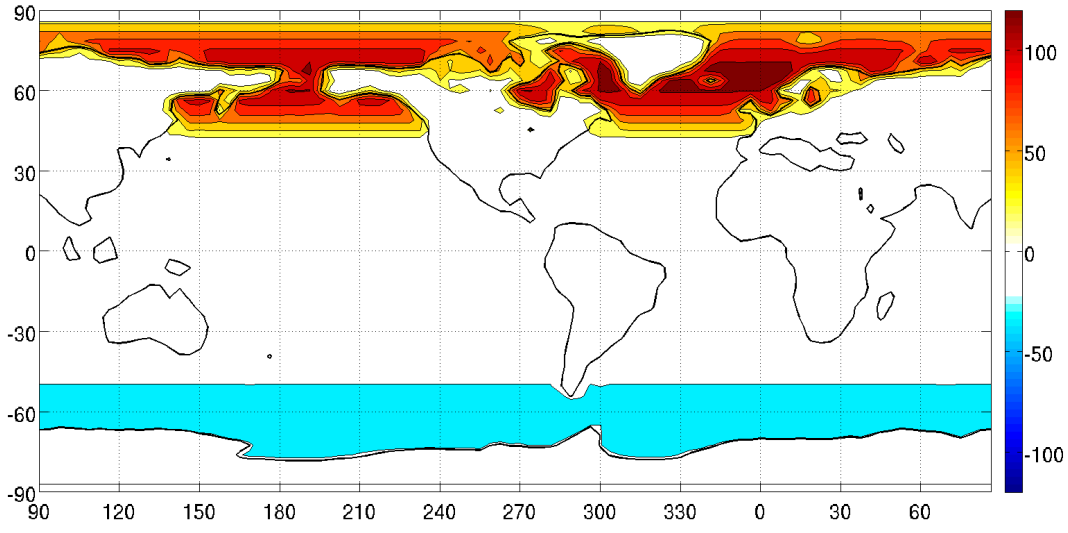

Figure 3.1: Forcing pattern with components in both hemispheres. The sign convention is positive out of sea. Contour interval 20 W/m^2.

A model configuration in which the tropical (30ºS-30ºN) SSTs are kept fixed, while the slab ocean is applied elsewhere is implemented to test the role of these SSTs in transmitting the signal from the extratropical regions to the tropics. For this configuration we conduct three forced experiments, applying the nh+sh, nh or sh forcing patterns, as well as a corresponding Control case. The experiments names are: *nh+sh_forcing_fix_trop_sst*, *nh_forcing_fix_trop_sst*, *sh_forcing_fix_trop_sst* and *Control_fix_trop_sst*, respectively.

Finally, to asses the role of the LST over Africa, we conduct a last series of simulations in which the tropical SSTs are kept fixed, the slab ocean model is applied elsewhere and, in addition, the LST over the African continent are not allowed to change (climatological temperatures of the land model are imposed). These experiments are named: *nh+sh_forcing_fix_trop_sst_fix_Africa*, *nh_forcing_fix_trop_sst_fix_Africa*, *sh_forcing_fix_trop_sst_fix_Africa* and *Control_fix_trop_sst_fix_Africa*, respectively.

In all the simulations the model was run for 40 years and the last 10 are used for averaging. Running the simulations for 40 years proved to be more than enough to reach the equilibrium; a time scale of 10 years was estimated to be the time span necessary for adjustment. In Table 3.1 we summarize the experiments.

3.3. SACZ response to extratropical forcing

In this section we display the results for the experiments in which the slab ocean model is applied globally. Most of the results are presented in the form of anomalies with respect to the corresponding control case. As the SACZ peaks in austral summer we will focus on this season, showing the DJF means.

To gain insight on the magnitude of the response to the imposed forcing we will show the global anomalies for the near surface air temperature (NSAT) while for the rest of the fields we will focus on the vicinity of the SACZ displaying the anomalies only in the region 60°S-30°N, 270°E-30°E, which includes South America and tropical and southern Atlantic Ocean (SATSA).

Table 3.1: Experiment summary.

Experiment Name	**Forcing Pattern**	**Fixed Tropical SST**	**Fixed Land Surface Temperature over Africa**
Control	None	No	No
nh+sh_forcing	nh+sh	No	No
nh_forcing	nh	No	No
sh_forcing	sh	No	No
Control_fix_trop_sst	None	Yes	No
nh+sh_forcing_fix_trop_sst	nh+sh	Yes	No
nh_forcing_fix_trop_sst	nh	Yes	No
sh_forcing_fix_trop_sst	sh	Yes	No
Control_fix_trop_sst_fix_Africa	None	Yes	Yes
nh+sh_forcing_fix_trop_sst_fix_Africa	nh+sh	Yes	Yes
nh_forcing_fix_trop_sst_fix_Africa	nh	Yes	Yes
sh_forcing_fix_trop_sst_fix_Africa	sh	Yes	Yes

Figure 3.2 shows the DJF NSAT anomalies for the *nh+sh_forcing*, *nh_forcing* and *sh_forcing* experiments. For the experiment *nh+sh_forcing* the response consists of a generalized warming (cooling) over the NH (SH) with absolute magnitudes decreasing from 70ºN (70ºS) toward the Equator. In the extratropics the most extreme response in the NH (SH) is a 16ºC (-20ºC) anomaly over the north Atlantic Ocean at 70ºN (over the Ross Sea). In the tropics the maximum response (11ºC) is obtained over the Sahara desert while over the oceans the signal has a W-E gradient in the northern tropics and an E-W gradient in the southern tropics, being the oceanic signal stronger in the NH than in the SH. According to Van der Wiel et al. (2016) the E-W gradient in the southern tropics (which implies an increase in the zonal SST gradient) would lead to an increase in the diagonality of the SPCZ and the SACZ. Finally, in the SACZ region the response to the extratropical forcing is weak (below -1ºC).

In the *nh_forcing* experiment (Figure 3.2 b) the response in the NH high latitudes is similar to the one obtained in the *nh+sh_forcing* experiment. Although weak (less or equal to 1ºC) there is some response in the SH. Over the SACZ a small region of positive NSAT anomalies is produced. For the *sh_forcing* experiment (Figure 3.2 c) the NSAT signal in the extratropics of the SH is similar to the one obtained in the *nh+sh_forcing* experiment and a weak (smaller than -2ºC) signal in the opposite hemisphere of the forcing is also created. Over the SACZ a temperature anomaly of -1ºC is detected. Overall, in terms of NSAT, the response to the forcing components is quasi linear being the differences between the sum of the responses of experiments with hemispheric forcing and the one with *nh+sh_forcing* experiment less than 1ºC in absolute value.

Figure 3.3 depicts the precipitation anomalies for the three experiments, in the SATSA sector. The strongest response is seen in the tropical band: the ITCZ is clearly shifted northward over western South America and Africa, while over eastern South America and the Atlantic ocean the ITCZ weakens. The SACZ is weakened and slightly shifted southward. Furthermore, a region of positive precipitation anomalies is generated in the Atlantic Ocean around 20ºN-30ºN with a SW-NE diagonal orientation. It is to be noted this region should not be regarded as a northward displacement of the ITCZ but as a secondary convergence zone itself: note the Control precipitation overlaid in Figure 3.3 a.

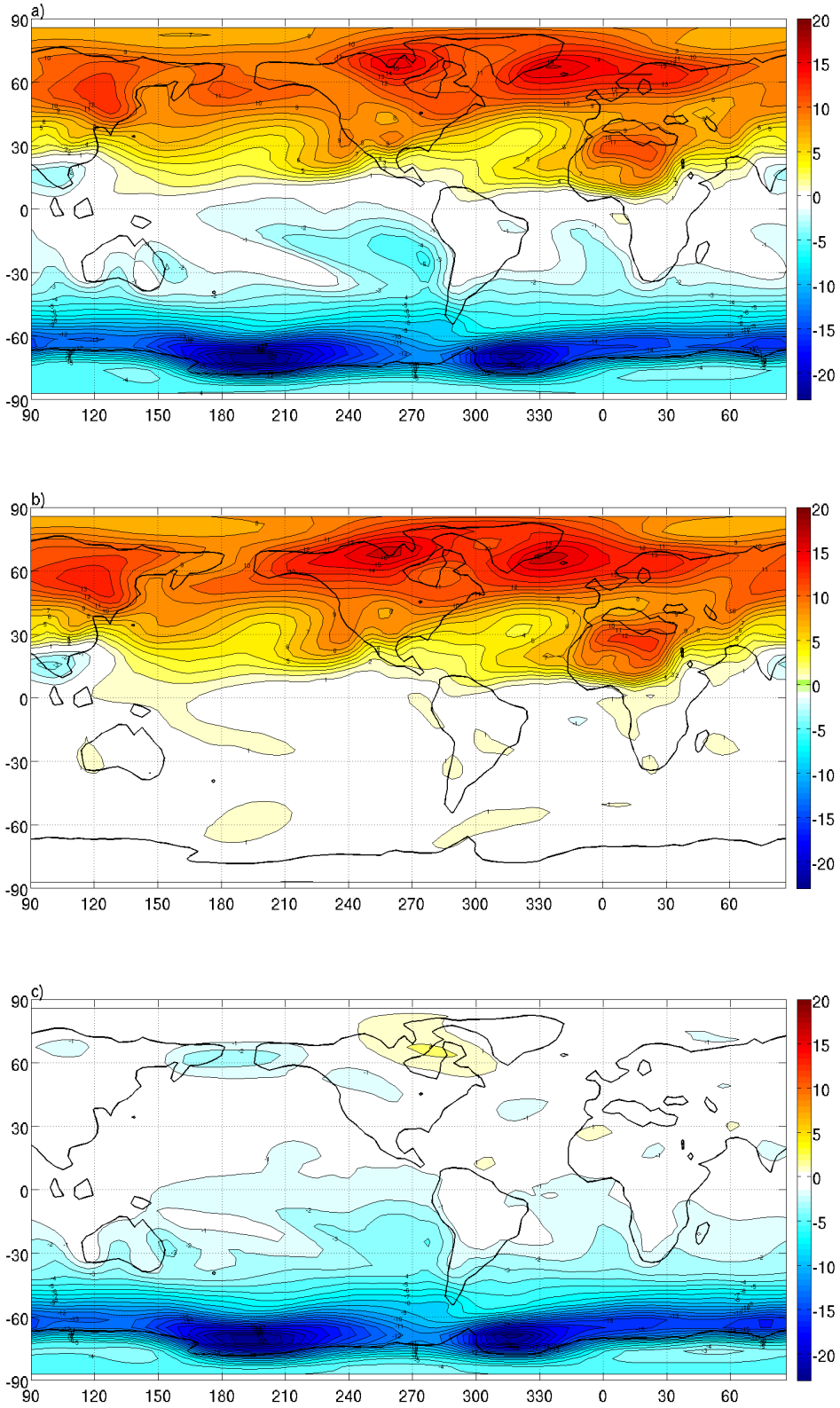

Figure 3.2: DJF mean anomalies with respect to the control of NSAT for: a. *nh+sh_forcing*, b. *nh_forcing* and c. *sh_forcing* experiments, respectively. Contour interval 1ºC.

The hemispheric simulations (Figure 3.3 b and 3.3 c) show signals in the SATSA region, being the *nh_forcing* simulation the one that produces the strongest anomalies. The northward displacement of the ITCZ over Africa and the positive precipitation anomaly zone in the Atlantic Ocean at 20ºN-30ºN noted in the *nh+sh_forcing* experiment are reproduced by the *nh_forcing* experiment, but not by the SH counterpart. Thus, this tropical north Atlantic diagonal precipitation band is caused by the warm pool of SST (up to 29ºC) generated due to decreased ocean-to-atmosphere heat fluxes between the Equator and 25ºN. The changes in surface heat fluxes are, in turn, due to weakened trades consequence of the strong weakening of the subtropical high as result of the NH extratropical imposed heating (Figure 3.4 a,b). The created SST anomaly, in turn, favors wind convergence and precipitation over the region.

Regarding the SACZ, the anomalies produced by the NH forcing are similar to the ones obtained when the forcings are applied in the two hemispheres. On the other hand, the application of the SH forcing produces only a weak positive anomalous signal. In this latter case the ITCZ clearly shifts northward over the western Atlantic basin. Thus, while in the ITCZ region both forcings tend to induce changes of the same sign, in the SACZ region the NH and SH forcings tend to oppose each other but with different strengths so that the NH forcing dominates the response in the experiment with combined forcing.

The similarity in the tropical surface response between the *nh+sh_forcing* and the *nh_forcing* experiments is clearly seen in the maps of mean sea level pressure (MSLP) over the whole Atlantic basin (Figure 3.4). The differences arise in the response over the SH extratropics where there are quasi zonally symmetric negative (positive) anomalies southward (northward) of 50ºS, which are consequence of the SH forcing (Figure 3.4 a, c). Also, there is an intensification of the south Atlantic subtropical high as result of both the NH and SH forcing. This response supports the fact that the SH forcing does not have a significant influence over the northern Atlantic, while the NH forcing indeed has an important influence on the southern Atlantic.

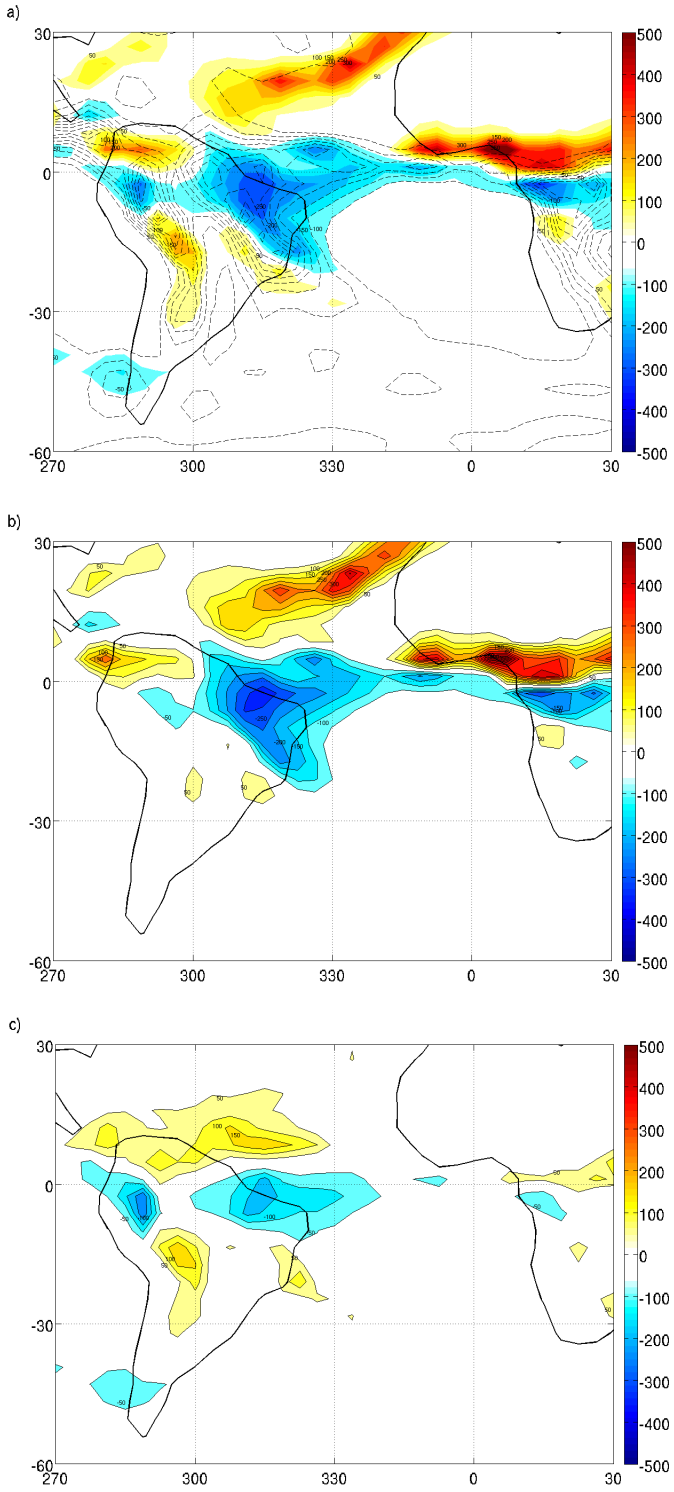

Figure 3.3: DJF mean anomalies with respect to the control of precipitation for: a. *nh+sh_forcing*, b. *nh_forcing* and c. *sh_forcing* experiments, respectively, in the SATSA region. Contour interval 50 mm/month. For reference, in a, the Control precipitation is plotted in dashed lines with countour interval 50 mm/month.

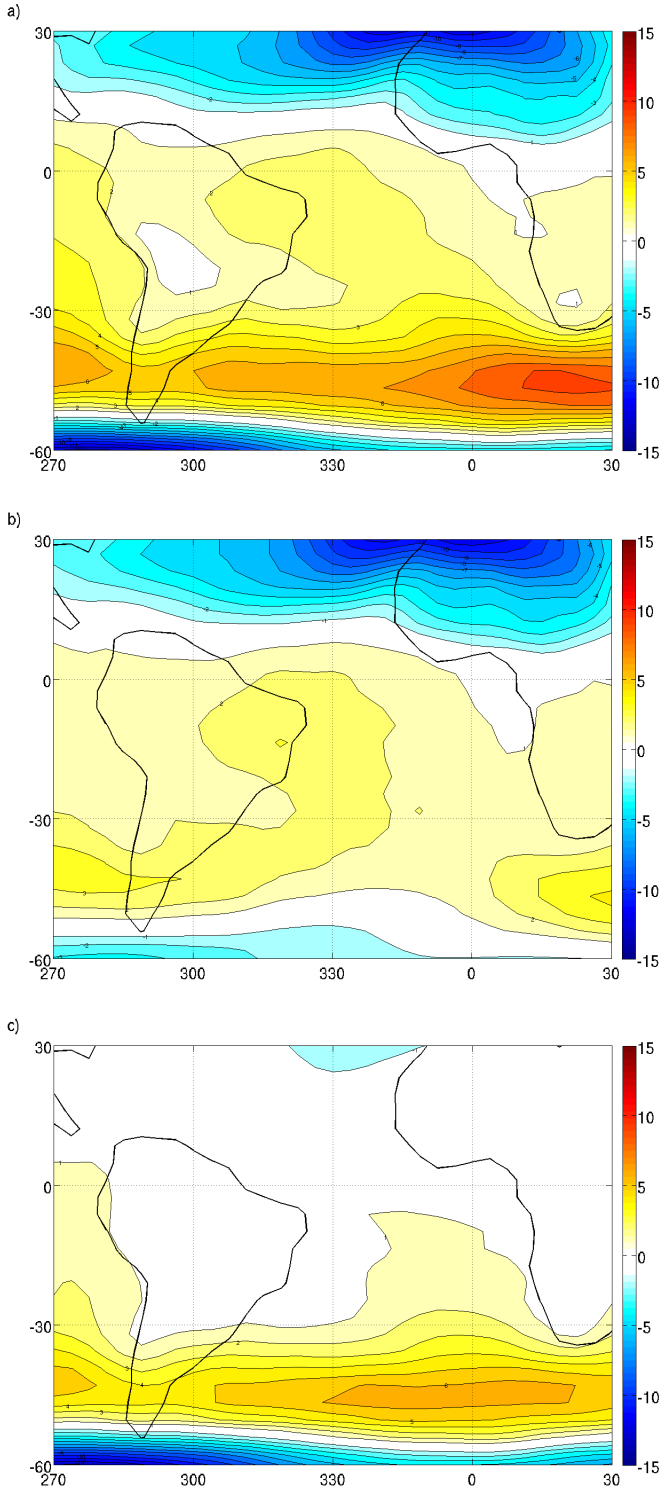

Figure 3.4: DJF mean anomalies with respect to the control of MSLP for: a. *nh+sh_forcing*, b. *nh_forcing* and c. *sh_forcing* experiments, respectively, in the SATSA region. Contour interval 1hPa.

The DJF near surface (950 hPa) winds changes with respect to the control in the SATSA region are shown in Figure 3.5 and are thoroughly consistent with the MSLP response and shift in the precipitation bands. In the *nh+sh_forcing* and *nh_forcing* experiments the strongest changes (10 m/s) occur over western equatorial Africa in agreement with a northward displacement of the ITCZ and over a diagonal SW-NE band in the tropical Atlantic Ocean between 15ºN and 25ºN which lead to the enhanced rain band mentioned above. There are also strong wind changes around 50-60ºS, 270-300ºE in the Southern Ocean, which are present in the *nh+sh_forcing* and s*h_forcing* experiments. Over the SACZ a weak anticyclonic anomaly is generated and seen in the experiments involving NH forcing.

To analyse the mean meridional circulation we consider the mass streamfunction Ψ_M defined as (e.g. Hartmann 1994): $\Psi_M = \frac{2\pi a \cos(\theta)}{g} \int_0^p [v]\,dp$ where a is Earth's radius, θ the latitude, g gravity, p pressure, v meridional wind and the square brackets denote zonal averages.

With an over bar denoting DJF temporal mean, Figure 3.6 depicts the mean meridional overturning circulation stream function $[\overline{\Psi_M}]$ anomalies with respect to the control run, calculated just over the Atlantic Ocean sector (defined as the portion of the globe between 307.5ºE and 7.5ºE) for the three experiments.

The *nh+sh_forcing* produces a negative anomaly region from 10ºS to 30ºN, indicating that a new uplift region is created around 30ºN in the Atlantic, in agreement with the surface winds convergence zone and positive precipitation anomalies found in the Atlantic Ocean around 20ºN-30ºN. As result there is a weakening of the northern Hadley cell and an intensification of the southern cell, associated with increased descent over the SACZ. In addition, a region of strong positive anomalies is found from 30ºN to 70ºN indicating changes in the Ferrel Cell.

The hemispheric experiments indicate that the SH forcing produces a weak response in terms of stream function. On the contrary, the NH forcing creates a similar anomaly pattern to the one created in the *nh+sh_forcing* experiment, in agreement with the similarities in the surface fields described previously.

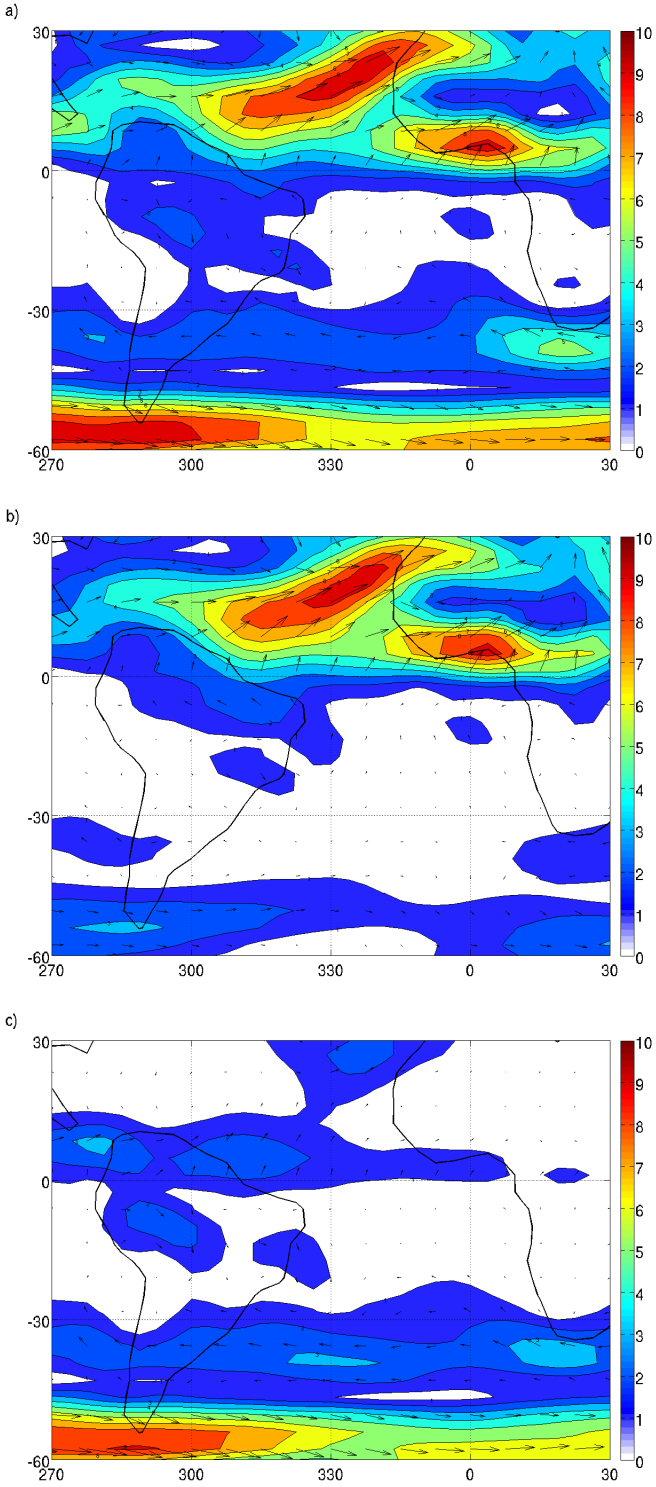

Figure 3.5: DJF mean anomalies with respect to the control of near surface (950 hPa) wind for: a. *nh+sh_forcing*, b. *nh_forcing* and c. *sh_forcing* experiments, respectively, in the SATSA region. Contour interval 1m/s.

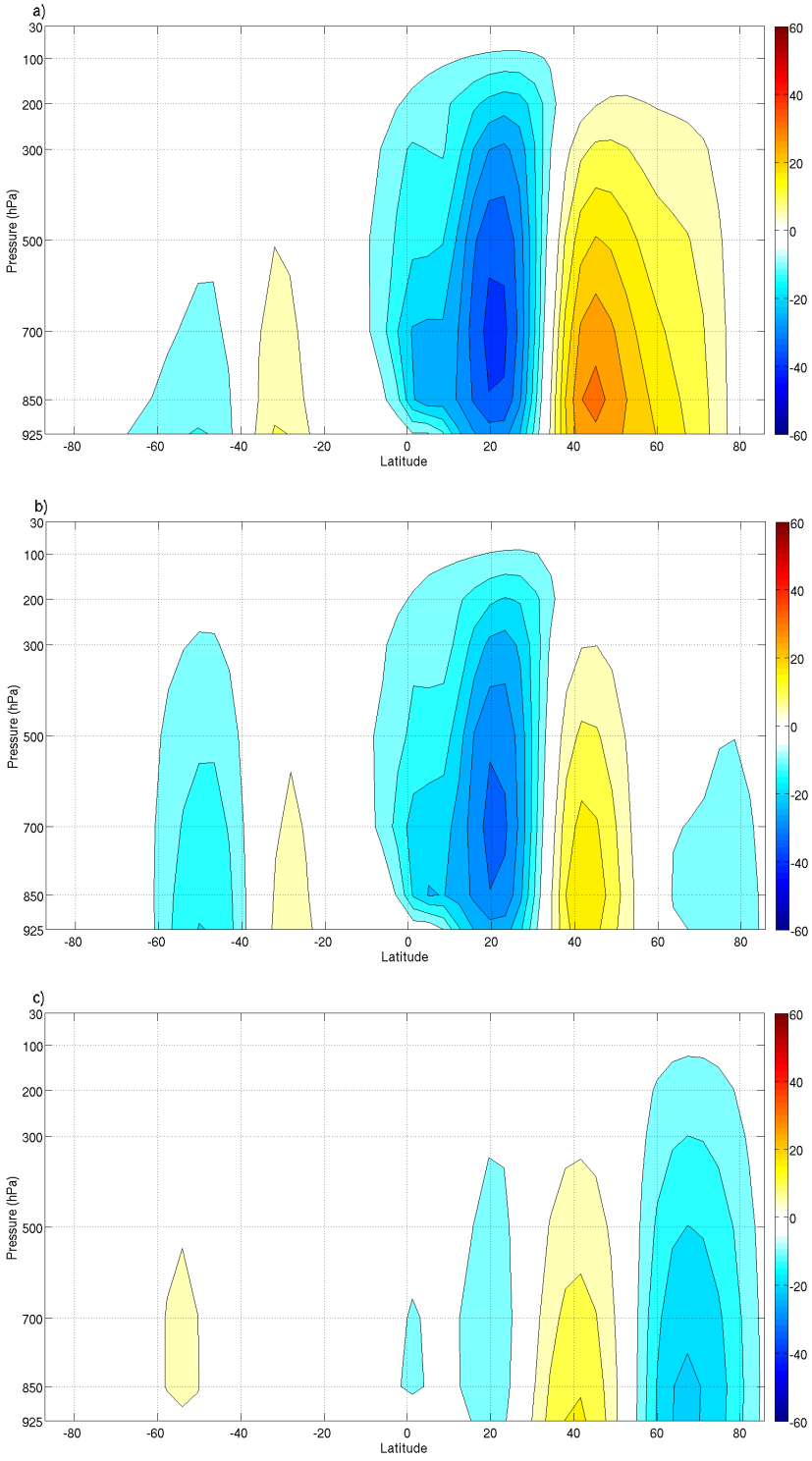

Figure 3.6: DJF mean anomalies with respect to the control of mean meridional overturning circulation stream function over the Atlantic Ocean sector /10^{10} for: a. *nh+sh_forcing*, b. *nh_forcing* and c. *sh_forcing_fix_trop_sst* experiments, respectively. Contour interval 5 m^2/s^2.

To complement the picture, Figure 3.7 shows the velocity potential and divergent wind anomalies at 200 hPa for the three experiments. For the experiment *nh+sh_forcing* a region of upper-level divergence (convergence) is noticed over the north tropical Atlantic (SACZ). Over the SACZ, the strongest gradient of the velocity potential (strongest convergent wind) is noted in two directions: a N-S component originating from the secondary convergence zone around 20ºN-30ºN in the Atlantic Ocean, and a NE-SW component originating from western equatorial Africa.

The hemispheric experiments indicate that the NH component of the forcing is the one that produces the upper-level convergence over SACZ, being the generated anomalies even stronger than those seen in the *nh+sh_forcing* simulation. The SH component of the forcing produces a weak signal over the SACZ, in the opposite direction (generating a weak divergence over the region).

In summary, we can conclude that the total response to the extratropical thermal forcing is predominantly linear with respect to the NH and SH components of the forcing. In particular, the SACZ is weakened by the forcing and this weakening is still produced when only the NH component of the forcing is applied. When the SH component is the only forcing, the SACZ shows some strengthening, which is overcome by the NH forcing. Thus, results indicate that the NH forcing exerts the strongest control on the SACZ's behaviour.

These results thus suggest the following mechanism to explain how the signal is transmitted from the NH extratropics to the SACZ. When the extratropical forcing in the NH is imposed it strongly weakens the north Atlantic subtropical high, weakening the trades and generating a positive SST anomaly to the north of the equator. This induces anomalous surface wind convergence between 20ºN and 30ºN and strong positive precipitation anomalies and generates an uplift region. In turn, this anomalous ascent promotes a change in the Hadley circulation over the tropical Atlantic Ocean in which anomalous descent is favoured over the SACZ, thus inhibiting the development of precipitation (see Figure 3.7).

The hypothesis proposed depends on the generation of a secondary near-surface convergence zone over the northern tropical Atlantic which then leads to changes in the Hadley cell. To test this mechanism we perform additional experiments in which the tropical SST is not allowed to respond

to changes in the surface heat fluxes and thus the secondary rainfall band should not develop.

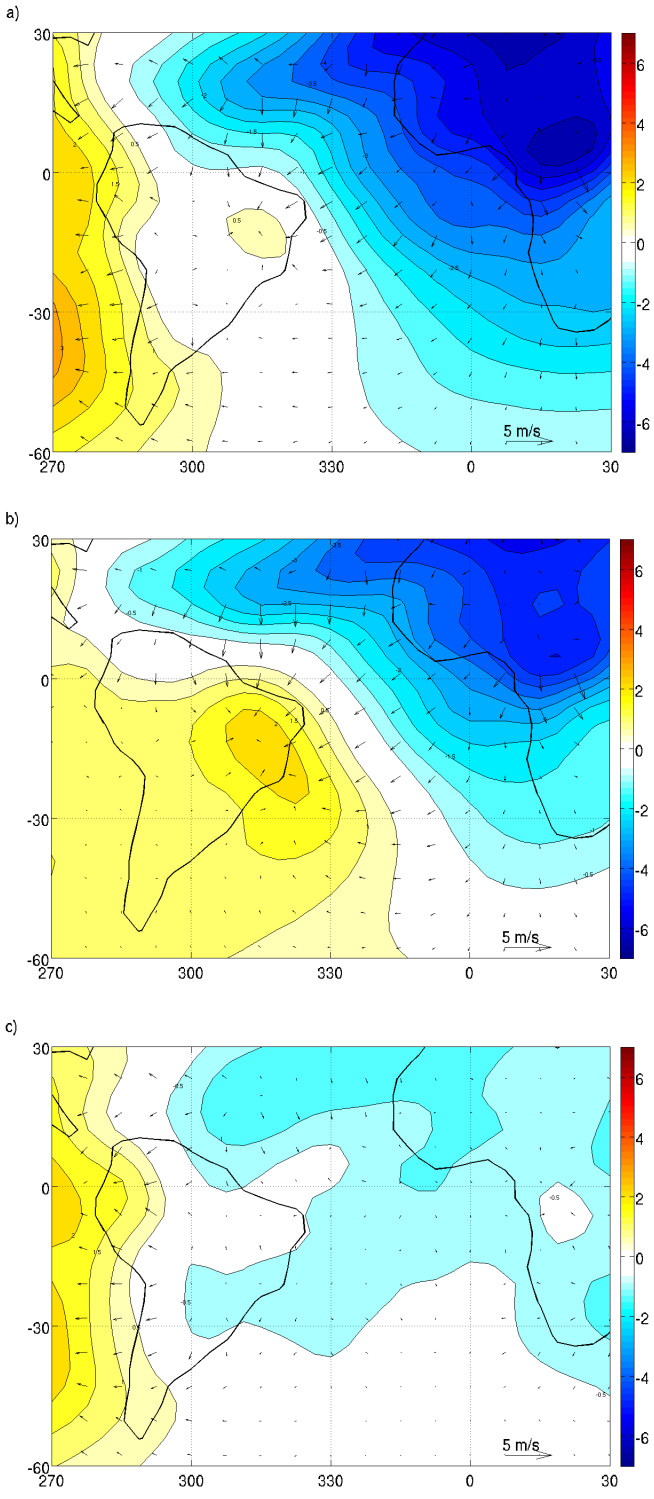

Figure 3.7: DJF mean anomalies with respect to the control of velocity potential (*10^6) and divergent wind for: a. *nh+sh_forcing*, b. *nh_forcing* and c. *sh_forcing* experiments, respectively. Contour interval 0.5 m^2/s.

3.4. SACZ response to the extratropical forcing: Roles of tropical SST and LST over Africa

We start this section briefly presenting the results in which the extratropical forcing (with its components in the two hemispheres) is applied, but the tropical SSTs are not allowed to change.

Figure 3.8 a shows the DJF precipitation anomalies for the experiment *nh+sh_forcing_fix_trop_sst* with respect to the corresponding control case for this configuration, for the SATSA area. As expected, the region of positive precipitation anomalies located in the Atlantic Ocean around 20ºN-30ºN completely vanishes. The response over the ITCZ is greatly reduced although some significant signal is still present over the Atlantic Ocean and Africa. Over the SACZ there is still some response indicating a weakening and slight southward shift as in the *nh+sh_forcing* but changes are much weaker (75% reduction in the signal). The signal obtained in the *nh+sh_forcing_fix_trop_sst* experiment is mostly reproduced by applying the NH portion of the forcing, in particular the northward displacement of the ITCZ over Africa and the weakening over SACZ; the SH forcing produces some signal over SACZ but is weak and of minor extension (not shown).

In the absence of tropical SST response the 200 hPa divergent wind anomalies over the SACZ are weaker (Figure 3.8 b) although a component originating in the region of ITCZ northward displacement over western equatorial Africa can be appreciated.

Therefore, the results obtained in this section confirm that the in the absence of a secondary near-surface convergence zone over the northern tropical Atlantic Ocean the SACZ response is much weaker remaining about 25% of the signal. Is it possible to explain the other 25% by changes in the ITCZ in western Africa? Talento and Barreiro (2015) found that the ITCZ response over Africa completely vanishes when, in addition to fixed tropical SST, the LST over continental Africa is not allowed to change. Therefore, to test the hypothesis that the remaining 25% of the SACZ' signal is remotely induced by the ITCZ changes over Africa, we conduct a last series of simulations in which both tropical SSTs and LSTs over Africa are kept fixed. In Figure 3.9 we show the results for the simulation with forcing in the two hemispheres.

As expected, the precipitation anomalies over Africa completely vanish while over the SACZ, although there are still some anomalies present, are reduced considerably (Figure 3.9 a). Divergent wind in upper levels (Figure 3.9 b) agree with the results of precipitation, not showing any significant signal over the SACZ.

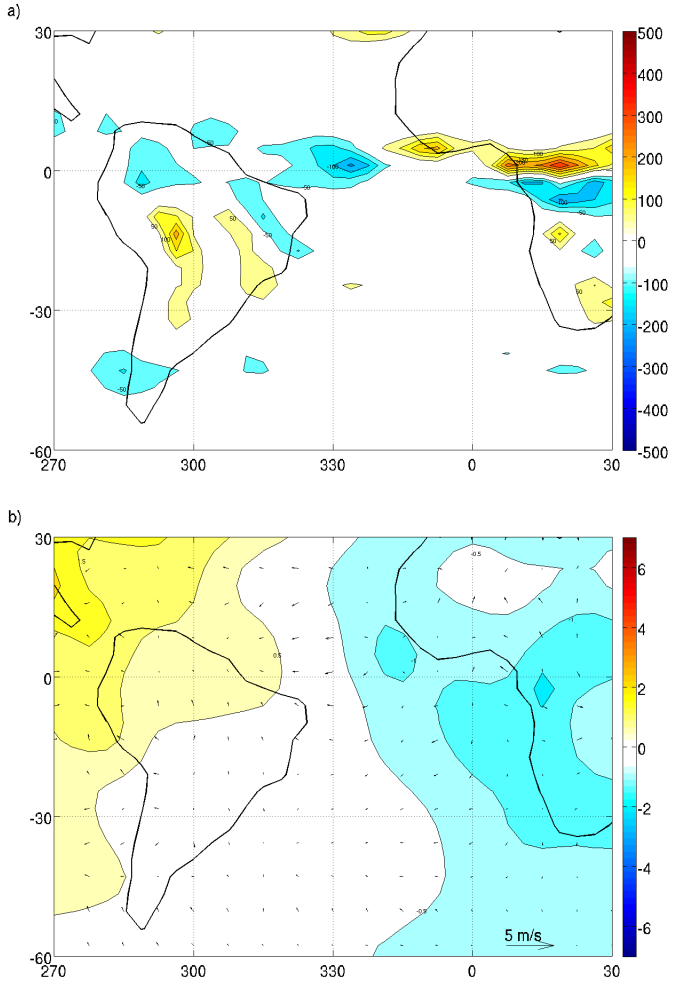

Figure 3.8: *nh+sh_forcing_fix_trop_sst* DJF mean anomalies with respect to the control in the SATSA region of: a. precipitation (contour interval 50 mm/month) and b. velocity potential (*10^6) and divergent wind (contour interval 0.5 m^2/s).

3.5. Summary and conclusions

We investigated the response of the SACZ to an extratropical thermal forcing in an AGCM coupled to a slab ocean model, with realistic surface boundary conditions. The imposed forcing consists of warming in the NH and cooling in the SH, with zero global mean. We further divide the forcing into its northern and southern components to asses their relative roles in affecting the SACZ.

We found that during its peak season (DJF) the SACZ is weakened by the imposed extratropical forcing and that the northern component of it is the one that exerts the most dominant role on this response. When the forcing is applied in the two hemispheres it produces a 31% reduction in the total SACZ rainfall, when only the NH forcing is applied the reduction amounts to 40%, while the application of the SH forcing produces a small increase in the SACZ rainfall.

These results are in agreement with the paleoclimatic and modeling studies that analyse the SACZ response to extratropical forcings.

From Strikis et al. (2015), and assuming linearity of the processes, a warming of the NH would lead to a SACZ weakening and a northward ITCZ shift over South America. Our results agree and also indicate that in the event of a NH warming the SACZ is weakened and that a northward ITCZ displacement occurs over western South America. However, in our simulations the eastern South America's ITCZ response does not shift but weakens, a discrepancy that could be model dependent.

Chiessi et al. (2009) proposed two mechanisms linking the SACZ to the AMO. The first one implied that a cooling of the western south Atlantic would lead to a SACZ weakening; we can not make any statements on this given that in our simulations such mechanism was not triggered (no significant SST changes were found in the vicinity of the SACZ in the western south Atlantic). The second mechanism associated a northward South American ITCZ shift with a SACZ weakening, which is in agreement with our results although we did not find any evidence related to changes in the low level jet (see Figure 3.5 b) as was suggested by Chiessi el al. (2009).

Regarding other model simulations, our findings are in accordance with the ones of Junquas et al. (2012) which indicate that the case of a NH warmer than the SH is expected to produce a weakening of the SACZ during DJF.

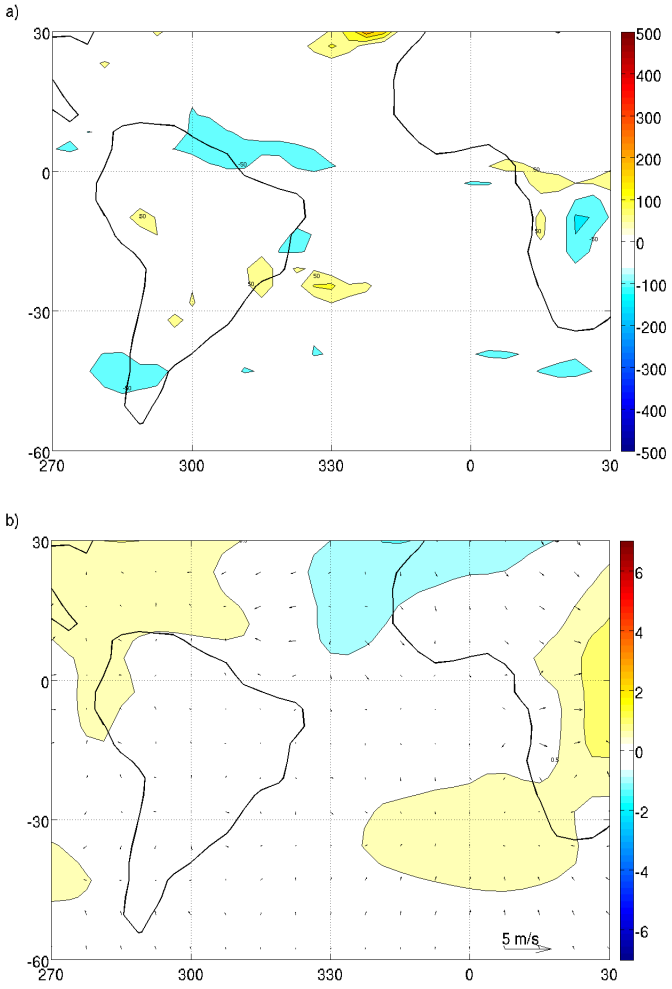

Figure 3.9: Same as Fig. 3.8 for the experiment *nh+sh_forcing_fix_trop_sst_fix_Africa*.

We further proposed that the communication of the signal from the northern extratropics to the SACZ is produced by two overlapping mechanisms. The first mechanism is related to the generation of a secondary convergence zone in the northern tropical Atlantic: when the forcing is applied, changes in the general circulation of the atmosphere occur in a way that a region of surface winds convergence is generated over the Atlantic Ocean in the latitude band 20ºN-30ºN; this

convergence and its associated ascent region further provoke changes in the tropical Hadley circulation over this basin that ends promoting an abnormal descent over the SACZ, inducing a precipitation decrease there. The second mechanism, explaining the remaining 25% of the precipitation decrease, relates changes in the African ITCZ to the SACZ: the extratropical forcing induces a northward ITCZ displacement over Africa, via a Walker-type of circulation this displacement favours subsidence over the northern portion of the SACZ and a consequent decrease in precipitation.

To test the viability of the proposed mechanisms we designed new experiments in which the same forcing patterns are applied but the model configuration is modified.

To test the first mechanism we conducted simulations in which the secondary convergence zone over the northern tropical Atlantic is not developed: simulations with fixed tropical SST. In this case the SACZ precipitation anomalies weaken significantly (75% of signal reduction) highlighting the fundamental role of the tropical SSTs in transmitting the information from the high latitudes to this tropical convergence zone.

The remaining 25% of the precipitation signal over the SACZ was linked to the second proposed mechanism via simulations in which, in addition to fixed tropical SSTs, a restriction over the LST over Africa was imposed. As shown in Talento and Barreiro (2015), not allowing the tropical SSTs nor the LST over Africa to change in response to the remote extratropical forcing will lead to the vanishing of the African ITCZ response and, in this case, this was also associated to the weakening of the SACZ precipitation signal.

In summary, we found that the SACZ response to a warming of the NH and a cooling of the SH high latitudes consists in a precipitation decrease and southward shift, and that the NH component of the forcing is the one that plays the dominant role. It would be desirable to repeat the experiments with other models and to search for this type of signal in climate change projections and Last Glacial Maximum simulations.

Chapter 4. Sensitivity of the tropical climate to an interhemispheric thermal gradient: the role of ocean dynamics

Abstract

This study aims to determine the role of the tropical ocean dynamics in the response of the climate to an extratropical thermal forcing. We analyse and compare the outcomes of coupling an atmospheric general circulation model (AGCM) with two ocean models of different complexity. In the first configuration the AGCM is coupled with a slab ocean model while in the second a Reduced Gravity Ocean (RGO) model is additionally coupled in the tropical region.

We find that the imposition of an extratropical thermal forcing (warming in the Northern Hemisphere and cooling in the Southern Hemisphere with zero global mean) produces, in terms of annual means, a weaker response when the RGO is coupled, thus indicating that the tropical ocean dynamics opposes the incoming remote signal. On the other hand, while the slab ocean coupling does not produce significant changes to the equatorial Pacific sea surface temperature (SST) seasonal cycle, the RGO configuration generates a strong warming in the centre-east of the basin from April to August balanced by a cooling during the rest of the year, strengthening the seasonal cycle in the eastern portion of the basin. We hypothesize that such changes are possible via the dynamical effect that zonal wind stress has on the thermocline depth. We also find that the imposed extratropical pattern affects El Niño Southern Oscillation, weakening its amplitude and low-frequency behaviour, possibly via a frequency entrainment mechanism associated to the intensification of the SST seasonal cycle in the eastern equatorial Pacific Ocean.

4.1. Introduction

Paleoclimatic data (Wang et al., 2004), 20th century observations (Folland et al., 1986) and numerical simulations (Chiang and Bitz, 2005; Kang et al., 2008, 2009; Cvijanovic and Chiang, 2013; Talento and Barreiro, 2015, 2016) have all suggested the capability of an extratropical thermal forcing to affect different features of the tropical climate. The general picture emerging from these studies is that the Inter Tropical Convergence Zone (ITCZ) tends to shift toward the warmer hemisphere at the same time that the atmospheric energy transport is modified to favour the transmission of energy to the colder hemisphere.

In particular, Talento and Barreiro (2015) use an atmospheric general circulation model (AGCM) coupled to a slab ocean model to quantify the relative roles of the atmosphere, tropical sea surface temperatures (SST) and continental surface temperatures in the ITCZ response to an extratropical thermal forcing. They find that if the tropical SSTs are not allowed to change, then the ITCZ response strongly weakens although it is not negligible, in particular, over the Atlantic Ocean and Africa. If, in addition, the land surface temperature over Africa is maintained fixed the ITCZ response completely vanishes, indicating that the ITCZ response to the extratropical forcing is not possible just trough purely atmospheric processes, but needs the involvement of either the tropical SST or the continental surface temperatures. With the same model configuration, Talento and Barreiro (2016) focus on the South Atlantic Convergence Zone (SACZ) and show that, during its peak in austral summer, its response to a warming in the Northern Hemisphere (NH) extratropics and a cooling in the Southern Hemisphere (SH) extratropics consists of a weakening, mostly due to the NH component of the forcing. Both studies showed strong changes in the tropical band where SST, surface winds and precipitation are strongly coupled. Nevertheless, in these studies important ocean dynamics are missing as the slab ocean can only simulate the thermodynamic exchange between the atmosphere and the ocean.

Chiang et al. (2008) explore the impact of an interhemispheric thermal gradient (ITG) on the tropical Pacific climate through simulations performed with an AGCM coupled to a medium-complexity model: a Reduced Gravity Ocean (RGO) model. They find that when the NH is warmer than the SH the annual mean equatorial zonal SST gradient strengthens, associated with an earlier onset and a later retreat of the seasonal cold tongue together with an intensification during the peak

cold season. They also find that El Niño Southern Oscillation (ENSO) activity is sensitive to the ITG, being small ITG optimal for the development of ENSO activity.

Lee et al. (2015) also use and AGCM coupled to a RGO model and analyse the impact of the glacial continental ice sheet topography on the tropical Pacific climate. They suggest that the thickness of the ice sheets, separate from the ice albedo effect, has a significant impact on the tropical climate. They identify two types of responses: a quasi-linear response directly associated with the topographic changes and a nonlinear response mediated through the tropical thermocline adjustment. They find that increasing the thickness of the continental ice sheets produces a southward displacement of the ITCZ and a weakening of the equatorial zonal SST gradient, caused by cooling (warming) in the western (eastern) equatorial Pacific, together with a thermocline deepening to the east. They note that the energy flux approach proposed in Kang et al. (2008, 2009) and Cvijanovic and Chiang (2013) does not appear to explain the ITCZ shifts in these experiments because even though the northern cross equatorial energy transport increases with the ice thickness, the mid-latitude transport decreases.

In this study we would like to further examine the role of equatorial ocean dynamics in the tropical response to an extratropical forcing. Differently from other studies, which focus on just one ocean model at a time, we will analyse and compare the response generated when an AGCM is coupled to a slab ocean model to that obtained when a RGO model is additionally coupled in the tropical oceans.

The chapter is organized as follows. In section 4.2 we describe the models used, with special emphasis in the description of the RGO model and its validation against observational data. The experiments performed are explained in section 4.3. The results can be find in section 4.4, discriminated as regarding annual means, seasonal cycles or ENSO. A summary and conclusions are presented in section 4.5.

4.2. Model Description

The atmospheric model used in this study is the Abdus Salam International Centre for Theoretical Physics (ICTP) AGCM (Molteni 2003; Kucharski et al. 2006) which is a full atmospheric model with simplified physics. We use the model version 40 in its 8-layer configuration and T30 (3.75ºx3.75º) horizontal resolution. Present-day boundary surface conditions, orbital parameters and greenhouse forcing are used.

We analyze the outcomes of coupling the AGCM with two ocean models of different complexity. In the first configuration the AGCM is coupled with a slab ocean model; a monthly-varying ocean heat flux correction is imposed in order to keep the simulated SST close to present-day conditions. In the second configuration, and in order to better reproduce the tropical ocean dynamics, a RGO model is coupled in the tropical region (30ºS-30ºN), while a slab ocean model is applied elsewhere. Also in this setup a monthly-varying ocean heat flux correction is imposed in order to keep the simulated SST close to present-day conditions in both models.

We proceed to describe the RGO model and to validate its results comparing with observational analogous.

4.2.1. Reduced Gravity Ocean Model Formulation

We use an extension of the classical 1 ½ layer RGO model, introduced by Cane (1979) to study the ENSO phenomenon. The extension of the model includes thermodynamics of the upper ocean and allows the prediction of the SST, as in Chang (1994).

The model consists of an upper layer in which mass, heat and momentum obey the conservation laws and a lower layer of infinite depth in which the velocity must be null so that the kinetic energy is finite. With this scheme the stratification in the ocean is simplified as a two layer fluid. The approximation is reasonable for the tropical ocean because of the existence of a sharp thermocline which inhibits the downward propagation of waves generated in the upper ocean (Zebiak, 1985).

Let subindex 1 denote the upper layer and 2 the bottom layer, as shown in Figure 4.1.

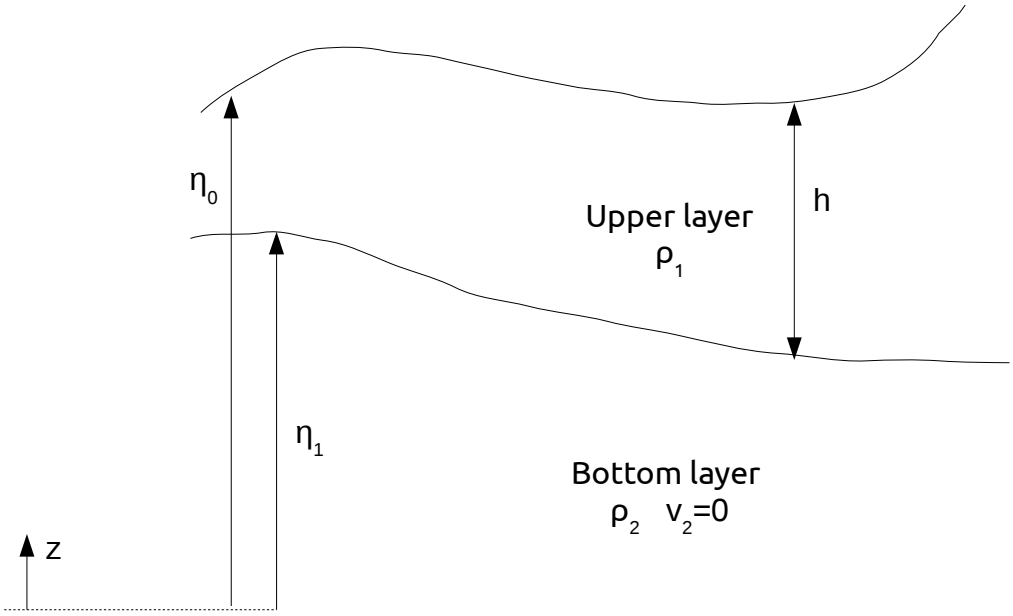

Figure 4.1: Schematic diagram of the vertical structure of the shallow-water model with 1 ½ layers.

Under the shallow water assumption and applying the hydrostatic equation for the upper layer:

$$\frac{dp_1}{dz} = -\rho_1 g$$

$$p_1 = -\rho_1 g z + Constant$$

$$p_1 = p_{atm} + \rho_1 g(\eta_0 - z)$$

$$\frac{1}{\rho_1}\nabla_H p_1 = \frac{1}{\rho_1}\nabla_H p_{atm} + g\nabla_H \eta_0 \qquad (1)$$

And for the bottom layer:

$$\frac{dp_2}{dz} = -\rho_2 g$$

$$p_2 = -\rho_2 g z + Constant$$

$$p_2 = p_{atm} + \rho_1 g \eta_0 + g\eta_1(\rho_2 - \rho_1) - \rho_2 g z$$

$$\frac{1}{\rho_2}\nabla_H p_2 = \frac{1}{\rho_2}\nabla_H p_{atm} + \rho_1 g \nabla_H \eta_0 + g(\rho_2 - \rho_1)\nabla_H \eta_1 \qquad (2)$$

The momentum equations for the layers are:

$$\frac{D\vec{v_{H1}}}{Dt} + f\vec{k}\times\vec{v_{H1}} = -\frac{1}{\rho_1}\nabla_H p_1$$

$$\frac{D\vec{v_{H2}}}{Dt} + f\vec{k}\times\vec{v_{H2}} = -\frac{1}{\rho_2}\nabla_H p_2$$ Considering null velocity in this layer $\nabla_H p_2 = 0$

Then, from (2): $\nabla_H p_{atm} = -\rho_1 g \nabla_H \eta_0 + g(\rho_1 - \rho_2)\nabla_H \eta_1$

Applying the former on (1):

$$\frac{1}{\rho_1}\nabla_H p_1 = -g\nabla_H \eta_0 + g\frac{\rho_1 - \rho_2}{\rho_1}\nabla_H \eta_1$$

$$\frac{-1}{\rho_1}\nabla_H p_1 = g'\nabla_H \eta_1$$ defining the reduced gravity as: $g' = g(\frac{\rho_2 - \rho_1}{\rho_1})$

Noting that $\eta_1 = \eta_0 - h$ $\nabla_H \eta_1 = \nabla_H \eta_0 - \nabla_H h$ and assuming that $\nabla_H \eta_0 \ll \nabla_H h$ (which is a good approximation for the tropical oceans) we obtain $\nabla_H \eta_1 = -\nabla_H h$

Finally, the momentum equation for the upper layer becomes:

$$\frac{D\vec{v}_{H1}}{Dt} + f\vec{k}\times\vec{v}_{H1} = -g'\nabla_H h \qquad (3)$$

On the other hand, the mass conservation for the upper layer leads to:

$$\nabla\cdot\vec{v}_1 = 0$$

$$\nabla_H\cdot\vec{v}_{H1} + \frac{\partial w_1}{\partial z} = 0$$

$$\int_{\eta_1}^{\eta_0}\frac{\partial w_1}{\partial z}dz = -\int_{\eta_1}^{\eta_0}\nabla_H\cdot\vec{v}_{H1}dz$$

$$w_1(\eta_0)-w_1(\eta_1) = -\nabla_H\cdot\vec{v}_{H1}(\eta_0-\eta_1)$$

$$\frac{D\eta_0}{Dt}-\frac{D\eta_1}{Dt} = -\nabla_H\cdot\vec{v}_{H1}(\eta_0-\eta_1)$$

$$\frac{Dh}{Dt} = -h\nabla_H\cdot\vec{v}_{H1}$$

$$\frac{\partial h}{\partial t}+\vec{v}_{H1}\cdot\nabla h+h\nabla_H\cdot\vec{v}_{H1} = 0$$

$$\frac{\partial h}{\partial t}+\nabla\cdot(\vec{v}_{H1}h) = 0 \qquad (4)$$

The system of equations formed by (3) and (4) is the Reduced Gravity Shallow Waters system of equations with 1 ½ layers.

Now, following Zebiak (1985) and Chang (1994), we will proceed to modify the shallow water system and include wind stress, a viscosity term and a thermodynamic equation.

Modifying (3) to include wind stress and viscosity:

$$\frac{\partial \vec{v_{H1}}}{\partial t} + \vec{v_1}\cdot\nabla \vec{v_{H1}} + f\vec{k}\times\vec{v_{H1}} = -g'\nabla_H h + \frac{\tau}{\rho} + \mu\Delta\vec{v_{H1}}$$

$$\frac{\partial \vec{v_{H1}}}{\partial t} + \vec{v_{H1}}\cdot\nabla_H \vec{v_{H1}} + w_1\frac{\partial \vec{v_{H1}}}{\partial z} + f\vec{k}\times\vec{v_{H1}} = -g'\nabla_H h + \frac{\tau}{\rho} + \mu\Delta\vec{v_{H1}}$$

$$\frac{\partial \vec{v_{H1}}}{\partial t} + \vec{v_{H1}}\cdot\nabla_H \vec{v_{H1}} + f\vec{k}\times\vec{v_{H1}} = -g'\nabla_H h + \frac{\tau}{\rho h} + \mu\Delta\vec{v_{H1}} - w_1\frac{\partial \vec{v_{H1}}}{\partial z} \qquad (5)$$

Last, the thermodynamic equation with a diabatic heating and a diffusivity term is:

$$\frac{DT}{Dt} = \frac{Q}{\rho C_p h} + k\Delta T$$

$$\frac{\partial T}{\partial t} + \vec{v_1}\cdot\nabla T = \frac{Q}{\rho C_p h} + k\Delta T$$

$$\frac{\partial T}{\partial t} + \vec{v_{H1}}\cdot\nabla_H T = \frac{Q}{\rho C_p h} + k\Delta T - w_1\cdot\frac{\partial T}{\partial z} \qquad (6)$$

In summary, the shallow waters (SW) equations with 1 ½ layers are:

$$\frac{\partial \vec{v}_{H1}}{\partial t} + \vec{v}_{H1}\cdot\nabla_H \vec{v}_{H1} + f\vec{k}\times\vec{v}_{H1} = -g'\nabla_H h + \frac{\tau}{\rho h} + \mu\Delta\vec{v}_{H1} - w\frac{\partial \vec{v}_{H1}}{\partial z} \qquad (5)$$

$$\frac{\partial h}{\partial t} + \nabla\cdot(\vec{v}_H h) = 0 \qquad (4)$$

$$\frac{\partial T}{\partial t} + \vec{v}_{H1}\cdot\nabla_H T = \frac{Q}{\rho C_p h} + k\Delta T - w_1\frac{\partial T}{\partial z} \qquad (6)$$

That system is comprised of 5 unknown scalar variables (the two components of $\vec{v}_1$, w_1, T and h) and has 4 scalar equations, thus, a new equation or parameterization must be incorporated in order to solve it.

In addition, it should not be expected that (SW) will give a correct solution close to the surface given that the whole upper layer is assumed homogeneous when , in reality, a turbulent well-mixed layer (mixed layer) exists close to the surface. Thus, to predict changes in the SST is important to better resolve the region closer to surface. To do so, a linear and homogeneous frictional layer is added to the model (see Figure 4.2). We will assume that the effective friction in this layer is much larger than below it, concentrating most of the induced Ekman transport.

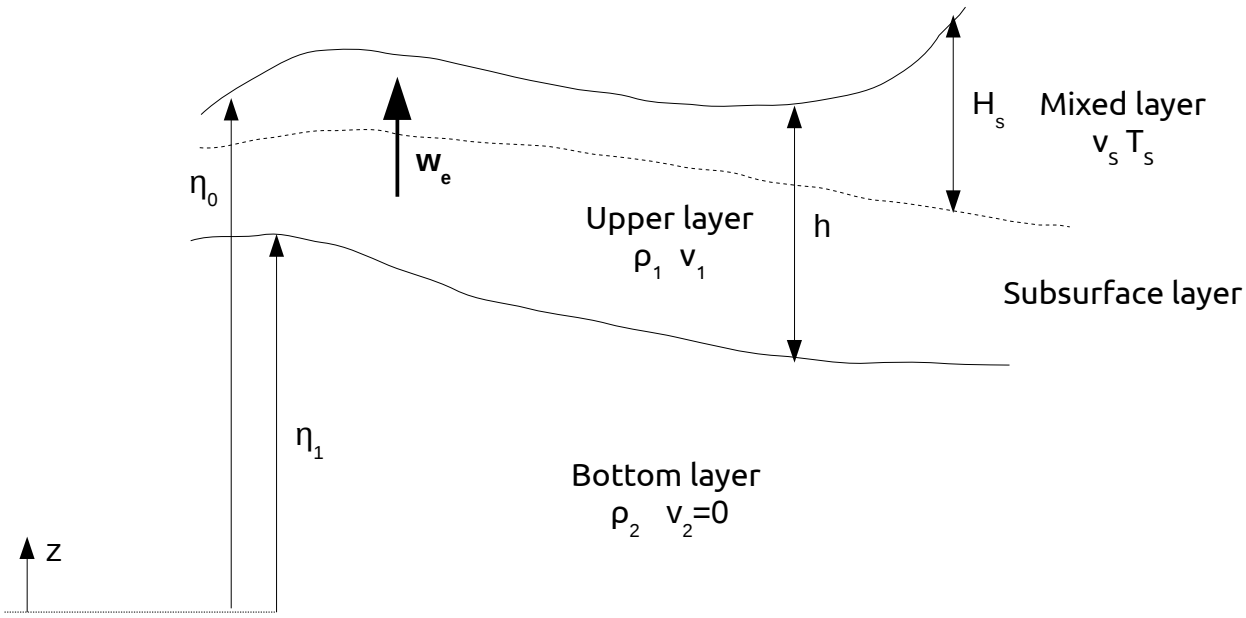

Figure 4.2: Schematic diagram of the vertical structure of the shallow waters model with 1 ½ layers and including a mixed layer in the surface.

The total velocity $\vec{v}_1$ already includes the frictional Ekman flow $\vec{v}_e$ although, by assumption, it is uniformly distributed throughout the entire upper layer. We subtract this flow from the near-surface current ($\vec{v}_s$) and then add it assuming it is uniformly distributed only in the mixed layer:

$$\vec{v}_1 = \vec{v}_S - \vec{v}_e \frac{(H - H_s)}{H}$$

Therefore, the horizontal velocity in the mixed layer $\vec{v}_s$ is:

$$\vec{v}_S = \vec{v}_1 + \vec{v}_e \frac{(H - H_s)}{H}$$

where H_S is the depth of the mixed layer and H the mean thermocline depth.

The components of $\vec{v}_e$ are determined by:

$$-f v_e = \frac{\tau_x}{\rho H_S} - r u_e$$

$$f u_e = \frac{\tau_y}{\rho H_S} - r v_e$$

in which *r* is the Rayleigh friction coefficient for the surface Ekman flow.

Then, the entrainment velocity w_e is determined by the divergence induced by the Ekman pumping: $w_e = H_S \nabla \cdot \vec{v}_S$

In (5) the vertical advection term can be parameterized as:

$$w \frac{\partial \vec{v}_{H1}}{\partial z} = w_e \frac{\vec{v}_{H1}}{h}$$

Going back to the thermodynamic equation (6), the term $w_1 \frac{\partial T}{\partial z}$ is parameterized as $w_e H(w_e) \frac{T - T_e}{H_S}$ in which T_e is the temperature of the entrained water beneath the mixed layer and H is the heavyside step function $H(x)=1 \ \ if\ x \geqslant 0;\ \ H(x)=0 \ \ if\ x<0$

T_e is given by: $T_e = (1-\gamma)T + \gamma T_d$ with γ between 0 and 1 and T_d the subsurface temperature parameterized in terms of the thermocline depth h as:

$$T_d = \overline{T_{50}} + \delta \frac{\partial \overline{T_{50}}}{\partial z}(h - \bar{h})$$

where $\overline{T_{50}}$ is the observed annual mean temperature at 50m of depth from Levitus (1982), δ is a parameter controlling the dependence of T_e on the thermocline depth and $\bar{h}$ is the annual mean thermocline depth when the model is forced with observed wind stress.

Finally, the system of equations becomes:

$$\frac{\partial \vec{v_{H1}}}{\partial t} + \vec{v_{H1}} \cdot \nabla_H \vec{v_{H1}} + f\vec{k} \times \vec{v_{H1}} = -g' \nabla_H h + \frac{\tau}{\rho h} + \mu \Delta \vec{v_{H1}} - w_e \frac{\partial \vec{v_{H1}}}{\partial z}$$

$$\frac{\partial h}{\partial t} + \nabla \cdot (\vec{v_H} h) = 0$$

$$\frac{\partial T}{\partial t} + \vec{v_{H1}} \cdot \nabla_H T = \frac{Q}{\rho C_p h} + k \Delta T - w_e H(w_e) \frac{T - T_e}{H_S}$$

$$\vec{v_S} = \vec{v_1} + \vec{v_e} \frac{(H - H_s)}{H}$$

$$-f v_e = \frac{\tau_x}{\rho H_S} - r u_e$$

$$f u_e = \frac{\tau_y}{\rho H_S} - r v_e$$

$$w_e = H_S \nabla \cdot \vec{v}_S$$

$$T_e = (1-\gamma) T + \gamma T_d$$

$$T_d = \overline{T_{50}} + \delta \frac{\partial \overline{T_{50}}}{\partial z} (h - \bar{h})$$

The unknown variables are: $\vec{v_{H1,}}$ h, w_e, T, T_e, $\vec{v}_S$, $\vec{v}_e$, T_d (11 scalar unknowns) and the number of scalar equations is 11 as well, resulting in a closed system.

We will consider the following values for the parameters: H_S = 50m (depth of mixed layer), H=150m (mean thermocline depth), $\gamma = 0.75$, $\delta = 1$, $\mu = K = 2 * 10^8 cm^2/s$, $\rho = 1 kg/m^3$, $C_p = 4{,}2 * 10^7 J/KgK$ and r= 2 1/day.

An annual-mean heat flux correction is applied to the surface layer of the ocean model, in order to keep the simulated SST close to present-day conditions. The resolution of the RGO model is 1º in latitude and 2º in longitude, applied in the 30ºS-30ºN tropical band. The model is run using an anomaly coupling strategy. That means that, for momentum and heat fluxes, the oceanic and atmospheric components of the model exchange anomalies computed relative to their own model annual mean. The modeled anomalies are then superimposed to the observed annual mean. Sponge layers of 5º wide are introduced at the northern and southern boundaries to eliminate artificial coastal Kelvin waves.

4.2.2. Reduced Gravity Ocean Model validation

A 70-years Control simulation in which the AGCM is coupled to the RGO in the tropics and the slab ocean model elsewhere is produced. The last 50 years of the Control run are used for averaging and comparison with observational analogous. We use the NOAA Extended Reconstructed SST V3b (Smith et al., 2008) and the near-surface winds from the NCEP-NCAR Reanalysis (Kalnay et al., 2006), for the period 1979-2013.

With the imposed heat flux correction, in the Control the simulated annual mean SST strongly resembles the observed pattern (not shown). In addition, the model reasonably captures the main characteristics of the seasonal cycle in the equatorial (2ºS-2ºN) Pacific and Atlantic oceans (Figure 4.3), although in the equatorial Pacific the de-meaned (annual mean removed) simulated SST pattern is weaker and does not extend as westward as the observations. Also, the Pacific cold tongue is not well developed during SH summer.

The Control simulation also reproduces the main mode of variability in the tropical Pacific Ocean quite realistically both in the spatial and temporal domains (Figure 4.4). The first coupled pattern arising from a Singular Value Decomposition (SVD) of the monthly SST and surface wind characterizes ENSO and explains 81% (62%) of the variability in the observations (simulation). The simulated pattern is weaker than the observed and with the SST anomaly maximum located too far eastward. The phase-locking to the seasonal cycle of the simulated pattern peaks during the end of the calendar year as do in the observations, but its distribution is more uniform throughout the year. Both simulated and observed spectra show significant peaks relative to a red noise null hypothesis from 16 to 60 months.

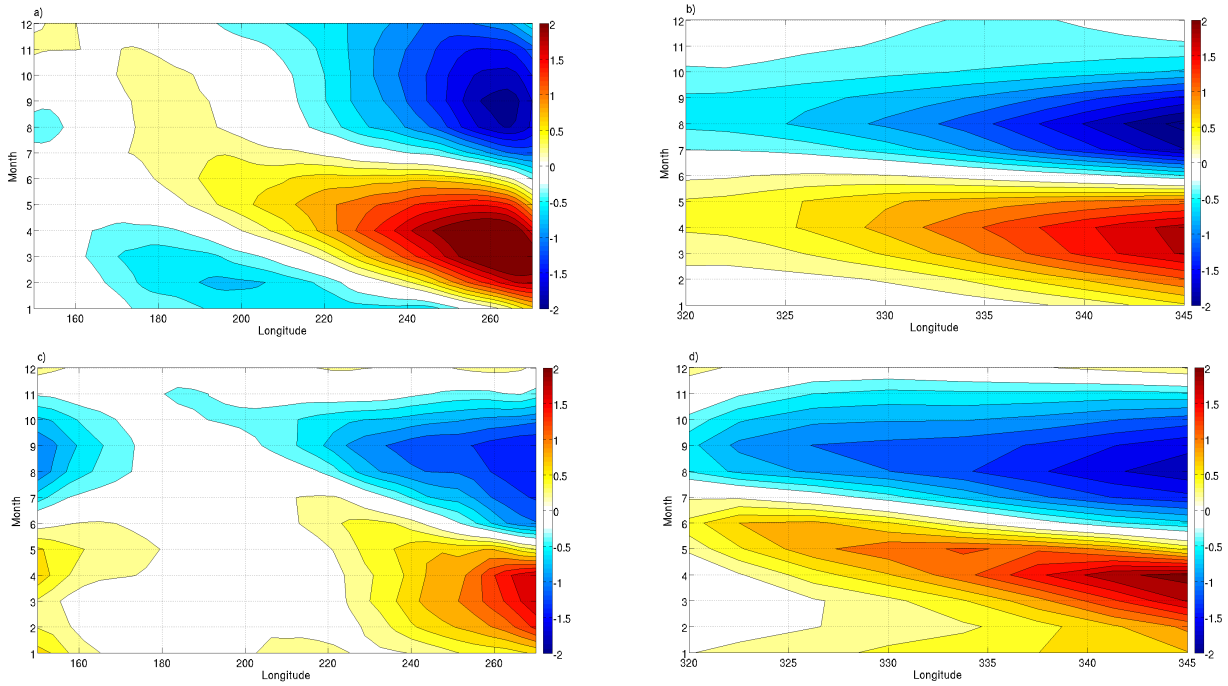

Figure 4.3: a. and b.: De-meaned SST seasonal cycle from NOAA SST data (Smith et al., 2008) in the Equatorial Pacific (2°S- 2°N, 150°E-270°E) and Atlantic (2°S-2°N, 320°E-345°E), respectively. c. and d.: De-meaned SST seasonal cycle for *Control_slab+rgo* in the Equatorial Pacific and Atlantic, respectively. Contour interval: 0.2°C.

4.3. Experimental Design

The experiments designed to study the response of the tropical climate to an extratropical thermal forcing are as follows.

The applied forcing pattern consists in cooling in one hemisphere and warming in the other poleward of 40°, applied only over ocean grid points, and with a resulting global average forcing equal to zero. This pattern is similar to the one used in Kang et al. (2008) and it is intended to represent the asymmetric temperature changes associated with glacial-interglacial and millennial-scale climate variability. The forcing pattern is superposed to a background state and is obtained as explained in the following paragraphs. Let θ denote latitude, ψ longitude and lsm the land surface mask i.e. lsm=1 over land, lsm=0 over sea.

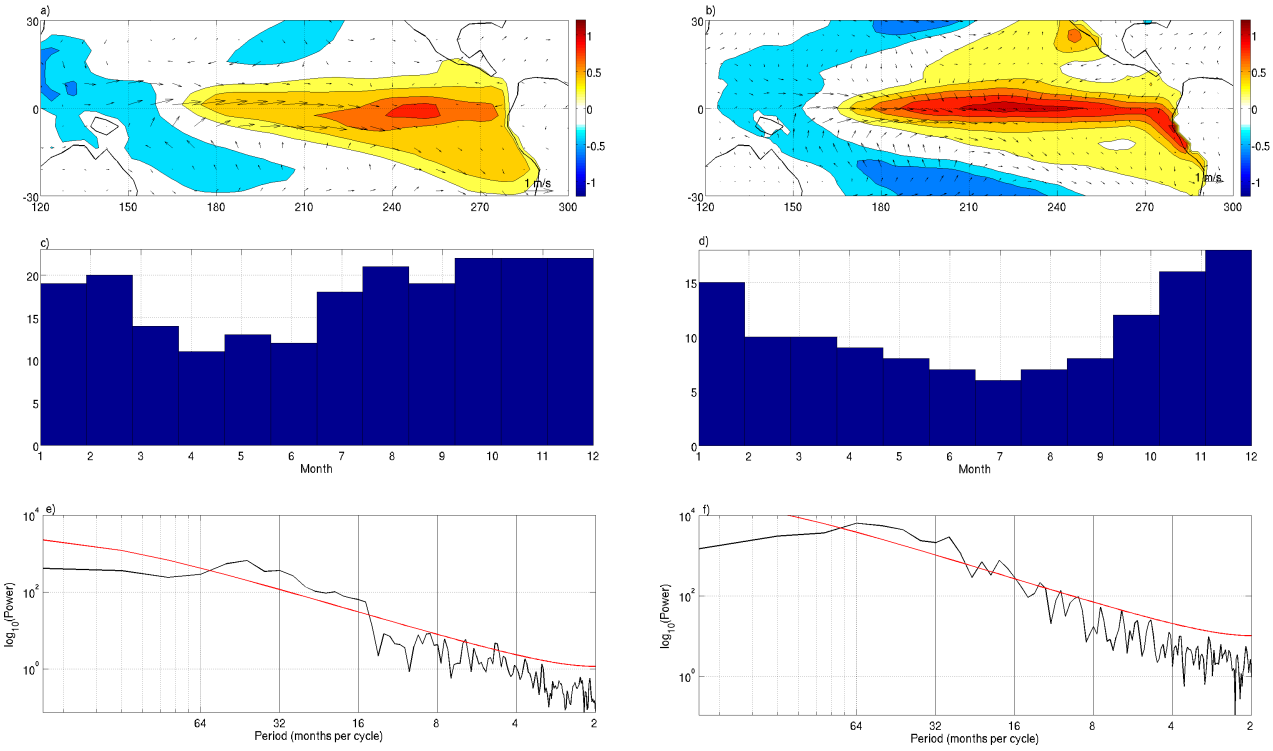

Figure 4.4: First SVD pattern of SST and near-surface winds in the tropical Pacific Ocean (30°S-30°N, 120°E-300°E) for the *Control_slab+rgo* experiment (left) and NOAA SST and reanalysis data (right; Smith et al., 2008; Kalnay et al., 2006). a. and b.: Spatial pattern; contour interval 0.2°C. c. and d.: Histogram showing phase-locking to the seasonal cycle. e. and f.: Spectral analysis, the red line indicates the red noise spectrum.

Consider h to be:

$$h(\theta,\psi) = -A\sin\left(\frac{\theta+40}{50}\pi\right)*(1-lsm(\theta,\psi)) \quad \text{for} \quad \theta\in[-90,-40]$$

$$h(\theta,\psi) = 0 \quad \text{for} \quad \theta\in[-40,40]$$

$$h(\theta,\psi) = -A\sin\left(\frac{\theta-40}{50}\pi\right)*(1-lsm(\theta,\psi)) \quad \text{for} \quad \theta\in[40,90]$$

where A (W/m^2) denotes the intensity of the forcing.

Then, let h_{SH} and h_{NH} be the integral of h over the SH and NH, respectively:

$$h_{SH} = \int_{\psi=0}^{\psi=2\pi} \int_{\theta=-\pi/2}^{\theta=0} h(\theta,\psi)\, d\theta\, d\psi$$

$$h_{NH} = \int_{\psi=0}^{\psi=2\pi} \int_{\theta=0}^{\theta=\pi/2} h(\theta,\psi)\, d\theta\, d\psi$$

Finally, the applied forcing pattern H is defined as:

$$H(\theta,\psi) = h(\theta,\psi) \quad \text{for} \quad \theta \in [-90,-40]$$

$$H(\theta,\psi) = 0 \quad \text{for} \quad \theta \in [-40,40]$$

$$H(\theta,\psi) = \frac{-h_{SH}}{h_{NH}} * h(\theta,\psi) \quad \text{for} \quad \theta \in [40,90]$$

We only consider the forcing pattern corresponding to the values A=0 (Control runs without any forcing) and A=50 W/m^2 (see Figure 4.5). The selected sign convention is positive out of sea. Therefore, positive values of the forcing could be thought as representing a situation where the atmosphere is dry and colder than the ocean below it so that there is a strong ocean-to-atmosphere net heat flux.

As mentioned before we use two ocean models, and for each setup a Control and a forced run are produced. When the AGCM is coupled to a slab ocean model, the experiments are named: *Control_slab* and *Forced_slab*. If an RGO is used in the tropical band, while the slab ocean model is applied elsewhere the corresponding experiments are named: *Control_slab+rgo* and *Forced_slab+rgo*. In all the simulations the model was run for 70 years and the last 50 are used for averaging. Running the simulations for 70 years proved to be more than enough to reach the equilibrium; a time scale of 10 years was estimated to be the time span necessary for adjustment. In Table 4.1 we summarize the experiments.

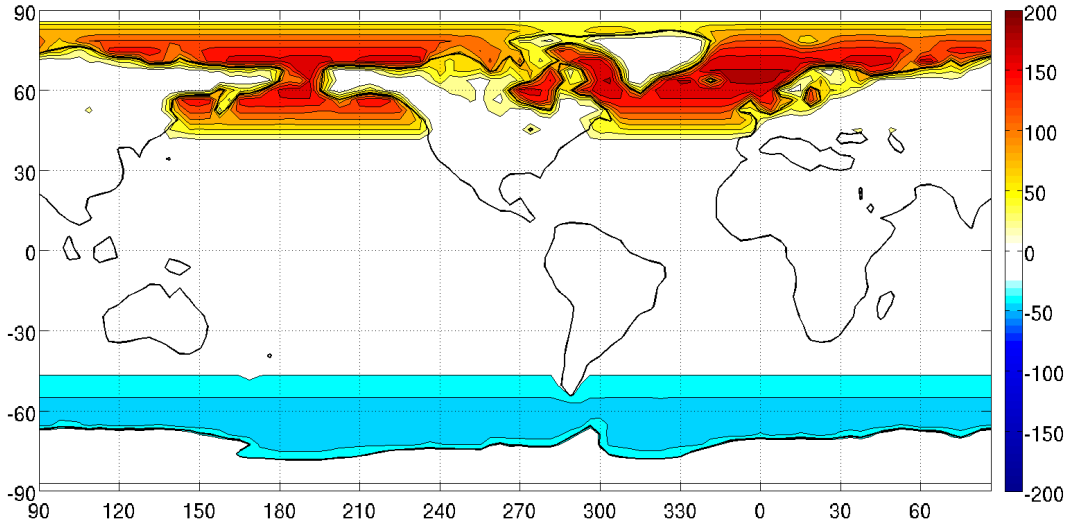

Figure 4.5: Forcing pattern. The sign convention is positive out of sea. Contour interval 20 W/m^2.

Table 4.1: Experiment summary.

Experiment Name	**Ocean model**	**Forcing pattern H**
Control_slab	Slab ocean model globally	A=0
Forced_slab	Slab ocean model globally	A=50 W/m^2
Control_slab+rgo	RGO model in 30°S-30°N, slab ocean model elsewhere	A=0
Forced_slab+rgo	RGO model in 30°S-30°N, slab ocean model elsewhere	A=50 W/m^2

4.4. Results

First we analyse and compare the annual mean anomalies generated by the extratropical forcing with the two configurations implemented. Second, we will focus in the tropical Pacific climate and study the changes produced to the seasonal cycle for both setups. Finally, we will briefly investigate possible changes in ENSO activity when the RGO is coupled in the tropical oceans.

4.4.1. Annual means

In this subsection we compare the results obtained with the two implemented configurations in terms of annual means of different fields. The results are presented in the form of anomalies with respect to the corresponding Control case.

Figure 4.6 shows the near surface air temperature (NSAT) anomalies with respect to the corresponding Control for the two configurations. In both experiments there is a generalized warming (cooling) in the NH (SH), while in the southern tropics a strengthening of the zonal gradient is evident. The most pronounced differences between the two configurations are seen in the tropical region, in which the slab+rgo configuration anomalies tend to be up to 1ºC weaker than the slab configuration anomalies. In particular, the equatorial Pacific cooling seen in the slab configuration is no longer present in the rgo+slab configuration, and the southeastern ocean basins do not cool as much. This suggests that, overall, ocean dynamics tends to oppose changes in the annual mean conditions. In the extratropics the differences between the two configurations are almost not noticeable, although regions of up to 2ºC are noted in the vicinity of the Antarctic Peninsula and Greenland.

As a consequence, tropical changes in precipitation are weaker when using the RGO: while in both experiments the most pronounced feature is a northward shift of the ITCZ, anomalies for the slab+rgo configuration are much weaker (Figure 4.7). Also, in the slab configuration strong changes of tropical precipitation are found equally over the three ocean basins, but for the slab+rgo setup the most intense anomalies are seen over the Atlantic Ocean concurrent with a still relatively strong

cross-equatorial SST gradient and suggesting a larger role for continental temperatures in controlling the position of the ITCZ (as in Talento and Barreiro, 2015). Changes in the subtropical convergence zones are also weaker in the slab+rgo configuration, differently from the southward shift seen in the slab configuration. In particular for the case of the South Atlantic Convergence Zone, this result is consistent with Talento and Barreiro (2016), which showed that during southern summer the weakening of the SACZ is related to the development of a region of strong rainfall in the tropical north Atlantic.

As expected from the above results, both experiments present similar patterns of near surface (950 hPa) wind anomalies (Figure 4.8): anomalous northward winds associated with the ITCZ northward displacement in the tropics, and anomalous westerly winds over the Southern Ocean. The *Forced_slab+rgo* response is weaker in the tropics but stronger over the Southern Ocean, compared to the *Forced_slab* response. Similar pictures of a weaker response in the case of slab+rgo configuration can be seen in upper-level winds, mean sea level pressure and mass stream-function (not shown).

To summarize, in Figure 4.9 we present the northward atmospheric energy transport for the Control and forced runs in the two configurations implemented. As can be seen, while the Control runs display almost an identical transport, the forced runs significantly disagree in magnitude in the tropical region, with the slab configuration producing the strongest changes with an increase of the transport toward the southern high latitudes. The energy flux equator is located around 17ºN (13ºN) for the slab (slab+RGO) configuration.

4.4.2. Seasonal Cycle

As the previous subsection showed, the most pronounced differences between the two implemented configurations are found in the tropical band. Therefore, for the analysis of variations in the seasonal cycle we will focus on the 30°S-30°N region.

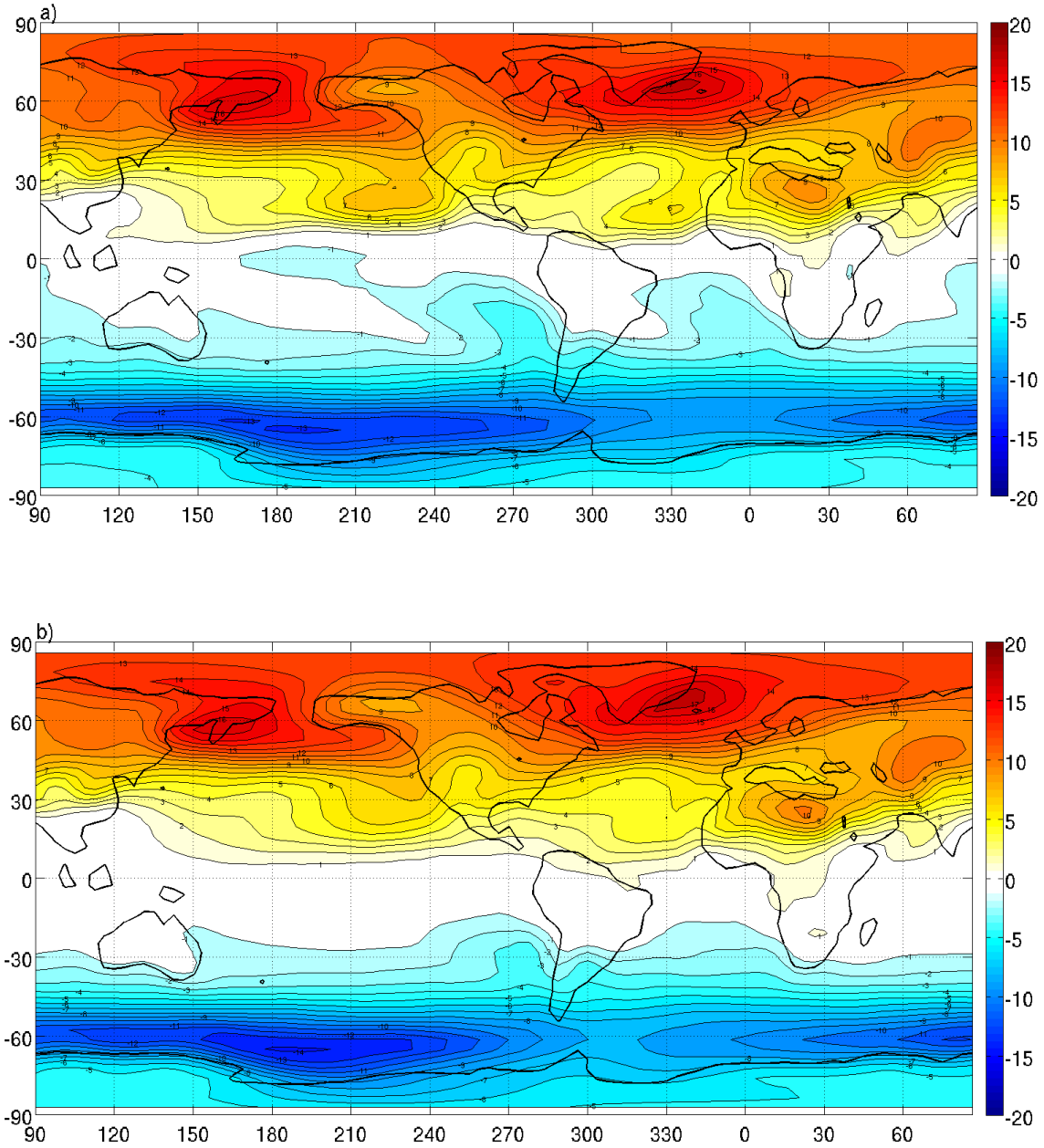

Figure 4.6: Annual mean anomalies with respect to the control of NSAT for: a. *Forced_slab* and b. *Forced_slab+rgo*, respectively. Contour interval 1°C.

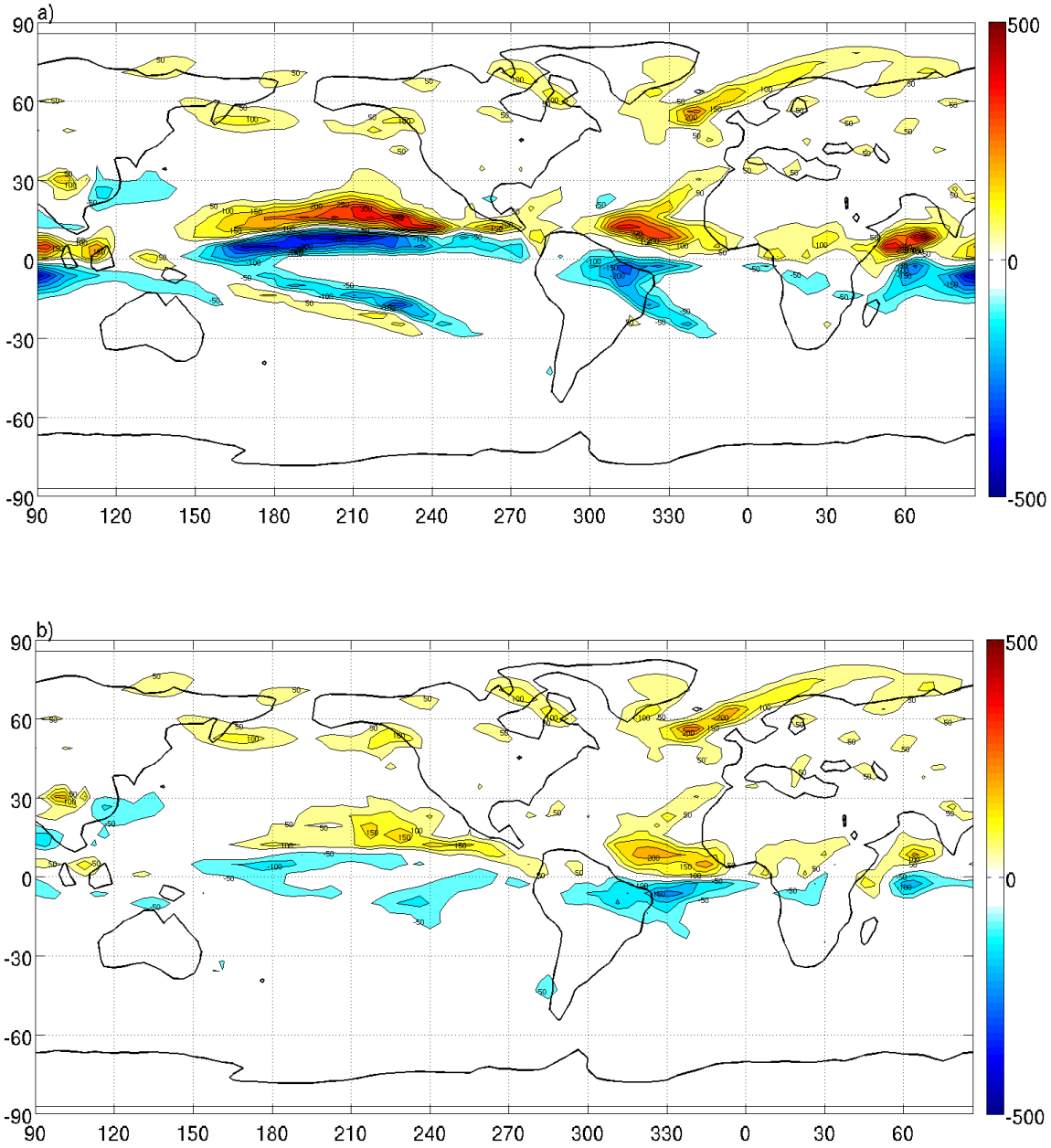

Figure 4.7: Annual mean anomalies with respect to the control of precipitation for: a. *Forced_slab* and b. *Forced_slab+rgo*, respectively. Contour interval 50 mm/month.

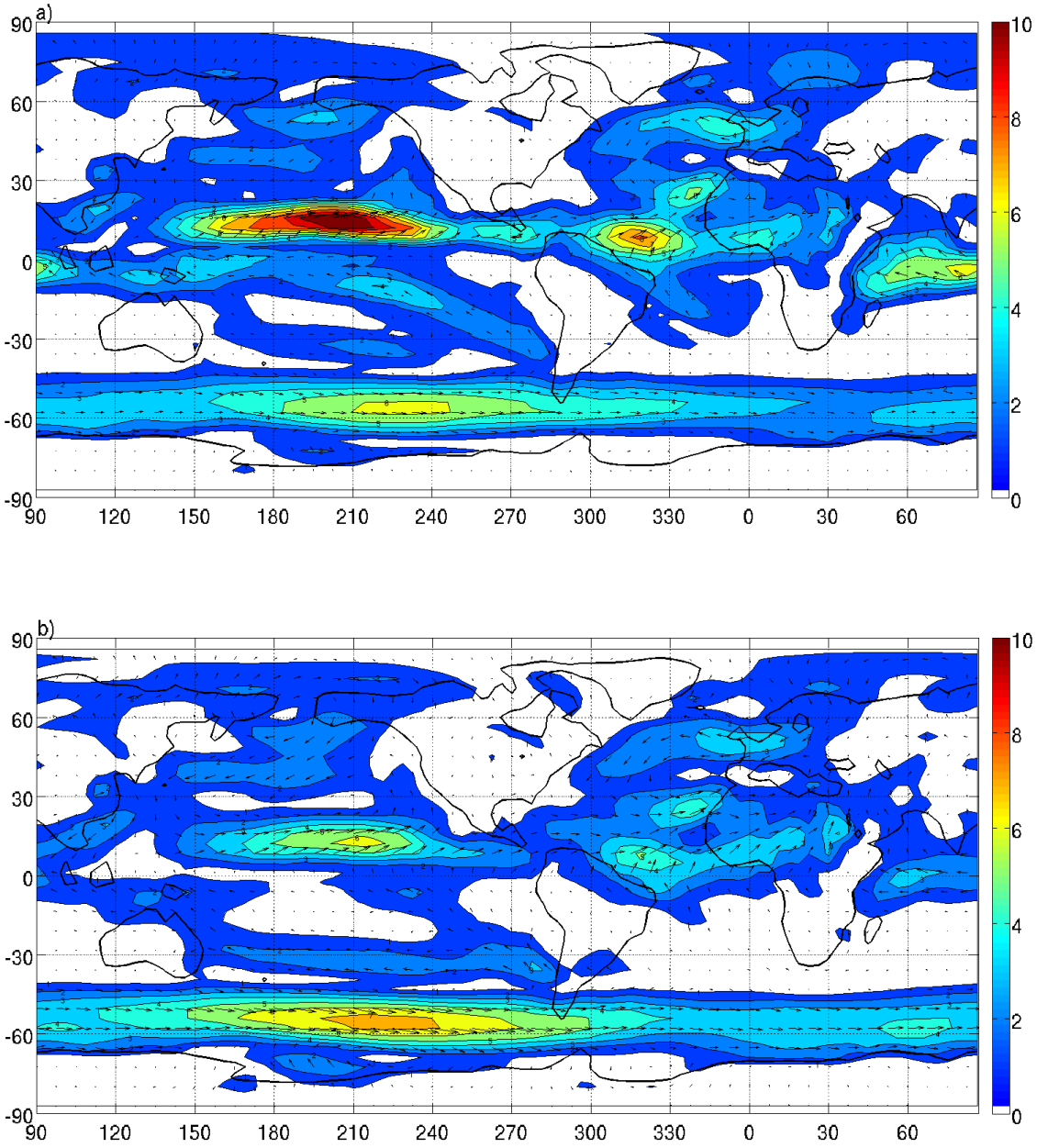

Figure 4.8: Annual mean anomalies with respect to the control of near-surface (950 hPa) wind for: a. *Forced_slab* and b. *Forced_slab+rgo*, respectively. Contour interval 1 m/s.

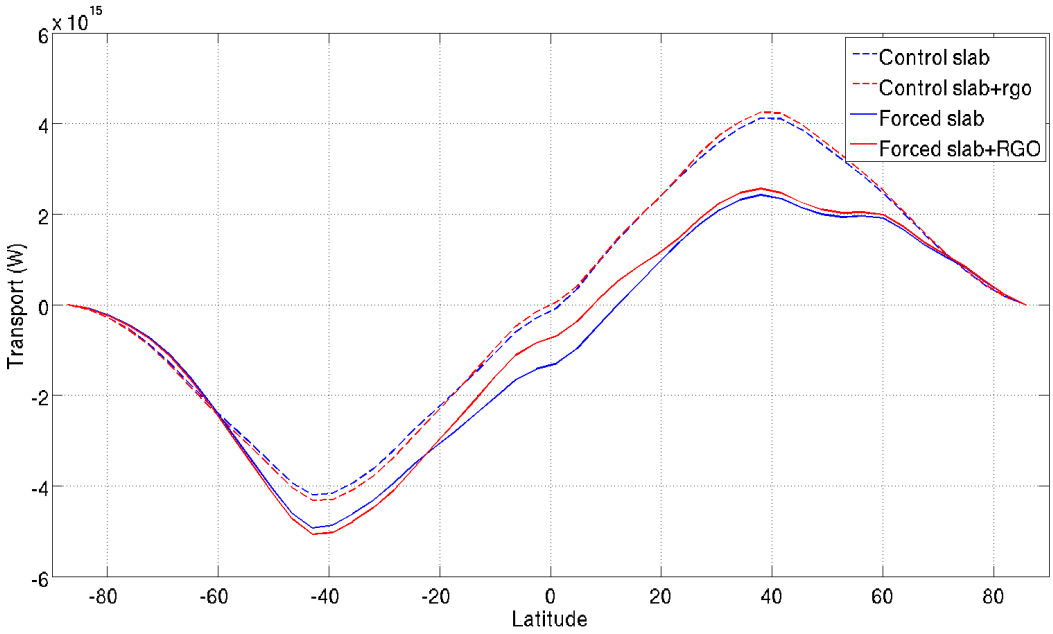

Figure 4.9: Northward atmospheric energy transport for the experiments: *Control_slab*, *Control_slab+rgo*, *Forced_slab* and *Forced_slab+rgo*.

Three-month means of SST and near-surface wind changes for the tropics are shown in Figure 4.10. In the Pacific Ocean, for the *Forced_slab* experiment negative SST anomalies are seen reaching the Equator (or even more to the north) in all 4 seasons, being September-November (SON) the period of strongest cooling and the June-August (JJA) period the one in which this negative anomalies have the weakest penetration onto the NH. Meanwhile, for the *Forced_slab+rgo* experiment the negative SST anomalies barely reach the Equator and, in fact, positive anomalies are the ones penetrating onto the SH for the seasons March-May (MAM) and JJA. Consistent with these changes in response, the equatorial anomalous winds in the slab configuration are mainly easterlies throughout the year, while in the slab+rgo configuration they have a marked northward component and are eastward during MAM season. Also, the equatorial Atlantic tends to warm up during most of the year when using the RGO model.

Equatorial (2ºS-2ºN) de-meaned seasonal cycles for near-surface zonal wind and SST anomalies in the Pacific basin for the two experimental configurations are shown in Figures 4.11 and 4.12, respectively. In *Forced_slab* there are eastward (westward) near-surface wind anomalies from December to May (June to November) distributed along the basin. The positive wind anomalies in

the *Forced_slab* are quite uniform along the basin, although there are maximums in the western and eastern ends during December-February (DJF). The negative anomalies during the second half of the year are maximal in the central-eastern basin. In the slab configuration, the equatorial SST response to these wind anomalies is, however, very weak (Figure 4.12 a). On the other hand, when the RGO is coupled (and although the annual mean anomalies were even weaker than for the slab configuration, Figure 4.6) there are significant changes occurring to the seasonal cycle of SST in the center-east of the basin: from April to August (October to December) the forced run produces a warming (cooling) of up to 1ºC (-0.8ºC). The location and timing of these anomalies lead to a substantial strengthening of the SST seasonal cycle in the eastern Pacific Ocean (overlap Figure 4.12 b on the *Control_slab+rgo* SST seasonal cycle showed in Figure 4.3 c).

The thermocline depth shows consistent changes when the RGO is used (Figure 4.13): a deepening in the east of the basin starting around March and finishing in July, consistent with the warmer SSTs seen in the region (with 1 month lag). Considering the wind anomalies of the slab setup (Figure 4.11 a) as the forcing pattern for the ocean dynamics derived from the extratropical signal, this thermocline deepening pulse appears to be initiated during the SH summer in the west of the basin (due to a weakening of the trades) and is propagated eastward as a Kelvin wave, reaching the eastern boundary 2 months later. The deepening of the eastern Pacific thermocline is concurrent with a shallowing in the western Pacific particularly from May to July, and vice versa (but less obvious) in other seasons of the year. In the second half of the year the strengthening of the trades locally shallows the thermocline in the eastern Pacific and the western Pacific recovers its mean depth.

In summary, the equatorial near-surface zonal wind changes caused by the extratropical forcing seen in the slab configuration induce dynamical ocean-atmosphere coupling that generates seasonal changes in the SST field when the RGO is used. This results in a late austral fall warming and a cooling in spring and summer in the equatorial eastern Pacific, leading to a strengthening of the SST seasonal cycle with consistent changes in the thermocline depth.

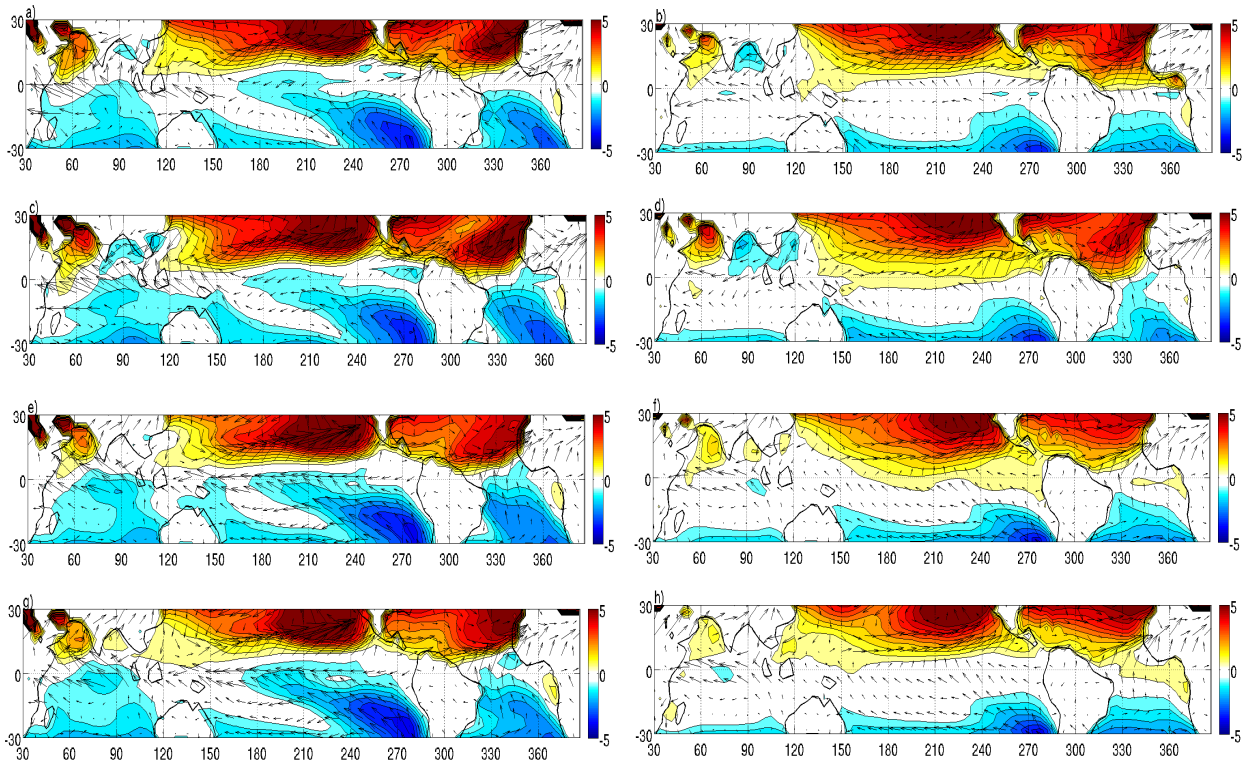

Figure 4.10: Seasonal SST and near-surface wind anomalies with respect to the control for *Forced_slab* (left) and *Forced_slab+rgo* (right). a. and b.: December-February; c. and d. March-May; e. and f.: June-August; g. and h.: September-November. Contour interval 0.5°C.

4.4.3. ENSO

In this subsection we investigate how the interannual variability in the tropical Pacific is affected by the interhemispheric SST gradient induced by the imposed forcing.

The leading pattern of co-variability of SST and near-surface wind in the tropical Pacific basin when the extratropical forcing is applied is weaker than that obtained when no forcing is implemented (Figure 4.14 a and b), and explains a smaller percentage of the total variability (46% compared to 62%). The phase-locking to the seasonal cycle (Figure 4.14 c and d) is also modified being more uniformly distributed and with a peak season going from July to the end of the calendar year. The frequency spectrum of the ENSO pattern under the effect of the extratropical forcing is characterized by shorter periods than in the absence of the forcing and has a peak at 24 months (Figure 4.14 f).

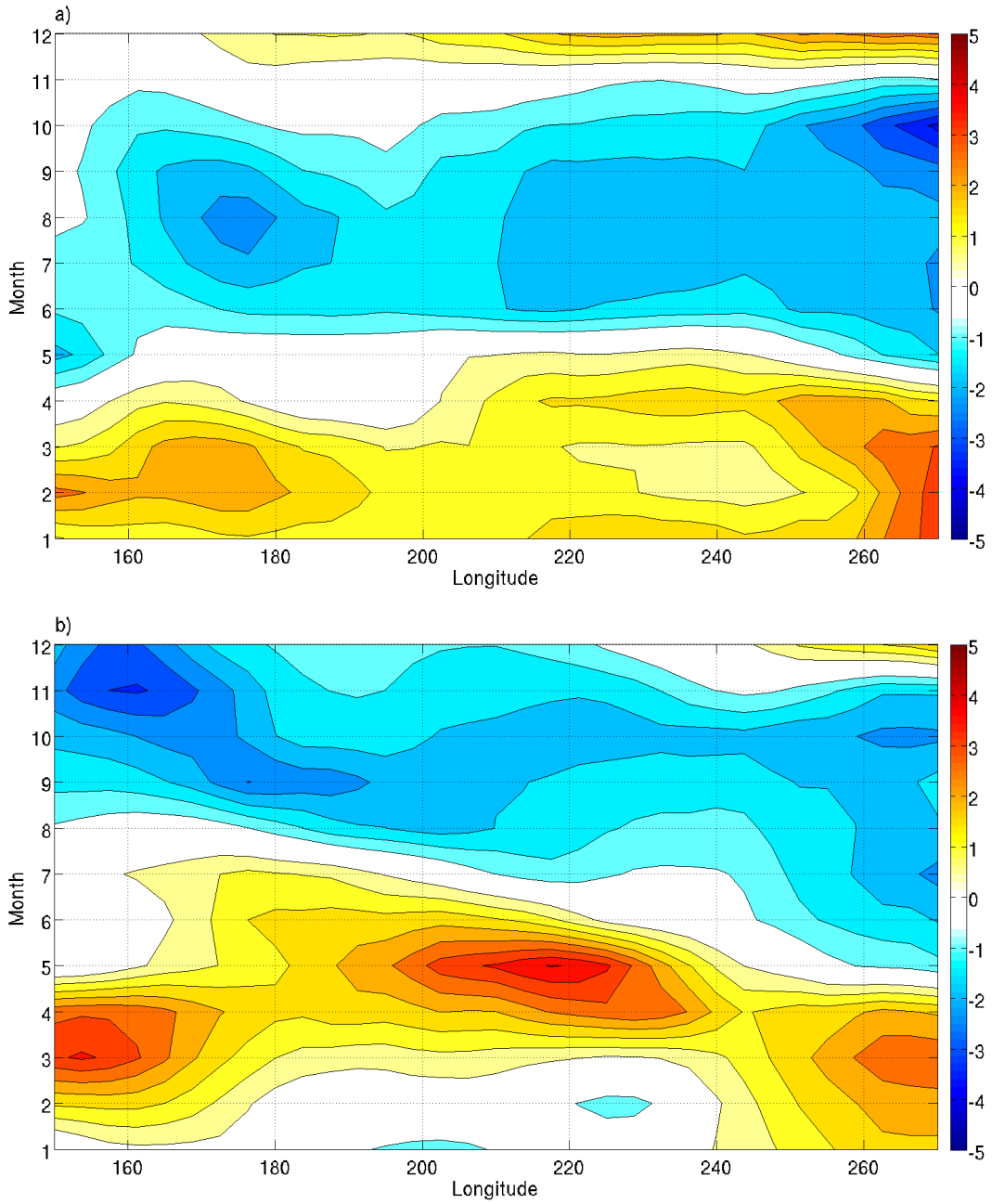

Figure 4.11: Equatorial Pacific Ocean (2°S-2°N, 150°E-270°E) de-meaned near-surface (950 hPa) zonal wind anomalies seasonal cycle for: a. *Forced_slab* and b. *Forced_slab+rgo* experiments, respectively. Contour interval: 0.5 m/s.

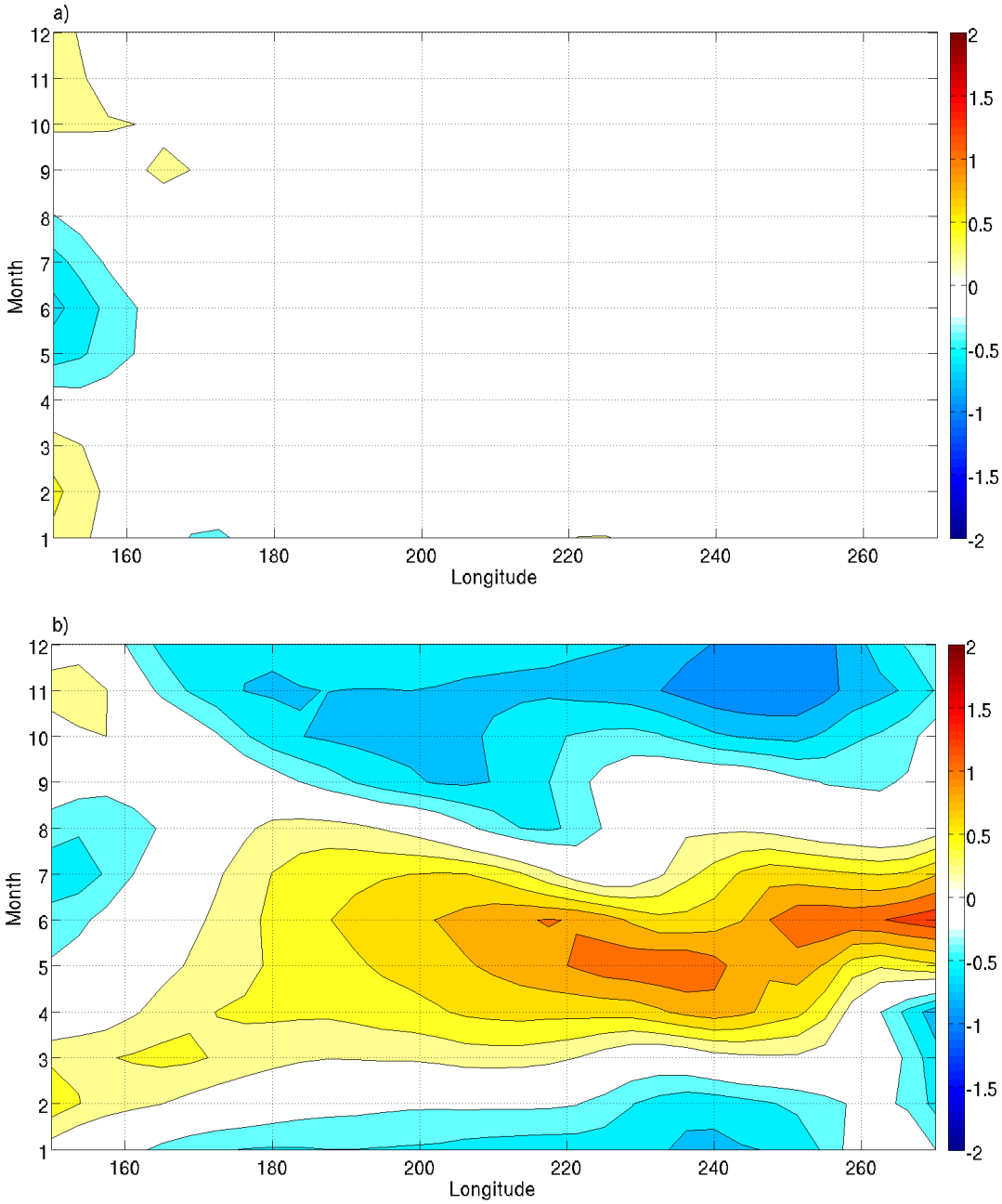

Figure 4.12: Equatorial Pacific Ocean (2°S-2°N, 150°E-270°E) de-meaned SST anomalies seasonal cycle for: a. *Forced_slab* and b. *Forced_slab+rgo* experiments, respectively. Contour interval: 0.2°C.

The weakening of the ENSO activity can be understood in relation to the changes produced by the extratropical forcing on the SST seasonal cycle in the eastern Pacific Ocean. According to the non-linear frequency entrainment mechanism (Chang et al., 1994) ENSO amplitude is anticorrelated

with the strength of the SST seasonal cycle. The frequency entrainment implies that a self exciting oscillator (like ENSO) will give up its intrinsic mode of oscillation in the presence of a strong external forcing (like a strong seasonal SST cycle) and acquire the frequency of the applied oscillating forcing. Therefore, in our case, as the extratropical forcing generates a significant strengthening of the east Pacific SST seasonal cycle, a weakening of ENSO is expected.

Assuming a linear behaviour holds, our result of ENSO weakening is also in agreement with Timmermann et al. (2007). These authors analyse fully coupled GCMs in the context of an Atlantic Meridional Overturning Circulation (AMOC) slowdown, producing a generalized cooling of the NH and warming in the SH, and find that most of the models predict a ENSO intensification attributed to a seasonal cycle weakening. The weakening of ENSO activity in the presence of an northward ITG is also consistent with the work of Chiang et al. (2008) who use a model configuration similar to ours: an AGCM coupled to a RGO model. Although they do not attempt to explain the causes, they find that ENSO is sensitive to ITG with maximal activity when the ITG is close to zero and a weakened performance as the gradient increases in any direction.

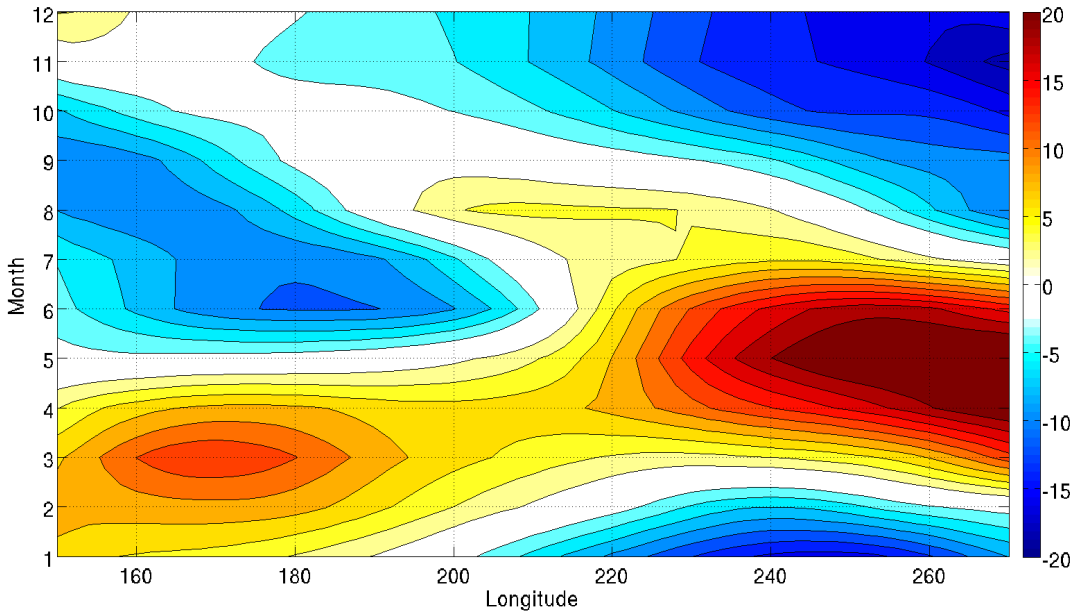

Figure 4.13: Equatorial Pacific Ocean (2°S-2°N, 150°E-270°E) de-meaned thermocline depth anomalies seasonal cycle for the *Forced_slab+rgo* experiment. Contour interval: 2 cm.

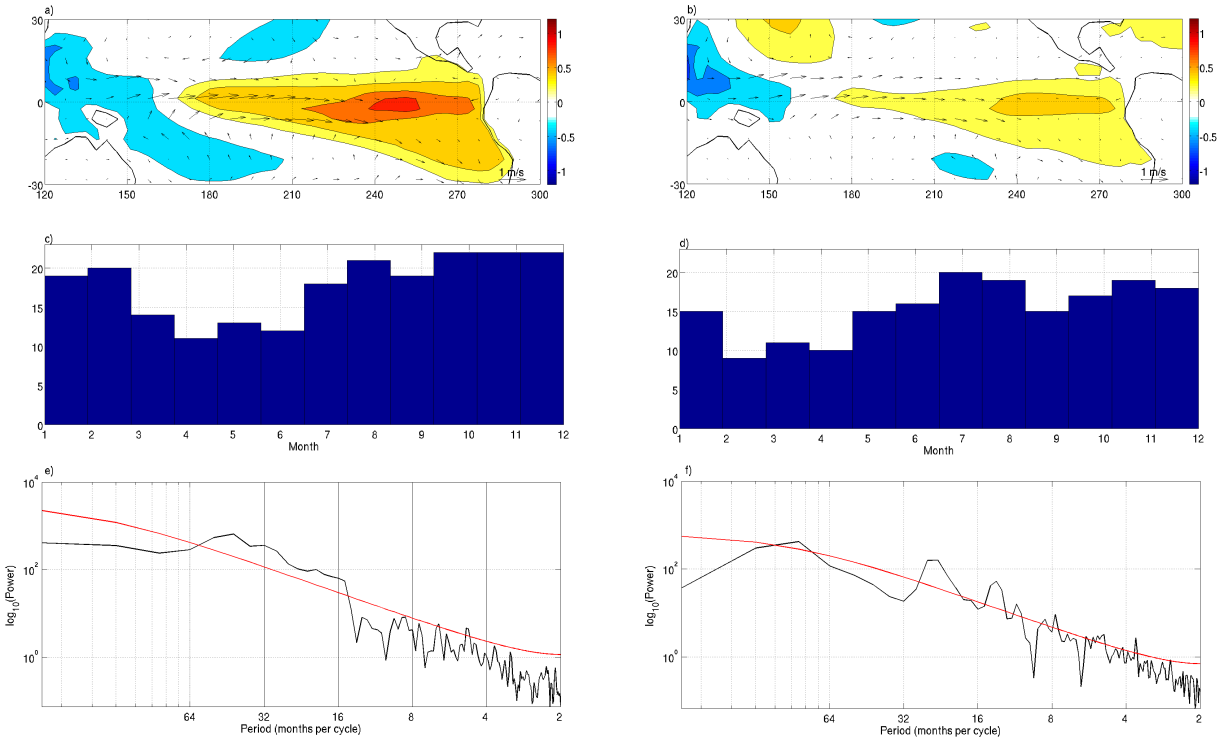

Figure 4.14: First SVD pattern of SST and near-surface winds in the tropical Pacific Ocean (30°S-30°N, 120°E-300°E) for the *Control_slab+rgo* (left) and *Forced_slab+rgo* experiments. a. and b.: Spatial pattern; contour interval 0.2°C. c. and d.: Histogram showing phase-locking to the seasonal cycle. e. and f.: Spectral analysis; the red line indicates the red noise spectrum.

4.5. Summary and Conclusions

We investigated and compared the response of the tropical climate to an extratropical thermal forcing in a hierarchy of models in which a AGCM was coupled either to a simple slab ocean model (just thermodynamic coupling) globally or with a combination of a RGO model in the tropical oceans and a slab ocean model elsewhere.

We found that the responses produced by the two types of configurations greatly differ in the tropical regions, being the signal produced with the RGO coupling weaker in terms of annual

means, indicating that regional dynamical air-sea interaction opposes to the remote signal. However, although the annual mean anomalies produced by this setup are weaker, the changes in the SST seasonal cycle are larger. In particular, over the equatorial Pacific Ocean, while the slab configuration produces no changes to the SST seasonal cycle, the RGO addition generates a profound warming in the centre-east of the basin from April to August balanced by a cooling in the rest of the year, yielding an almost null integration in the annual mean but also implying a significant strengthening of the seasonal cycle in the eastern Pacific. The response of the seasonal cycle to the imposed extratropical forcing is qualitatively similar to the one obtained by Chiang et al. (2008) in similar experiments, although in our case positive SST anomalies reach the eastern boundary of the basin not permitting an earlier onset of the seasonal cold tongue as these authors find in their simulations. We hypothesize that the changes in the SST seasonal cycle are possible via the effect that the zonal wind stress has on the thermocline depth: the remote forcing produces positive anomalies of zonal wind stress to be exerted in the first half of the calendar year; in particular, the significant weakening of the trades over the western portion of the basin around February and March induces a thermocline deepening pulse that propagates eastward in the form of a Kelvin wave, reaching the eastern boundary 2 months later, and generating a warming of the SST over that region as a result. In the second half of the year stronger trades in the central-eastern basin shallow the thermocline producing a local cooling of the SST. Since these mechanisms are not available under the slab configuration, the wind stress seasonal cycle changes are not able to produce any SST changes.

Finally, we briefly analysed, within the RGO setup, possible changes to ENSO activity and found that under the effect of the extratropical forcing significant changes are produced both in the spatial and temporal domains with a weaker SST pattern and a time series that lacks low-frequency variability. We associated the weakening of the ENSO activity to the intensification of the SST seasonal cycle in the eastern equatorial Pacific Ocean, via the frequency entrainment mechanism. As future climate projections tend to agree in the fact that global warming will have an important northward ITG component (NH warming faster than the SH; Friedman et al., 2013), the possible sensitivity of ENSO to ITG is of primary relevance. However, current state of the art fully coupled climate models do not seem to agree in the projected future changes in ENSO characteristics and no clear evidence for a correlation with ITG has been detected in future climate projections (Stevenson, 2012; Tascheto et al., 2014).

Chapter 5. Thesis Summary and Conclusions

The goal of this thesis is to study the response of the ITCZ and the SACZ to an extratropical thermal forcing in a series of numerical simulations performed with an AGCM coupled to either a low or medium complexity ocean model, using realistic surface boundary conditions in all the cases. The relative roles of the atmosphere, SST, LST, hemispheric component of the forcing and tropical ocean dynamics have been investigated and some physical mechanisms mediating in the extratropical to tropical teleconnection have been proposed and tested.

The selected extratropical thermal forcing consists of warming in the NH and cooling in the SH poleward of 40°, with zero global average, and is inspired by the AMO pattern. The AMO is considered to be a natural mode of oscillation associated with fluctuations in the intensity of the thermohaline circulation in the North Atlantic which is, in turn, regarded to be associated with abrupt warming or cooling events in the high latitudes of the Atlantic Ocean. Although driven by different physical mechanism, this type of pattern and its associated interhemispheric thermal gradient additionally resembles the extratropical signature of the projected temperature changes for the 21st century, a scenario in which the NH is projected to warm faster than the SH with special amplification in the high latitudes of the NH.

In all the numerical experiments performed once the forcing pattern was applied a transient period of about 10 years was required for the system to reach an equilibrium. Although in this thesis we mainly focused on the stationary state, we note the potential and the necessity of the study of the transient term to shed light on relevant physical processes communicating the extratropical signal to lower latitudes of the globe.

In Chapter 2 we concentrated on the annual mean response of the ITCZ to the imposed extratropical forcing, separating the roles of the atmosphere, SST and LST on the communication of the remote signal to the tropics. The modelling configuration used in this chapter consisted of the AGCM coupled to slab ocean and land models.

We found that if both ocean and land slab models are applied globally the ITCZ response to the extratropical forcing consists in a shift toward the warmer hemisphere and that as the magnitude of the forcing increases the larger the shift and the precipitation response, but there are no significant changes in the width of tropical band.

Experiments in which the slab models were turned off and replaced by climatological fixed fields in specific regions were designed in order to investigate the roles of ocean and/or land thermodynamic coupling with the atmosphere in transmitting the remote pulse. In particular, in a simulation in which the slab land model is applied globally but the tropical SSTs are kept fixed we found that the ITCZ response notably weakens although non negligible ITCZ response is still present over the Atlantic Ocean and Africa with precipitation anomalies of the order of 20% and 60%, respectively, of the magnitude obtained without the SST restriction. This result highlights the primary role of the tropical SSTs in controlling the ITCZ response in most of the globe but indicates that, in particular, over the Atlantic and Africa some other process is also of relevance. We hypothesized that the effect of the forcing on the LST over Africa is the process that would explain the prevailing ITCZ response in the absence of tropical SST response. To demonstrate that we performed another experiment in which fixed LST over Africa is incorporated as an additional constraint and found that, in this case, the ITCZ response completely vanishes. Therefore, our results indicate that the ITCZ response to the extratropical forcing is not possible just trough purely atmospheric processes, but needs the involvement of either the tropical SST or the continental surface temperatures.

We proposed and tested one physical mechanism that mediates in the extratropical to tropical teleconnection in case the response of the tropical SSTs is inhibited: once the forcing is imposed, a general warming occurs in the high latitudes of the NH, leading to an increase in the specific humidity. Changes in the circulation advect humidity toward northern Africa, increasing the humidity there and enhancing the clear-sky longwave greenhouse effect leading to a warming of the surface beneath. As the warming is associated with a decrease in the regional sea level pressure it drives the ITCZ northward over the continent. Some other processes may also play a role in the warming experienced by northern Africa, as it is still triggered (although in a weaker way) when the clear-sky component of the longwave radiation is not allowed to react to the extratropical forcing. The deepening on the understanding on such processes could be a possible line for future work.

In Chapter 3 we use the same modelling setup as in chapter 2, but with a focus on the SACZ, a feature of the tropical climate whose response to an extratropical thermal forcing had not been addressed previously in the literature.

We found that during its peak season, DJF, the SACZ weakens in response to the extratropical forcing. This finding is consistent with paleoclimatic evidence and also with future climate projections that associate the future interhemispheric asymmetric warming with a decrease in precipitation over the SACZ. In addition, in a series of experiments in which the forcing is divided into its northern and southern components, we concluded that the SACZ weakening is mostly a response to the NH component of the forcing

Regarding the physical mechanisms linking the NH high latitude forcing to the SACZ, we proposed and tested two processes. The first proposed mechanism is related to the generation of a secondary convergence zone in the northern tropical Atlantic: when the forcing is applied, changes in the general circulation of the atmosphere occur in a way that a region of surface winds convergence is generated over the Atlantic Ocean in the latitude band 20ºN-30ºN; this convergence and its associated ascent region further provoke changes in the tropical Hadley circulation over this basin that promotes anomalous descent over the SACZ, inducing a precipitation decrease there. The testing of this mechanism involved a numerical experiment in which the secondary convergence zone over the northern tropical Atlantic is not developed: simulations with fixed tropical SST. In this case the SACZ precipitation anomalies weaken significantly (75% of signal reduction) highlighting the fundamental role of the tropical SSTs in transmitting the information from the high latitudes to this tropical convergence zone. The second proposed mechanism links, via a Walker-type of circulation, the northward ITCZ displacement over Africa with subsidence over the northern portion of the SACZ and a consequent decrease in precipitation. Evidence supporting this mechanism was provided via simulations in which neither the tropical SSTs nor the LST over Africa were allowed to change in response to the remote signal, giving as a result a null response of the African ITCZ as well as a weakening of the SACZ precipitation signal.

In Chapter 4 we concentrated on the role of the tropical ocean dynamics. For this purpose the AGCM was coupled to a slab ocean model or to a combination of a RGO model in the tropical oceans and a slab ocean model elsewhere and the outcomes of such experiments were analysed and

compared. The results revealed that the annual-mean response is weaker when the RGO is included, indicating that the tropical ocean dynamics acts to offset the annual-mean effect of the extratropical forcing. On the other hand, while the slab configuration produces almost no changes to the equatorial Pacific SST seasonal cycle, the RGO coupling generates a significant strengthening of the cycle in the eastern portion of the basin. The changes in the SST seasonal cycle seem to be associated to the thermocline adjustment to the zonal wind stress: the remote forcing produces a significant weakening of the trades over the western portion of the basin around February and March inducing a thermocline deepening pulse that propagates eastward as a Kelvin wave, reaching the eastern boundary 2 months later, and generating a warming of the SST over that region as a result. In the second half of the year stronger trades in the central-eastern basin shallow the thermocline producing a local cooling of the SST. The design of new numerical experiments to quantify the relative roles of the thermocline depth, Ekman dynamics and horizontal advection on the SST response would be a reasonable next step to further investigate how the tropical ocean dynamic modifies the remote signal once it reaches the tropical regions.

Furthermore, the detected changes in the equatorial Pacific Ocean motivated the study of the possible effect of the remote signal on ENSO's properties. We found that indeed ENSO is sensitive to the imposed extratropical thermal forcing, which produced a weakening of its intensity and reduction in its low-frequency variability. We associated the weakening of the ENSO activity to the intensification of the SST seasonal cycle in the eastern equatorial Pacific Ocean, via the frequency entrainment mechanism, proposed by Chang et al., 1994.

In summary, in this thesis a variety of simulated sensitivity studies were performed to assess the extratropical impact on the tropical climate and three main results are highlighted. First, we suggested that the LST (in particular over the Sahara desert) might play an important role in mediating in the transmission of information from the high latitudes to the tropical regions. Second, we presented numerical evidence that indicates that the SACZ can be affected by an extratropical thermal forcing with a behaviour that does not replicate the ITCZ response of shifting towards the warmer hemisphere. Third, our simulations revealed that the tropical ocean dynamics plays a major role in the extratropical to tropical teleconnection and tends to oppose the effect the forcing would generate if only a thermodynamic coupling was allowed, at least in terms of annual-means; the inclusion of tropical ocean dynamics also allows for changes in the equatorial Pacific SST seasonal

cycle, generating a strengthening of the cycle in the eastern portion of the basin which, in turn, favours a weakening of ENSO activity.

Regarding the future outlook, much is still to investigate. All the results of this thesis were obtained using a simplified physics AGCM and low to medium complexity ocean models which allowed to perform a large number of sensitivity tests under different configurations. The next step would be to implement similar experiments in higher complexity models, which may provide different results and possibly indicate the importance of other mechanisms not present in the configuration used here. Even without switching to higher complexity models there are still some aspects that we think deserve a further look. Notably the study of the transient state and the quantification of the role of other mechanisms that could be of relevance such as tropical clouds and the influence of the thermocline adjustment. In addition, the study of the response of the SACZ (and other less studied features of the tropical climate) to extratropical forcings needs to be taken much further, compiling information from paleoclimatic data, observations, numerical simulations and future climate projections. In particular, the detection of changes in the SACZ in CMIP5 historical and 21st century runs would be interesting.

References

Adler, R. F., Huffman, G. J., Chang, A., Ferraro, R., Xie, P. P., Janowiak, J., ... & Gruber, A. (2003). The version-2 global precipitation climatology project (GPCP) monthly precipitation analysis (1979-present). *Journal of hydrometeorology*, *4*(6), 1147-1167.

Baines, P. G., & Folland, C. K. (2007). Evidence for a rapid global climate shift across the late 1960s. *Journal of Climate*, *20*(12), 2721-2744. doi: 10.1175/JCLI4177.1

Barreiro, M., Fedorov, A., Pacanowski, R., & Philander, S. G. (2008). Abrupt climate changes: how freshening of the northern Atlantic affects the thermohaline and wind-driven oceanic circulations. *Annu. Rev. Earth Planet. Sci.*, *36*, 33-58.

Barreiro, M., & Philander, S. G. (2008). Response of the tropical Pacific to changes in extratropical clouds. *Climate dynamics*, *31*(6), 713-729. doi: 10.1007/s00382-007-0363-5

Biasutti, M., Battisti, D. S., & Sarachik, E. S. (2004). Mechanisms controlling the annual cycle of precipitation in the tropical atlantic sector in an atmospheric GCM*. *Journal of climate*, *17*(24), 4708-4723.

Boccaletti, G., Pacanowski, R. C., George, S., Philander, H., & Fedorov, A. V. (2004). The thermal structure of the upper ocean. *Journal of physical oceanography*, *34*(4), 888-902. doi: 10.1175/2008MWR2277.1

Broccoli, A. J., Dahl, K. A., & Stouffer, R. J. (2006). Response of the ITCZ to Northern Hemisphere cooling. *Geophysical Research Letters*, *33*(1). doi: 10.1029/2005GL024546

Broecker, W. S., Peteet, D. M., & Rind, D. (1985). Does the ocean-atmosphere system have more than one stable mode of operation?. *Nature*, *315*(6014), 21-26.

Bryden, H. L., Longworth, H. R., & Cunningham, S. A. (2005). Slowing of the Atlantic meridional overturning circulation at 25 N. *Nature*, *438*(7068), 655-657. doi: 10.1038/nature04385

Burls, N. J., & Fedorov, A. V. (2014). What controls the mean east–west sea surface temperature gradient in the equatorial Pacific: The role of cloud albedo. *Journal of Climate*, *27*(7), 2757-2778. doi: 10.1175/JCLI-D-13-00255.1

Cane, M. A. (1979). The response of an equatorial ocean to simple wind stress patterns. I-Model formulation and analytic results. II-Numerical results. Journal of Marine Research: 37: 233-299.

Carvalho, L. M., Jones, C., & Liebmann, B. (2004). The South Atlantic convergence zone: Intensity, form, persistence, and relationships with intraseasonal to interannual activity and extreme rainfall. *Journal of Climate*, *17*(1), 88-108. doi: 10.1175/1520-0442(2004)017<0088:TSACZI>2.0.CO;2

Chang, P. (1994). A study of the seasonal cycle of sea surface temperature in the tropical Pacific Ocean using reduced gravity models. *Journal of Geophysical Research: Oceans*, *99*(C4), 7725-7741.

Chang, P., Wang, B., Li, T., & Ji, L. (1994). Interactions between the seasonal cycle and the Southern Oscillation-Frequency entrainment and chaos in a coupled ocean-atmosphere model. *Geophysical Research Letters*, *21*(25), 2817-2820.

Chang, P., Ji, L., & Li, H. (1997). A decadal climate variation in the tropical Atlantic Ocean from thermodynamic air-sea interactions. *Nature*, *385*(6616), 516-518.

Chiang, J. C., Cheng, W., & Bitz, C. M. (2008a). Fast teleconnections to the tropical Atlantic sector from Atlantic thermohaline adjustment. *Geophysical Research Letters*, *35*(7).

Chiang, J. C., Fang, Y., & Chang, P. (2008b). Interhemispheric thermal gradient and tropical Pacific climate. *Geophysical Research Letters*, *35*(14).

Chiang, J. C., Kushnir, Y., & Giannini, A. (2002). Deconstructing Atlantic Intertropical Convergence Zone variability: Influence of the local cross-equatorial sea surface temperature gradient and remote forcing from the eastern equatorial Pacific. *Journal of Geophysical Research: Atmospheres*, *107*(D1). Doi: 10.1029/2000JD000307

Chiang, J. C., & Bitz, C. M. (2005). Influence of high latitude ice cover on the marine Intertropical Convergence Zone. *Climate Dynamics*, *25*(5), 477-496. doi: 10.1007/s00382-005-0040-5

Chiang, J. C., & Friedman, A. R. (2012). Extratropical cooling, interhemispheric thermal gradients, and tropical climate change. *Annual Review of Earth and Planetary Sciences*, *40*(1), 383. doi: 10.1146/annurev-earth-042711-105545

Chiessi, C. M., Mulitza, S., Pätzold, J., Wefer, G., & Marengo, J. A. (2009). Possible impact of the Atlantic Multidecadal Oscillation on the South American summer monsoon. *Geophysical Research Letters*, *36*(21). doi: *10.1029/2009GL039914*

Collins, M., R. Knutti, J. Arblaster, J.-L. Dufresne, T. Fichefet, P. Friedlingstein, X. Gao, W.J. Gutowski, T. Johns, G. Krinner, M. Shongwe, C. Tebaldi, A.J. Weaver and M. Wehner, 2013: Long-term Climate Change: Projections, Commitments and Irreversibility. In: Climate Change 2013: The Physical Science Basis. Contribution of Working Group I to the Fifth Assessment Report of the Intergovernmental Panel on Climate Change [Stocker, T.F., D. Qin, G.-K. Plattner, M. Tignor, S.K. Allen, J. Boschung, A. Nauels, Y. Xia, V. Bex and P.M. Midgley (eds.)]. Cambridge University Press, Cambridge, United Kingdom and New York, NY, USA.

Cvijanovic, I., & Chiang, J. C. (2013). Global energy budget changes to high latitude North Atlantic cooling and the tropical ITCZ response. *Climate dynamics*, *40*(5-6), 1435-1452.

Dansgaard, W., Johnsen, S. J., Clausen, H. B., Dahl-Jensen, D., Gundestrup, N. S., Hammer, C. U., ... & Bond, G. (1993). Evidence for general instability of past climate from a 250-kyr ice-core record. *Nature*, *364*(6434), 218-220.

Delworth, T. L., & Mann, M. E. (2000). Observed and simulated multidecadal variability in the Northern Hemisphere. *Climate Dynamics*, *16*(9), 661-676.

Dickson, R. R., Meincke, J., Malmberg, S. A., & Lee, A. J. (1988). The “great salinity anomaly” in the northern North Atlantic 1968–1982. *Progress in Oceanography*, *20*(2), 103-151.

Doyle, M. E., & Barros, V. R. (2002). Midsummer low-level circulation and precipitation in subtropical South America and related sea surface temperature anomalies in the South Atlantic. *Journal of Climate*, *15*(23), 3394-3410. doi: 10.1175/1520-0442(2002)015<3394:MLLCAP>2.0.CO;2

Flato, G. M., & Boer, G. J. (2001). Warming asymmetry in climate change simulations. *Geophysical Research Letters*, *28*(1), 195-198.

Folland, C. K., Palmer, T. N., & Parker, D. E. (1986). Sahel rainfall and worldwide sea temperatures, 1901–85. *Nature*, *320*(6063), 602-607. doi:10.1038/320602a0

Friedman, A. R., Hwang, Y. T., Chiang, J. C., & Frierson, D. M. (2013). Interhemispheric temperature asymmetry over the twentieth century and in future projections. *Journal of Climate*, *26*(15), 5419-5433. doi: 10.1175/JCLI-D-12-00525.1

Frierson, D. M., Hwang, Y. T., Fučkar, N. S., Seager, R., Kang, S. M., Donohoe, A., ... & Battisti, D. S. (2013). Contribution of ocean overturning circulation to tropical rainfall peak in the Northern Hemisphere. *Nature Geoscience*, *6*(11), 940-944. doi: 10.1038/NGEO1987

Giannini, A., Saravanan, R., & Chang, P. (2003). Oceanic forcing of Sahel rainfall on interannual to interdecadal time scales. *Science*, *302*(5647), 1027-1030. doi: 10.1126/science.1089357

Grimm, A. M., Pal, J. S., & Giorgi, F. (2007). Connection between spring conditions and peak summer monsoon rainfall in South America: Role of soil moisture, surface temperature, and topography in eastern Brazil. *Journal of Climate*, *20*(24), 5929-5945. doi: 10.1175/2007JCLI1684.1

Gu, D., & Philander, S. G. (1997). Interdecadal climate fluctuations that depend on exchanges between the tropics and extratropics. *Science*, *275*(5301), 805-807.

Haarsma, R. J., Selten, F. M., Weber, S. L., & Kliphuis, M. (2005). Sahel rainfall variability and response to greenhouse warming. *Geophysical Research Letters*, *32*(17).

Hansen, J., Ruedy, R., Sato, M., & Lo, K. (2010). Global surface temperature change. *Reviews of Geophysics*, *48*(4). doi: 10.1029/2010RG000345

Hansen, J., Sato, M., Kharecha, P., & Schuckmann, K. V. (2011). Earth's energy imbalance and implications. *Atmospheric Chemistry and Physics*, *11*(24), 13421-13449.

Hastenrath, S., & Heller, L. (1977). Dynamics of climatic hazards in northeast Brazil. *Quarterly Journal of the Royal Meteorological Society*, *103*(435), 77-92.

Hartmann, D.L. (1994) Global Physical Climatology. International Geophysics Series, vol 56, Academic Press.

Hartmann, D. L., Klein Tank, A. M. G., Rustucci, M., Alexander, L. V., Bronnimann, S., Charabi, Y., ... & Soden, B. J. (2013). Observations: Atmosphere and Surface in: Climate Change 2013: The Physical Science Basis. Contribution of working group I to the fifth assessment report of the intergovernmental panel on climate change. *Cambridge University Press, Cambridge, United Kingdom and New York, NY, USA*.

Held, I. M., & Soden, B. J. (2006). Robust responses of the hydrological cycle to global warming. *Journal of Climate*, *19*(21), 5686-5699.

Holton, J.R. (2004) An Introduction to Dynamic Meteorology, 4th ed. International Geophysics Series, vol 88, Academic Press.

Horel, J. D., & Wallace, J. M. (1981). Planetary-scale atmospheric phenomena associated with the Southern Oscillation. *Monthly Weather Review*, *109*(4), 813-829.

Hoskins, B. J., & Karoly, D. J. (1981). The steady linear response of a spherical atmosphere to thermal and orographic forcing. *Journal of the Atmospheric Sciences*, *38*(6), 1179-1196.

Hoskins, B. J., & Valdes, P. J. (1990). On the existence of storm-tracks. *Journal of the atmospheric sciences*, *47*(15), 1854-1864.

Hughen, K. A., Southon, J. R., Lehman, S. J., & Overpeck, J. T. (2000). Synchronous radiocarbon and climate shifts during the last deglaciation. *Science*, *290*(5498), 1951-1954.

Junquas, C., Vera, C., Li, L., & Le Treut, H. (2012). Summer precipitation variability over Southeastern South America in a global warming scenario. *Climate Dynamics*, *38*(9-10), 1867-1883. doi: 10.1007/s00382-011-1141-y

Kalnay, E., Kanamitsu, M., Kistler, R., Collins, W., Deaven, D., Gandin, L., ... & Zhu, Y. (1996). The NCEP/NCAR 40-year reanalysis project. *Bulletin of the American meteorological Society*, *77*(3), 437-471.

Kang, S. M., Held, I. M., Frierson, D. M., & Zhao, M. (2008). The response of the ITCZ to extratropical thermal forcing: Idealized slab-ocean experiments with a GCM. *Journal of Climate*, *21*(14), 3521-3532. doi: 10.1175/2007JCLI2146.1

Kang, S. M., Frierson, D. M., & Held, I. M. (2009). The tropical response to extratropical thermal forcing in an idealized GCM: The importance of radiative feedbacks and convective parameterization. *Journal of the atmospheric sciences*, *72*(9). doi: 10.1175/2009JAS2924.1

Kerr, R. A. (2000). A North Atlantic climate pacemaker for the centuries. *Science*, *288*(5473), 1984-1985. doi: 10.1126/science.288.5473.1984

Kodama, Y. M. (1992). Large-scale common features of subtropical precipitation zones (the Baiu frontal zone, the SPCZ, and the SACZ). Part I: Characteristics of subtropical frontal zones. *J. Meteor. Soc. Japan*, *70*, 813-836.

Kodama, Y. M. (1993). Large-scale common features of subtropical convergence zones (the Baiu frontal zone, the SPCZ, and the SACZ). Part II: Conditions of the circulations for generating the STCZs. *J. Meteor. Soc. Japan*, *71*, 581-610.

Koutavas, A., & Lynch-Stieglitz, J. (2004). Variability of the marine ITCZ over the eastern Pacific during the past 30,000 years. In *The Hadley Circulation: Present, Past and Future* (pp. 347-369). Springer Netherlands.

Kucharski, F., Molteni, F., & Bracco, A. (2006). Decadal interactions between the western tropical

Pacific and the North Atlantic Oscillation. *Climate dynamics*, *26*(1), 79-91. doi: 10.1007/s00382-005-0085-5

Lee, S. Y., Chiang, J. C., & Chang, P. (2015). Tropical Pacific response to continental ice sheet topography. *Climate Dynamics*, *44*(9-10), 2429-2446.

Levitus, S. (1982). Climatological atlas of the world ocean. *NOAA Prof. Pap.*, *13*, *US Government Printing Office, Washington DC.*

Lin, J. L. (2007). The double-ITCZ problem in IPCC AR4 coupled GCMs: Ocean-atmosphere feedback analysis. *Journal of Climate*, *20*(18), 4497-4525. doi: 0.1175/JCLI4272.1

Lindzen, R. S., & Nigam, S. (1987). On the role of sea surface temperature gradients in forcing low-level winds and convergence in the tropics. *Journal of the Atmospheric Sciences*, *44*(17), 2418-2436.

Liu, Z., & Alexander, M. (2007). Atmospheric bridge, oceanic tunnel, and global climatic teleconnections. *Reviews of Geophysics*, *45*(2).

Liu, Y., Guo, L., Wu, G., & Wang, Z. (2010). Sensitivity of ITCZ configuration to cumulus convective parameterizations on an aqua planet. *Climate dynamics*, *34*(2-3), 223-240. doi: 10.1007/s00382-009-0652-2

Liu, Z., & Yang, H. (2003). Extratropical control of tropical climate, the atmospheric bridge and oceanic tunnel. *Geophysical Research Letters*, *30*(5). doi: 10.1029/2002GL016492

Lorenz, D. J., & Hartmann, D. L. (2001). Eddy-zonal flow feedback in the Southern Hemisphere. *Journal of the atmospheric sciences*, *58*(21), 3312-3327.

Manabe, S., & Stouffer, R. J. (1995). Simulation of abrupt climate change induced by freshwater input to the North Atlantic Ocean. *Nature*, *378*(6553), 165-167.

Marengo, J. A., Liebmann, B., Grimm, A. M., Misra, V., Silva Dias, P. L., Cavalcanti, I. F. A., ... & Saulo, A. C. (2012). Recent developments on the South American monsoon system. *International Journal of Climatology*, *32*(1), 1-21. doi: 10.1002/joc.2254

Mahajan, S., Saravanan, R., & Chang, P. (2011). The role of the wind-evaporation-sea surface temperature (WES) feedback as a thermodynamic pathway for the equatorward propagation of high-latitude sea ice-induced cold anomalies. *Journal of Climate*, *24*(5), 1350-1361.

Molteni, F. (2003). Atmospheric simulations using a GCM with simplified physical parametrizations. I: Model climatology and variability in multi-decadal experiments. *Climate Dynamics*, *20*(2-3), 175-191.

Nicholson, S. E., & Palao, I. M. (1993). A re-evaluation of rainfall variability in the sahel. Part I. Characteristics of rainfall fluctuations. *International Journal of Climatology*, *13*(4), 371-389.

Nogués-Paegle, J., & Mo, K. C. (1997). Alternating wet and dry conditions over South America during summer. *Monthly Weather Review*, *125*(2), 279-291.

Peterson, L. C., Haug, G. H., Hughen, K. A., & Röhl, U. (2000). Rapid changes in the hydrologic cycle of the tropical Atlantic during the last glacial. *Science*, *290*(5498), 1947-1951.

Philander, S. G. H., Gu, D., Lambert, G., Li, T., Halpern, D., Lau, N. C., & Pacanowski, R. C. (1996). Why the ITCZ is mostly north of the equator. *Journal of climate*, *9*(12), 2958-2972.

Rahmstorf, S. (1996). Bifurcations of the Atlantic thermohaline circulation in response to changes in the hydrological cycle. *Oceanographic Literature Review*, *5*(43), 435.

Schlesinger, M. E., & Ramankutty, N. (1994). An oscillation in the global climate system of period 65-70 years. *Nature*, *367*(6465), 723-726.

Schneider, T., Bischoff, T., & Haug, G. H. (2014). Migrations and dynamics of the intertropical convergence zone. *Nature*, *513*(7516), 45-53.

Smith, T. M., Reynolds, R. W., Peterson, T. C., & Lawrimore, J. (2008). Improvements to NOAA's historical merged land-ocean surface temperature analysis (1880-2006). *Journal of Climate*, *21*(10), 2283-2296.

Song, X., & Zhang, G. J. (2009). Convection parameterization, tropical Pacific double ITCZ, and upper-ocean biases in the NCAR CCSM3. Part I: Climatology and atmospheric feedback. *Journal of Climate*, *22*(16), 4299-4315.

Stríkis, N. M., Chiessi, C. M., Cruz, F. W., Vuille, M., Cheng, H., Souza Barreto, E. A., ... & Bernal, J. P. (2015). Timing and structure of Mega-SACZ events during Heinrich Stadial 1. *Geophysical Research Letters*, *42*(13), 5477-5484. doi: 10.1002/2015GL064048

Stevenson, S. L. (2012). Significant changes to ENSO strength and impacts in the twenty-first century: Results from CMIP5. *Geophysical Research Letters*, *39*(17). doi:10.1029/2012GL052759

Stouffer, R. J., Yin, J., Gregory, J. M., Dixon, K. W., Spelman, M. J., Hurlin, W., ... & Hu, A. (2006). Investigating the causes of the response of the thermohaline circulation to past and future climate changes. *Journal of Climate*, *19*(8), 1365-1387.

Sun, D. Z., Zhang, T., & Shin, S. I. (2004). The effect of subtropical cooling on the amplitude of ENSO: A numerical study. *Journal of climate*, *17*(19), 3786-3798.

Svensson, A., Andersen, K. K., Bigler, M., Clausen, H. B., Dahl-Jensen, D., Davies, S. M., ... & Röthlisberger, R. (2008). A 60 000 year Greenland stratigraphic ice core chronology. *Climate of the Past*, *4*(1), 47-57.

Talento, S., & Barreiro, M. (2012). Estimation of Natural Variability and Detection of Anthropogenic Signal in Summertime Precipitation over South America. *Advances in Meteorology*, *2012*. doi: 10.1155/2012/725343

Talento, S., & Barreiro, M. (2015). Simulated sensitivity of the tropical climate to extratropical thermal forcing: tropical SSTs and African land surface. *Climate Dynamics*, 1-20. doi: 10.1007/s00382-015-2890-9

Talento, S., & Barreiro, M. (2016) Control of the South Atlantic Convergence Zone by extratropical

thermal forcing. Under review.

Taschetto, A. S., Gupta, A. S., Jourdain, N. C., Santoso, A., Ummenhofer, C. C., & England, M. H. (2014). Cold tongue and warm pool ENSO events in CMIP5: mean state and future projections. *Journal of Climate*, *27*(8), 2861-2885. doi: 10.1175/JCLI-D-13-00437.1

Timmermann, A., Okumura, Y., An, S. I., Clement, A., Dong, B., Guilyardi, E., ... & Stouffer, R. J. (2007). The influence of a weakening of the Atlantic meridional overturning circulation on ENSO. *Journal of Climate*, *20*(19), 4899-4919.

Thompson, D. W., Wallace, J. M., Kennedy, J. J., & Jones, P. D. (2010). An abrupt drop in Northern Hemisphere sea surface temperature around 1970. *Nature*, *467*(7314), 444-447. doi: 10.1038/nature09394

Uppala, S. M., Kållberg, P. W., Simmons, A. J., Andrae, U., Bechtold, V. D., Fiorino, M., ... & Li, X. (2005). The ERA-40 re-analysis. *Quarterly Journal of the Royal Meteorological Society*, *131*(612), 2961-3012. doi:10.1256/qj.04.176

Van Der Wiel, K., Matthews, A. J., Joshi, M. M., & Stevens, D. P. (2016). Why the South Pacific convergence zone is diagonal. *Climate Dynamics*, *46*(5-6), 1683-1698. doi: 10.1007/s00382-015-2668-0

Vecchi, G. A., & Soden, B. J. (2007). Global warming and the weakening of the tropical circulation. *Journal of Climate*, *20*(17), 4316-4340. doi: 10.1175/JCLI4258.1

Vellinga, M., & Wood, R. A. (2002). Global climatic impacts of a collapse of the Atlantic thermohaline circulation. *Climatic change*, *54*(3), 251-267.

Vera, C., Higgins, W., Amador, J., Ambrizzi, T., Garreaud, R., Gochis, D., ... & Nogues-Paegle, J. (2006). Toward a unified view of the American monsoon systems. *Journal of Climate*, *19*(20), 4977-5000.

Wang, Y. J., Cheng, H., Edwards, R. L., An, Z. S., Wu, J. Y., Shen, C. C., & Dorale, J. A. (2001). A high-resolution absolute-dated late Pleistocene monsoon record from Hulu Cave, China. *Science*, *294*(5550), 2345-2348.

Wang, X., Auler, A. S., Edwards, R. L., Cheng, H., Cristalli, P. S., Smart, P. L., ... & Shen, C. C. (2004). Wet periods in northeastern Brazil over the past 210 kyr linked to distant climate anomalies. *Nature*, *432*(7018), 740-743. doi: :10.1038/nature03067

Yang, H., & Liu, Z. (2005). Tropical–extratropical climate interaction as revealed in idealized coupled climate model experiments. *Climate dynamics*, *24*(7-8), 863-879. doi: 10.1007/s00382-005-0021-8

Yoshimori, M., & Broccoli, A. J. (2008). Equilibrium response of an atmosphere-mixed layer ocean model to different radiative forcing agents: Global and zonal mean response. *Journal of Climate*, *21*(17), 4399-4423. doi: 0.1175/2008JCLI2172.1

Zebiak, S.E. (1985) Tropical atmosphere-ocean interaction and the El Niño/Southern Oscillation Phenomenon. PhD Thesis, Massachusetts Institute of Technology. Dept. of Earth, Atmospheric, and

Planetary Sciences.

Zhang, L., & Wang, C. (2013). Multidecadal North Atlantic sea surface temperature and Atlantic meridional overturning circulation variability in CMIP5 historical simulations. *Journal of Geophysical Research: Oceans*, *118*(10), 5772-5791. doi: 10.1002/jgrc.20390

Zhang, R., & Delworth, T. L. (2005). Simulated tropical response to a substantial weakening of the Atlantic thermohaline circulation. *Journal of Climate*, *18*(12), 1853-1860.